

論文 / 著書情報  
Article / Book Information

|                   |   |
|-------------------|---|
| 題目(和文)            | ゼオライト内包ニッケル触媒によるバイオマス由来アルコールからの水素および合成ガスの製造に関する研究   |
| Title(English)    | Study on the Production of Hydrogen and Syngas from Biomass-Derived Alcohols using Zeolite-Encapsulated Nickel Catalysts  |
| 著者(和文)            | ArayawateSirintra   |
| Author(English)   | Sirintra Arayawate  |
| 出典(和文)            | 学位:博士(工学),<br>学位授与機関:東京工業大学,<br>報告番号:甲第12622号,<br>授与年月日:2023年12月31日,<br>学位の種別:課程博士,<br>審査員:多湖 輝興,関口 秀俊,下山 裕介,松本 秀行,横井 俊之  |
| Citation(English) | Degree:Doctor (Engineering),<br>Conferring organization: Tokyo Institute of Technology,<br>Report number:甲第12622号,<br>Conferred date:2023/12/31,<br>Degree Type:Course doctor,<br>Examiner:,,,, |
| 学位種別(和文)          | 博士論文  |
| Type(English)     | Doctoral Thesis   |

## 2023 Doctoral Thesis

Study on the Production of Hydrogen and Syngas from Biomass-Derived Alcohols using  
Zeolite-Encapsulated Nickel Catalysts

(ゼオライト内包ニッケル触媒によるバイオマス由来アルコールからの水素および合  
成ガスの製造に関する研究)

Tokyo Institute of Technology, School of Materials and Chemical Technology

Department of Chemical Science and Engineering

Graduate Major in Chemical Science and Engineering

Tago Laboratory

Sirintra ARAYAWATE

### Abstract

The objective of this research is the highly efficient production of hydrogen or syngas from biomass-derived aqueous alcohol solutions, and the ethanol steam reforming reaction (ESR reaction) using Ni-based catalysts was conducted. The problems with the ESR reaction are catalyst deactivation due to carbon deposition and hydrothermal degradation. To solve these problems, Ni@Silicalite-1 catalyst was developed by encapsulating Ni particles within Silicalite-1, a hydrophobic porous material, and the ESR activities at the reaction temperatures of 500-700 °C were compared to conventional catalyst prepared by wetness impregnation (Ni/Silicalite-1). Because Ni particle size in Ni@Silicalite-1 maintained at 3 – 5 nm during ESR without sintering, Ni@Silicalite-1 provided a higher ethanol conversion and hydrogen yield than Ni/Silicalite-1.

**Keywords:** Ethanol Steam Reforming; Zeolite supported metal catalysts; Ni nanoparticles; Thermal stability;

## Acknowledgement

The completion of my doctoral degree would have been impossible without support from a group of people. First, I would like to express my sincere gratitude to my academic advisor, Prof. Teruoki Tago for all kindness, all support, and caring attention throughout the way of my PhD study here. Moreover, I would like to thank the thesis committee for their contributions and comments to improve my research quality. Also, I would like to extend my sincere thanks to Assist. Prof. Hiroyasu Fujitsuka and Assist. Prof. Kentaro Kimura for their research guidance. I would like to acknowledge MEXT Scholarship that provided me a full scholarship opportunity with living allowance for 3 years of my PhD study in IGP(C) program at Tokyo Tech.

I would like to thank my junior research mate, Ms. Yokosawa for always helping and supporting during experiments and various research presentation preparation. I am also grateful to all Tago lab members, all students and our lab secretary, Ms. Tabata, for their help with lab work, and administrative work. I would also acknowledge support from a Grants-in-Aid for Scientific Research [21K18845 and 21H01700] for a partial budget support on my research, and Ookayama Materials Analysis Division for facilities support.

Apart of laboratory, this journey would be impossible without my very nice Thai friends: Nui, Tang, and friends for their emotional support. I would also like to thank the other group of friends who supported me in my cooking session, and nice friends at my part-time place. My PhD journey will be lonelier and more difficult without them. I am also thankful to Health support center staff, especially Ms. Son, my counselor, who helps me to understand my thoughts, emotions, and deal with them better.

The last group of people I would like to thank is “Family”, my father, my mother, my dad, my brother, my sister, my all-time best friend, and my inner self friend. Their belief in me keeps motivating me not to surrender all difficulties I faced along the way. I would also like to thank my favorite artists, especially Billkin, PP Krit, Heartrocker, and all talented chefs around the world for all entertainments, inspiration, and bringing happiness to me during this journey.

Miss Sirintra Arayawate

## Table of Contents

|  |           |
|--|-----------|
| <b>Abstract</b>  | <b>2</b>  |
| <b>Acknowledgement</b>   | <b>3</b>  |
| <b>Table of Contents</b>   | <b>4</b>  |
| <b>Chapter 1 : Introduction</b>  | <b>1</b>  |
| 1.1. Research background   | 1         |
| 1.1.1. Hydrogen production processes and technologies                              | 2         |
| 1.1.2. Biomass reforming from different carbon source for hydrogen production      | 7         |
| 1.1.3. Types of Ethanol reforming  | 14        |
| 1.1.4. ESR in applications: Reaction process and reactors                          | 15        |
| 1.2. Bio-ethanol reforming for hydrogen production                                 | 28        |
| 1.2.1. Ethanol reforming reaction pathways   | 29        |
| 1.2.2. Catalyst for ethanol steam reforming (ESR)                                  | 30        |
| 1.2.3. Ni-based catalyst for ESR: support and preparation techniques               | 31        |
| 1.2.4. Encapsulation structure of metal nanoparticles                              | 37        |
| 1.3. Problem statement   | 40        |
| 1.4. Objectives  | 40        |
| 1.5. Scope of the study  | 41        |
| <b>Chapter 2 : Preparation of Ni@Silicalite-1 with Ni-Phyllosilicate precursor</b> | <b>43</b> |
| 2.1. Introduction  | 43        |
| 2.1.1. Goal and criteria for “ESR ideal catalyst”                                  | 43        |
| 2.2.2. Zeolite formation mechanism via hydrothermal synthesis: General knowledge   | 44        |
| 2.2.2.1. Hydrothermal synthesis of zeolites  | 44        |
| 2.2.2.2. Hydrothermal synthesis parameters that effect the properties of zeolites  | 47        |
| 2.2.2.3. Zeolite preparation with seed utilization (seeding)                       | 49        |
| 2.2.3. Ni-phyllosilicate: structure and advantages                                 | 50        |
| 2.2. Experimental  | 52        |
| 2.2.1. Preparation of Ni-PS precursors   | 53        |
| 2.2.2. Preparation of Ni@Silicalite-1  | 54        |
| 2.2.3. Materials Characterization (before reaction tests)                          | 56        |
| 2.3. Results and discussion  | 58        |
| 2.3.1. Explanation of Ni@Silicalite-1 formation mechanism                          | 58        |
| 2.3.2. Effect of Ni-phyllosilicate condition                                       | 61        |

|  |            |
|--|------------|
| 2.3.2.1. Effect of the use of precursor in the preparation of Ni@Silicalite-1 (1-step vs 2-step preparation)                   | 61         |
| 2.3.2.2. Precursor calcination and porosity  | 63         |
| 2.3.2.3. Precursor dissolution: dissolution time   | 66         |
| 2.3.3. Effect of hydrothermal synthesis condition towards zeolite formation  | 67         |
| 2.3.3.1. Effect of H <sub>2</sub> O:Si ratio   | 67         |
| 2.3.3.2. Effect of hydrothermal synthesis temperature  | 68         |
| <b>Chapter 3 : Study of reaction mechanism and pathway of ethanol steam reforming on Ni over Silicalite-1</b>                  | <b>71</b>  |
| 3.1. Introduction  | 71         |
| 3.1.1. Ethanol steam reforming reaction pathway  | 71         |
| 3.1.2. Ethanol steam reforming reaction mechanism on Ni-zeolite catalyst   | 73         |
| 3.2. Experimental  | 75         |
| 3.3. Results and discussion  | 76         |
| 3.3.1. Calculation of chemical equilibrium concentration of ESR  | 77         |
| 3.3.2. Effect of different reaction temperature towards ESR reaction mechanism on Ni over Silicalite-1 catalyst                | 79         |
| 3.3.3. Proposed reaction mechanism on Ni@Silicalite-1  | 81         |
| 3.3.3.1. Ethanol adsorption and its surface reaction   | 81         |
| 3.3.3.2. Water adsorption and its surface reaction   | 85         |
| <b>Chapter 4 : Investigation of Catalytic activity of Ni@Silicalite-1</b>  | <b>88</b>  |
| 4.1. Introduction  | 88         |
| 4.2. Experimental  | 92         |
| 4.2.1. ESR activity test   | 92         |
| 4.2.2. Catalyst characterization (after the reaction test)   | 94         |
| 4.3. Results and discussion  | 95         |
| 4.3.1. Effect of Ni location on catalysts towards ethanol conversion and product selectivity in different reaction temperature | 95         |
| 4.3.2. Effect of steam-to-carbon ratio in feed   | 104        |
| 4.3.3. Stability Test  | 106        |
| <b>Chapter 5 : Conclusion and recommendations</b>  | <b>112</b> |
| <b>References</b>  | <b>114</b> |
| <b>Biography</b>   | <b>122</b> |

## Chapter 1 : Introduction

### 1.1. Research background

Hydrogen gas ( $H_2$ ) has important roles in chemical production process and energy aspect. In chemical production processes, hydrogen has been used across industries. It is used as a reactant, reducing agents, carrier gas, and as a source of heat. The process involving hydrogen gas includes ammonia synthesis (as a reactant), hydrogenation reactions in saturated fatty acid or solid fats production (in foods, beverages, cosmetics, and industrial processes), ethylene glycol production, and pharmaceuticals production. Hydrogen gas is also used in petroleum refining as in a hydrocracking process (making more valuable products from the long-chain hydrocarbon) and desulfurization process which is a process of sulfur removal using hydrogen gas. In methanol and hydrogen peroxide production, hydrogen is used as a feedstock. In chemical synthesis, hydrogen is used to modify functional groups to obtain the desired products. In metal and semiconductor industries, hydrogen is used as a reducing agent for producing pure metal and cleaning surfaces prior to thin film deposition.

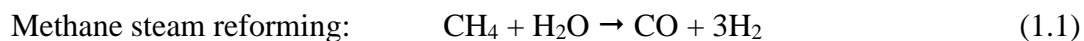
In energy aspect, hydrogen energy is in “spotlight” of this field. Energy crisis, fossil fuel depletion, and environmental problems are the reasons for the development of renewable and sustainable energy, and hydrogen is a selection in this category. Hydrogen energy is a clean energy carrier with a high heating value and energy density per unit mass [1]. The transition away from fossil fuel, one way is the use of hydrogen, could lower the use of fossil fuel, carbon emission, and pollution; therefore, energy security is ensured, and sustainability can be promoted [2]. Hydrogen fuel cells are examples of using hydrogen as an energy which is increasingly developed recently by several automotive companies. The market size of hydrogen gas is increased yearly in both industrial and energy sectors [3]. Research and innovation in production technologies, storage, transportation, infrastructure, and utilization of hydrogen, including its cost and safety has been investigating and developing by researchers as challenges to overcome and realize the use of hydrogen.

### 1.1.1. Hydrogen production processes and technologies

Over the past few decades, there have been a lot of studies focused on hydrogen energy because of its eco-friendly and can be a sustainable energy option. Hydrogen provides energy density per unit of mass, making it stand out among alternative fuels. Various approaches have been investigated to generate hydrogen, including thermochemical techniques such as reforming and hydrocarbon or organic matter gasification, electrolysis methods splitting water into hydrogen and oxygen, and biological processes that using microbial activity to produce hydrogen through natural reactions. Various kinds of hydrogen production and technologies are listed as follows [4]:

#### 1. Steam reforming of methane

The process of methane steam reforming, referred to as MSR or SMR, is an extensively utilized industrial technique to generate hydrogen and carbon monoxide (syngas) by reacting to methane (CH<sub>4</sub>) and water (H<sub>2</sub>O). This method is significantly important in today's hydrogen production since it is the most common method of hydrogen production which is utilized globally. Methane and high-temperature steam are mixed with the presence of catalyst. The reaction proceeds to form carbon monoxide and hydrogen (named the mixture as syngas). The chemical reaction is shown in Eq. (1.1). The reaction undergoes in an endothermic reaction, typically conducted at an elevated temperature in a range of 700 – 1000 °C, and moderate pressure.



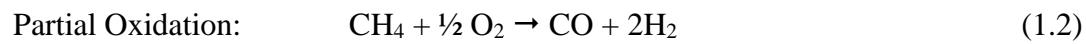
The catalyst that is normally used is often a Ni-based catalyst. The produced syngas serves as a valuable intermediary product extensively employed in diverse industrial processes. The hydrogen derived from this procedure is fundamental in applications such as ammonia production, methanol synthesis, and fuel cell utilization. Since the production is high in hydrogen as a large-scale hydrogen production, therefore, it is also provided a high carbon dioxide and carbon monoxide. These are considered as greenhouse gases which the further process includes capture, store, or repurpose the CO<sub>2</sub> produced during this process to mitigate its environmental impact.

#### 2. Partial Oxidation (POX)

This is the reaction that partially oxidized a hydrocarbon feedstock, typically methane, derived from fossil fuels, and other hydrocarbons, with a limited amount of oxygen or air as shown in Eq. (1.2). This controlled combustion yields a mixture of



hydrogen (H<sub>2</sub>), carbon monoxide (CO), and other gases. The reaction system is an exothermic reaction, releasing heat, which can be utilized in process heating or serve other purposes. This reaction typically occurs at elevated temperatures, between 1200 – 1600 °C, and under moderate pressure conditions. The precise balance of oxygen to hydrocarbon in stoichiometric terms is essential to obtain the effluents with a targeted syngas composition (H<sub>2</sub>/CO ratio) which relates to a further utilization of obtained syngas.



### 3. Gasification process

Gasification, a kind of thermochemical process, is used to produce hydrogen by converting carbon-based materials into a mixture of gases, primarily hydrogen and carbon monoxide [5]. This method involves heating the carbon-rich feedstock, such as coal, biomass, agricultural and forestry residue, in a controlled environment with a limited amount of oxygen or steam. During gasification, the carbonaceous feedstock undergoes a chemical transformation, breaking down into its gaseous components, including hydrogen and carbon monoxide. The resulting gas mixture, syngas, can be further processed to extract and purify to get hydrogen for various applications. Gasification is an efficient and versatile method, making the utilization of diverse feedstocks to generate hydrogen, and making the route of clean and valuable energy carrier to be more feasible.

### 4. Autothermal Reforming (ATR)

Autothermal Reforming (ATR) is a technique utilized to generate hydrogen by combining a partial oxidation and a steam reforming within a single reactor. It is considered as an effective and adaptable method for hydrogen production from hydrocarbon feedstocks such as natural gas, methane, propane, etc. Hydrocarbon feedstock is mixed with either oxygen or air and steam, and then elevated to high temperatures from 700 – 1100 °C, in the presence of a catalyst. Heat is required to proceed with the reaction since it is an endothermic steam reforming reaction. The chemical reactions of ATR can be shown by the following equations:



Syngas is a product of the system which can undergo subsequent water-gas shift reaction and purification steps to procure a higher purity of hydrogen. Since the amount

of oxygen and steam are controlled feeding into the reaction system, a well-proportioned mixture of hydrogen and carbon monoxide can be achieved. This mixture can be further purified to pure hydrogen, and further utilized in fuel cells and chemical manufacturing.

## 5. Thermochemical water splitting

It is a hydrogen production process that is utilizing high-temperature chemical reactions to break water molecules ( $\text{H}_2\text{O}$ ) into hydrogen ( $\text{H}_2$ ) and oxygen ( $\text{O}_2$ ). Thermochemical water splitting relies on heat generated from external sources or renewable energy (e.g., nuclear, or concentrated solar power). As its name thermochemical, the water splitting in this process involves several chemical reactions and they occur at different temperature stages. The chemical reactions in thermochemical water splitting process are listed below in two steps:



where  $\text{MO}_x$  is a metal oxide, M is the metal, and x is the oxidation state



Various metal oxides or compounds act as catalysts or redox materials to facilitate these reactions. The high-temperature step involves the reduction of the metal oxide to release oxygen, and the low-temperature step involves re-oxidizing the reduced metal oxide with water vapor to regenerate the original metal oxide. Besides metal oxide, several methods, for example, sulfur-based cycles, are being researched for improving hydrogen production efficiency. Hydrogen obtained at low temperatures is collected and utilized for various applications. Thermochemical water splitting has the advantage of being driven by high-temperature heat sources, making it compatible with concentrated solar power or other heat sources. Integration of the thermochemical water splitting with other types of renewable energy for process heating is even more encouraged the efficient and sustainable hydrogen production.

## 6. Electrolysis

Electrolysis is an electrochemical process that splits water ( $\text{H}_2\text{O}$ ) into its constituent elements, hydrogen ( $\text{H}_2$ ) and oxygen ( $\text{O}_2$ ). Water is broken down using electrodes which are commonly made of platinum or other conductive materials. In electrolysis process, a current is passing through water. Hydrogen ions ( $\text{H}^+$ ) migrate towards cathode, the negatively charged electrode, gaining electrons to form hydrogen

gas ( $\text{H}_2$ ). Simultaneously, oxygen ions ( $\text{O}^{2-}$ ) migrate towards anode, the positively charged electrode), losing electrons to form oxygen gas ( $\text{O}_2$ ). The redox reactions at the electrodes during electrolysis are as follows:



There are two main types of electrolysis, including Proton Exchange Membrane (PEM), and Alkaline Electrolysis. PEM is suitable for smaller-scale applications, also requiring precise control and rapid response. It is a system with polymer electrolyte membranes operating at low pressure and temperature. It can be integrated to hydrogen fueling station. Another type is alkaline electrolysis. Alkaline electrolyte with high temperature and pressure. It provides less efficient than PEM but widely used for large-scale hydrogen production. The obtained hydrogen can be collected and used in further applications. As with other hydrogen production technology, if the electricity provided to the process comes from renewable sources, the resulting hydrogen is considered as a sustainable energy.

## 7. Photoelectrochemical water splitting (PEC)

PEC can be called Photocatalytic Water Splitting. It utilizes a solar energy to split water into hydrogen and oxygen on a specialized semiconductor photoelectrode, which absorbs solar energy and drives the water-splitting reactions. Several steps are included, photo absorption, charge separation, and water splitting reactions. The semiconductor as a photoelectrode absorbs photons from sunlight, generating electron-hole pairs. When the enough energy from adsorbed photons surpasses the bandgap of semiconductor, the next step of charge separation can be proceeded. The excited electron and holes are separated within the semiconductor material. The migration occurs according to charge opposition: electron (negative charge) migrates to the surface that reduction takes place (where that hydrogen is produces), while the hole (missing of electron) migrates to the surface the oxidation takes place (where that oxygen is produced). Water splitting reaction occurs in this hydrogen evolution (HER) and oxygen evolution (OER) manners. Researchers are now trying to improve its efficiency and practical application from its potential for green hydrogen production. The challenges include the development of photoelectrode, materials of semiconductor, design optimization for commercialization.





## 8. Biological hydrogen production [6, 7]

This type of hydrogen production utilizes the help of microorganisms, including bacteria or microalgae with the ability of producing hydrogen. These microorganisms are cultivated, breakdown the organic feedstocks, which are organic waste or biomasses, and produce hydrogen as a metabolic by-product under the control condition.

There are two types of fermentation, including dark fermentation (no light) and photo-fermentation (with the presence of light). The dark fermentation bacteria are Clostridium, Enterobacter, and Escherichia coli. For the group of photo-fermentation, Photosynthetic bacteria, such as Rhodobacter and Rhodospseudomonas, utilize light energy to produce hydrogen. The produced matters are hydrogen, carbon dioxide, and by-products. The hydrogen produced can be captured and utilized as a clean fuel. This technology is under the development stage. It still provides a low hydrogen yield and is very sensitive to environmental factors, but it holds a promise for sustainable and renewable hydrogen production.

## 9. Others hydrogen production technologies

The example lists as follows are the hydrogen production that is utilizing renewable energy source which is a crucial component for transition to a clean and sustainable energy. They are promising approaches for energy production. Stand-alone are now in practical production already for some options, some are now under development for improving their efficiency and feasibility for larger scale production, also integration.

- Hydrogen from Wind Power (Wind-to-Hydrogen): excess electricity generated from a wind turbine can be further utilized in electrolysis. It can also be an energy source for all types of hydrogen production as well.
- Hydrogen from Hydropower (Hydro-to-Hydrogen): the same as the wind turbine electricity generation, the hydropower can be a source of energy provided for hydrogen production.
- Geothermal Hydrogen Production [8]: geothermal energy derived from earth's natural heat, which is the heat that being stored underneath the earth's surface can be utilized in electricity production. Those transformed energy are being utilized in

thermochemical or electrolytic processes to meet the process condition at high temperature or high voltage requirements for hydrogen production.

- Ocean Thermal Energy Conversion (OTEC) for Hydrogen Production: it utilizes the temperature difference in ocean water to generate electricity. The warm water at ocean surface is used to vaporize a working fluid to drive a turbine in electricity generation, then the cold water from deeper ocean is used for condensation. The electricity can be utilized in thermochemical or electrolytic processes, as same as wind power, hydro power, and geothermal energy, for hydrogen production.

In order to choose the hydrogen production process in a practical application, several factors need to be considered to ensure efficiency, sustainability, cost-effectiveness, and environmental impact. These are the aspects for consideration.

- 1) Feedstock Availability and its cost
- 2) Yield and Efficiency of the process
- 3) Production cost and Economic viability
- 4) Energy source of the process and integration with renewable energy source
- 5) Environmental Impact and Carbon Footprint together with waste and by-products management
- 6) Capacity and Scaling-up possibilities
- 7) Integration with existing infrastructure
- 8) Hydrogen Purity and Quality
- 9) End-Use Applications
- 10) Storage and Distribution of both feedstocks and products
- 11) Safety, Regulation and Policy Environment
- 12) Research and Innovation

### **1.1.2. Biomass reforming from different carbon source for hydrogen production**

Biomass reforming for hydrogen production is the thermochemical process, which biomass feedstocks are heated in the controlled environment with oxygen or steam to break down the carbonaceous component in the molecular structure in the biomass into syngas, containing carbon monoxide, hydrogen, and some other gases. Gasification, pyrolysis, and steam reforming are examples of the processes in this category, but nowadays with mostly gasification. The product gases can be subsequently reacted in water-gas shift reactions or

undergone the separation processes to increase the hydrogen content and purity of the obtained syngas.

Different carbon sources can be used, and each type of material has its own composition and characteristics, therefore, different advantages and disadvantages are affected to the efficiency and feasibility of hydrogen production. The selection of suitable carbon sources for hydrogen production is according to the feedstock availability (including a regional availability), processing cost, energy content, and the consideration on sustainability of using the material, etc. Examples of carbon sources in hydrogen production are listed below.

Wood and woody biomass, for example, wood chips and saw dust, consist of lignin and cellulose, which can be gasified to produce syngas, and this syngas is further separated for pure hydrogen. Agriculture residues, such as corn stover, rice straw, and wheat straw, are rich in cellulose and hemicellulose. They are also suitable feeds for biomass gasification.

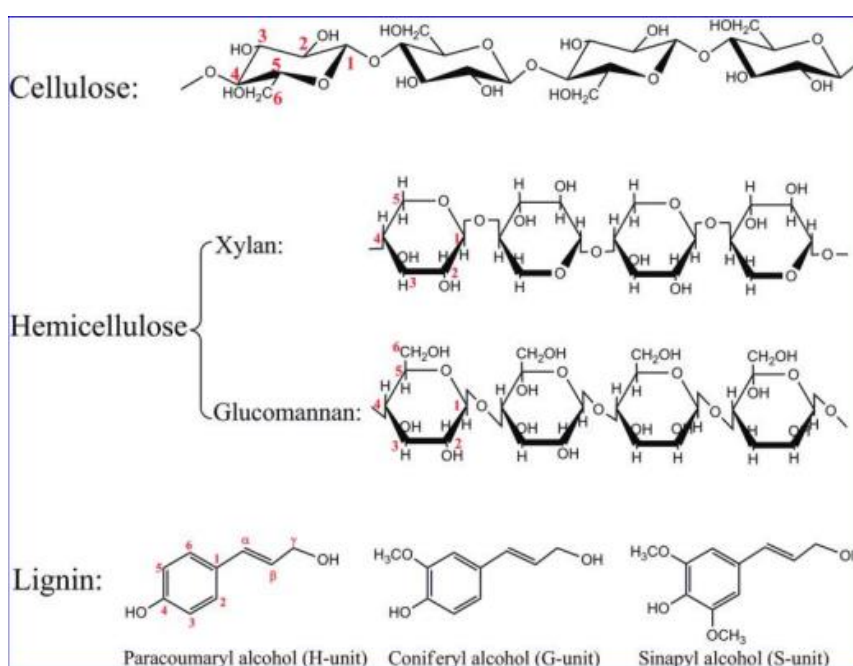


**Figure 1.1.** Structures of cellulose, hemicellulose, and lignin [9].

Consideration of key components in wood and agricultural residue, lignin, cellulose, and hemicellulose are three main components in the consideration of being the source of syngas production, subsequently hydrogen production. These three materials are the major components of plant cell walls, they all have their own properties and characteristics when become a carbon source for hydrogen production.

Lignin is a cross-linked aromatic polymer made up complexly from phenolic compound, which is not carbohydrate-like as cellulose and hemicellulose. It has high

resistance towards chemical and biological degradation; therefore, it is a reason for making lignin a stable carbon source for gasification. Since it is rich in carbon, it provides a high energy content and yields a substantial amount of hydrogen per unit mass, higher than cellulose and hemicellulose. Moreover, the syngas from lignin gasification often provides a favorable hydrogen-to-carbon monoxide ratio for certain applications of hydrogen production.

Cellulose is a linear polymer of repeating glucose units linked by  $\beta$ -1,4-glycosidic bonds. For digestion, it requires cellulase enzymes to break down the glycosidic bonds into glucose, for example, the biological processes like fermentation. For gasification to produce syngas, cellulose consists of higher oxygen content compared to lignin, therefore, the more carbon dioxide (CO<sub>2</sub>) can be obtained mixing in the product gas. With this result, the H<sub>2</sub>/CO ratio in the obtained syngas may not be as high as with some other feedstocks and need to be adjusted for further applications.

Hemicellulose is a branched polymer composed of various sugar monomers, including glucose, xylose, mannose, and others, which its composition can be varied due to the plant source. It is more easily hydrolyzed compared to cellulose, which makes hemicellulose more accessible for biological fermentation. For gasification, the obtained syngas composition depends on the sugar type presented. It often provides syngas with higher H<sub>2</sub>/CO ratio compared to cellulose gasification and makes this obtained syngas to be more suitable for hydrogen production process.

Energy crops (bioenergy crops) are a big group of plants which provide a high potential for energy production. It is a fast-growing plant and mainly used in energy fields such as biomass, biofuels production, or other forms of renewable energy. It provides a sustainable and reliable source of energy from their fast-growing ability.

The properties of energy crops include a high in biomass yield, high energy content (energy density), suitable for biofuel feedstocks, and adaptability. This group of crops can grow quickly per unit of the area used and yield large amounts of plant material, e.g., leaves, stems, seeds, or roots, which can be converted into energy. Compared to the traditional crops, the energy crops often provide a higher energy content, i.e., they can produce more energy when processed or converted into biofuels. The energy crops can be used as feedstocks for various biofuel production processes, including ethanol production from sugarcane, or corn, biodiesel production from oilseeds like soybeans or palm, biogas production from switchgrass or miscanthus. For adaptability, the crops are chosen from their ability to grow in

a variety of environmental conditions without requiring excessive care, such as excessive water or fertilizer inputs.

The common energy crops examples are switchgrass, miscanthus, sugarcane, willow, poplar trees, jatropha. Some of these crops are directly used as biomass feed in gasification, some are also used in biofuel production, such as bioethanol or biodiesel. The use of biofuel in hydrogen production will be mentioned in the next section. However, some energy crops are foods, therefore, it is important to manage the cultivation in a sustainable manner toward food security, biodiversity, and land use.

Besides plant-based carbon sources, other carbon-containing based materials can also be used in hydrogen production. Algae is also used as a hydrogen-rich plant. The cultivated algae are transported as an accumulated biomass, then is gasified to produce hydrogen-rich syngas. Kinds of organic waste, including Municipal Solid Waste (MSW) and animal waste, which also consists of organic components, can be used as a source of syngas production. The use of these solid waste could help in both waste minimization and hydrogen production. Biodegradable plastics are also the new candidates since they are made from biomass sources. They can be used as feedstock for biomass reforming for hydrogen production as other types of biomasses.

Biofuels are fuels that are derived from renewable sources, including plants, algae, and animal wastes. They are sustainable alternatives to the conventional fossil fuel that we use nowadays which are finite and in a way of depletion. Biofuels are used in renewable hydrogen production through various processes as listed below.

- 1) Biological hydrogen production (Dark fermentation): some microorganisms, for example, Clostridium and Enterobacter strain, can produce hydrogen gas as a by-product through dark fermentation. Organic compounds or other biofuels serve as substrates for the bacteria in enzymatic reactions.
- 2) Biological hydrogen production (Photofermentation): some photosynthetic bacteria, such as purple non-sulfur bacteria, can utilize the organic substrates, i.e., biofuel as a carbon source, to produce hydrogen gas in the presence of light.
- 3) Hydrogen production from algae: certain types of microalgae can produce biofuels during their growth and those biofuels are undergoing the reforming process yielding hydrogen gas.
- 4) Thermochemical conversion of biofuels: biodiesel, bioethanol, and biogas are used as feedstocks in thermochemical processes such as steam reforming or gasification and



converted into syngas. Bioethanol steam reforming or bioethanol catalytic reforming yields a hydrogen-rich gas. Biodiesel steam reforming or biodiesel pyrolysis are also utilized in hydrogen production with other byproducts. Biogas from the anaerobic digestion of organic wastes, which primarily consists of methane and carbon dioxide, can be reformed through steam reforming to produce hydrogen-rich gas.

The use of biomasses and biofuels in hydrogen production as the alternative carbon sources show benefits in terms of renewable and sustainable energy production. Nowadays, hydrogen production from biomass via gasification and pyrolysis has been implemented. To increase hydrogen yield, steam reforming and water-gas shift reaction are combined. The utilization of bio-liquid fuel has been in the investigation, considering bioethanol, it has advantages as follows [10].

1. Higher energy density in liquid fuel as bioethanol is obtained compared to original solid biomass. Liquid fuel also provides advantages in storage and transportation. Bioethanol for hydrogen production is easier, more practical, and more energy is obtained from its high hydrogen yield. This advantage can lead to efficiency in large scale production and distribution.
2. Reduction of preprocessing process: comparing the preprocessing process of biomass for gasification utilization, especially the lignocellulosic biomass, they are required the size reduction, drying, and other pretreatments. The fermentation and purification to obtain bioethanol requires fewer preprocessing steps, therefore the conversion to hydrogen is more efficient.
3. Higher overall process efficiency can be obtained from bioethanol reforming from its high energy efficiency. The operating temperature of liquid fuel reforming is a lot lower than the gasification temperature. There are some arising concerns of energy consumption from distillation and purification of ethanol, therefore, the durable and functionable catalyst in various feedstock, in terms of concentration and impurity, is very important for the application and lower the energy consumption in the preprocessing steps.
4. Lower carbon emissions are obtained in the case of bioethanol. The production of bioethanol from renewable feedstocks can lower the greenhouse gas emissions compared to biomass, especially the biomass involving deforestation or land-use changes.

5. The feedstock availability is found to be easier than feedstock for general biomass. Bioethanol is typically produced from corn, sugarcane, or cellulosic materials which are cultivated specifically for fuel production, vegetable wastes, nonedible lignocellulosic, or algae. Therefore, the feedstocks are often readily for the production and managed smoothly compared to various biomass that can be varied by the growing region and season of cultivation.
6. The well-established technologies, and infrastructure such as steam reforming of methane or autothermal reforming can be used with bioethanol steam reforming with minor modifications. The existing distribution and infrastructure of bioethanol utilization as transportation fuel can be combined for hydrogen production purpose. The feasibility for scaling up for bioethanol reforming for hydrogen production can be improved.

There are still several factors in consideration as challenges for research and development, including the feed stock sources, energy inputs required for production, operations, and material processing, also the emissions associated with biomass conversion, biofuel production, and hydrogen production from these biomaterial sources.

According to the different sources of hydrogen production, the produced hydrogen can be classified into different categories from their origins, production methods, and the environmental impacts from the production methods. The different types of hydrogen are listed as shown.

- 1) Green hydrogen: hydrogen that is produced with renewable energy sources including wind, solar, hydroelectric power as an energy source of water electrolysis to hydrogen and oxygen. This is the most desirable type of hydrogen since there is almost zero or no carbon emissions which shows sustainability and is environmentally friendly.
- 2) Blue hydrogen: hydrogen that is produced from natural gas, which is mainly methane. The production process is either steam reforming or autothermal reforming. The product gas also consists of carbon dioxide gas, but the carbon capture and storage (CCS) system are installed. The efficiency of CCS system is the key element for the consideration of the degree of process's environmental friendliness. Therefore, the carbon footprint of the process could be reduced. With this combination of process and CCS system, it could be a transition towards a low-carbon hydrogen production (green hydrogen).

- 3) Gray hydrogen: this is a common hydrogen production process nowadays. The simple concept for understanding is “a blue hydrogen production without CCS system”. It still has a higher carbon emission to the atmosphere.
- 4) Brown hydrogen: coal or lignite are used as the traditional hydrogen production method. High amounts of CO<sub>2</sub> and CO are released into the atmosphere. According to the study of international energy agency (IEA), around a fifth of hydrogen was still produced by coal.
- 5) Yellow hydrogen: solar power has been utilized as a power source of electrolysis producing hydrogen. In some cases, yellow hydrogen refers to hydrogen from electrolysis that utilizes the mix of renewable and fossil fuel energy.
- 6) Pink hydrogen (or purple/red): the term for hydrogen production process that utilizes nuclear energy for water hydrolysis. Even though it is a very low carbon emission but the concerns and challenges of using nuclear is making this kind of hydrogen becomes more complicated.
- 7) Turquoise hydrogen: this is a special term for hydrogen production falling in between green and blue hydrogen, it is a method of utilizing pyrolysis of methane into hydrogen and solid carbon, with the carbon capture and storage system of the obtaining carbon black.
- 8) White hydrogen: this type of hydrogen is from nature which occurs from underground deposits. They can be accessed via well drilling. The example locations which have been exploring are Mali, Brazil, and Australia. The production cost is very cheap compared to gray hydrogen. It is considered as a carbon-free fuel, but the environmental concerns come from the extraction methods.

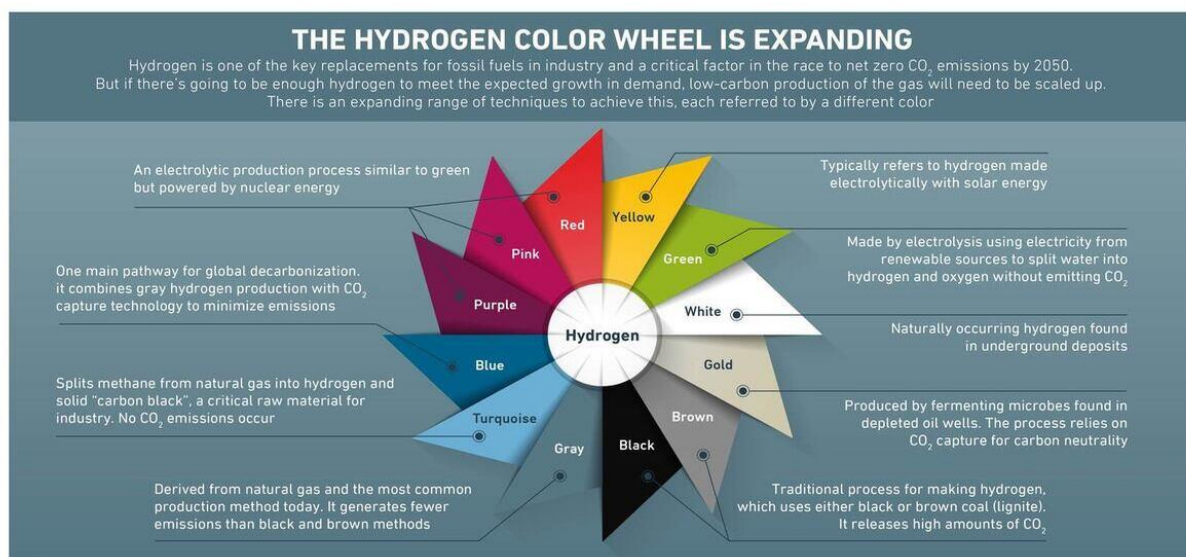


**Figure 1.2.** Classification of hydrogen according to their origins [11].

### 1.1.3. Types of Ethanol reforming

Ethanol could be reformed in various reactions and with different oxidizing agents. Ethanol reforming is the process to convert ethanol into hydrogen-rich gas. Each reforming process has its advantages and disadvantages in terms of process efficiency, product gas selectivity, operating condition, and equipment complexity. To select types of the process, several factors are considered, including the desired hydrogen yield, desired H<sub>2</sub>/CO (in case of syngas-aimed production), feedstocks availability, energy efficiency of the process, etc. Several types of ethanol reforming process can be listed as follows:

#### 1) Steam reforming (SR)

Steam reforming is a method of converting ethanol into hydrogen which is widely used. Ethanol is a reaction with high-temperature steam in the presence of catalyst to produce hydrogen, carbon monoxide and carbon dioxide. The process is normally carried out at high reaction temperatures of 700 – 1100 °C. A catalyst that is often used is a Ni-based catalyst.



#### 2) Partial oxidation (POX)

Partial oxidation is a reaction where ethanol is reacting with a limited amount of oxygen (O<sub>2</sub>) or air. The produced gas consists of hydrogen, carbon monoxide, and carbon dioxide. The reaction temperature is as high as 1200 – 1600 °C, and this reaction can be carried out in the presence or absence of a catalyst.



#### 3) Autothermal reforming (ATR)

Autothermal reforming is a combination of steam reforming and partial oxidation in which both steam and limited amount of oxygen are applied in the system yielded hydrogen, carbon monoxide, and carbon dioxide. It can be carried out at intermediate temperatures. The advantage is that this reaction provides better control of the hydrogen-to-carbon monoxide ratio (H<sub>2</sub>/CO) of the produced gas, which makes the product gas more compatible with the utilization of the produced syngas.



#### 4) Plasma reforming

Plasma reforming uses plasma (ionized gas) to dissociate ethanol into hydrogen and other gases as by-products. It provides high-energy conditions for ethanol molecules dissociation but relatively done at low temperatures. Ethanol is exposed to a high-temperature plasma, causing it to decompose into hydrogen, carbon monoxide, carbon dioxide, and other gases.

#### 5) Sorption-Enhanced Steam Reforming (SESR)

This type of ethanol reforming combines steam reforming with a sorbent material that captures carbon dioxide produced during the reaction. The advantage is that the reduction of carbon dioxide in the system makes equilibrium shift to the product side, therefore, the amount of hydrogen gas production is enhanced.

### **1.1.4. ESR in applications: Reaction process and reactors**

Ethanol steam reforming is a promising hydrogen production technology which can be used to serve for on-demanded hydrogen. Research and development are ongoing nowadays to improve its efficiency, reduce the costs of production and supported infrastructures, and integration with renewable energy sources as green hydrogen energy. It shows a great potential for the transition from fossil-based energy to hydrogen-based energy.

Considering the full process of catalytic reforming of bioethanol, the process is divided into three parts, upstream process which are the bioethanol production, ethanol steam reforming process which is the part of the reaction take place, and the final part of the downstream process which are including hydrogen purification and utilization. The full process as mentioned is illustrated in Figure 1.3.

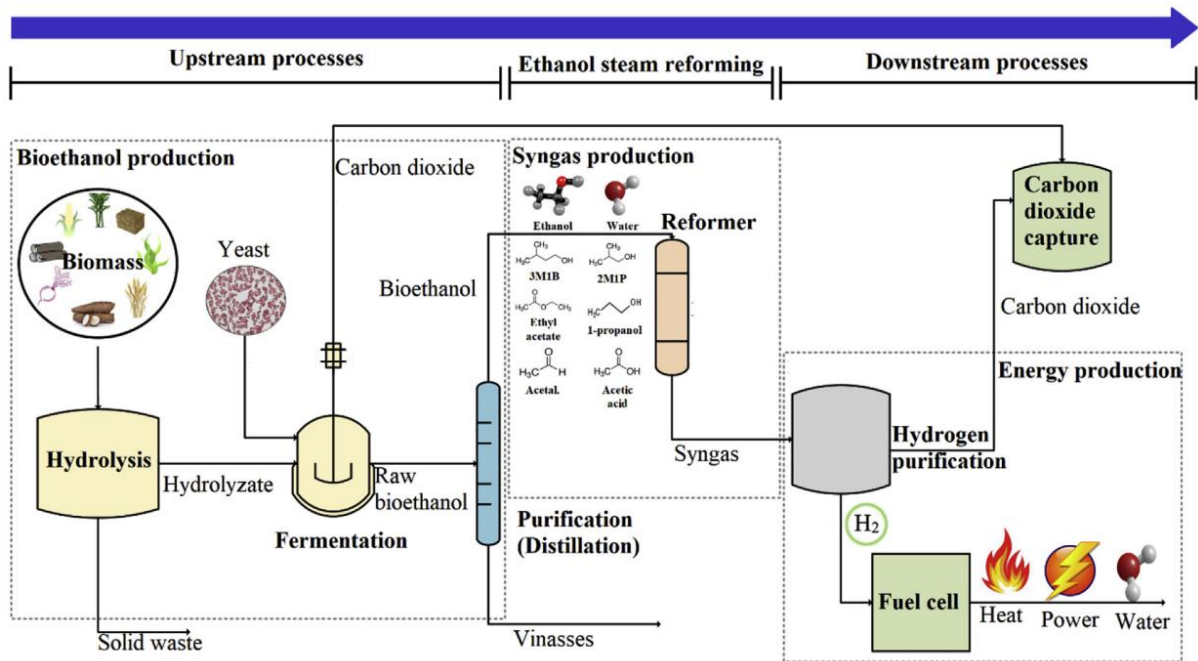


**Figure 1.3.** Overall process of catalytic conversion of bioethanol for hydrogen production [12].

There are several aspects of considering ethanol steam reforming as hydrogen production process to be a real application.

- 1) ESR reaction: it is the reaction that reacts ethanol with high-temperature steam in the presence of a catalyst to produce hydrogen, together with carbon monoxide, carbon dioxide, and possible by-products.
- 2) Catalyst: the material which is used to enhance the reaction rate and efficiency of ethanol steam reforming. Ni-based catalysts have been used in an application.
- 3) Operating conditions: the elevated temperature is typically used in the range of 700 – 1100 °C. The elevated pressure can also be utilized to drive the reaction forward. The exact operating conditions depend on the catalysts used and reactor design.
- 4) Reactor Design: various reactor configurations can be used for ESR, including fixed-bed reactors, fluidized bed reactors, and membrane reactors. The selection of reactor design and configuration depends on efficiency, catalyst compatibility, and scalability.
- 5) Desired product gas composition: product gas composition of ESR mainly consists of hydrogen, carbon monoxide, and carbon dioxide. The concentration of hydrogen produced can be varied by operating conditions and types of catalysts.
- 6) Purity of produced hydrogen: since the produced gas is a mixture of hydrogen, carbon monoxide, carbon dioxide, and possible by-products. To further utilize hydrogen or

syngas for specific processes, purification is required. Pressure swing adsorption (PSA) or membrane separation are commonly used for the purification process.

- 7) Application of the produced hydrogen: it can be utilized for various applications, including fuel cell vehicles, power generation through fuel cells, industrial processes, and as a feedstock for other chemical processes.
- 8) Integration with renewable energy: ethanol used as a reactant in ESR can be derived from renewable sources such as biomass or energy crops. It is aligning with sustainability. Integration of ESR with other types of renewable energy sources like solar or wind power for the energy provided in the production process can further enhance its sustainability.
- 9) Sustainability and environmental benefits: utilizing ethanol from renewable sources instead of the use of fossil fuel-based fuel for hydrogen production. It can significantly reduce greenhouse gas emissions, contributing to sustainable energy.

From overall aspects for consideration, the key elements of ethanol steam reforming reaction process are needed to be considered in more details, in order to realize the ESR in applications

1) Ethanol ( $C_2H_5OH$ ):

an alcohol biofuel which is commonly derived from renewable sources such as biomass, including sugarcane, corn, cassava, or cellulosic materials (through fermentation process). Usually, the crude bioethanol obtained from fermentation has an ethanol concentration of 4 – 12 vol%. Compared to the stoichiometric ratio of ethanol-to-water which is 1:3, the ratio of crude bioethanol falls between 1:25 to 1:77, a lot of water presence in a crude bioethanol. In the operating aspect, water evaporation or distillation as a cost of energy is required to prepare the proper feed for the reformer. In the aspect of transportation, the larger volume from water components makes the transportation to be more difficult, but it might not be a concern for on-site hydrogen production, which the transportation is excluded. If considering the utilization as blending additives in gasoline which required a pure ethanol, utilization of ethanol mixture with water in hydrogen production has a potential for energy supply.

There are several studies that try to study the feasibility of diluted bioethanol for hydrogen production, for example, Figure 1.4. Figure 1.5. Excess water favors the hydrogen production at lower temperature as shown in the simulation results. The

temperature could be lower by 300 – 350 °C in the utilization of crude bioethanol (without distillation) to obtain the same hydrogen yield as the utilization of 1:3 molar ratio of ethanol to water reforming. By the way, the increasing of steam-to-carbon increases the heat deficit of ethanol steam reforming [13]. The water separation from crude bioethanol seems indispensable at the presence study, therefore, the optimization between the cost of crude ethanol distillation and the lowering reaction temperature are needed to be verified to make the process feasibility.

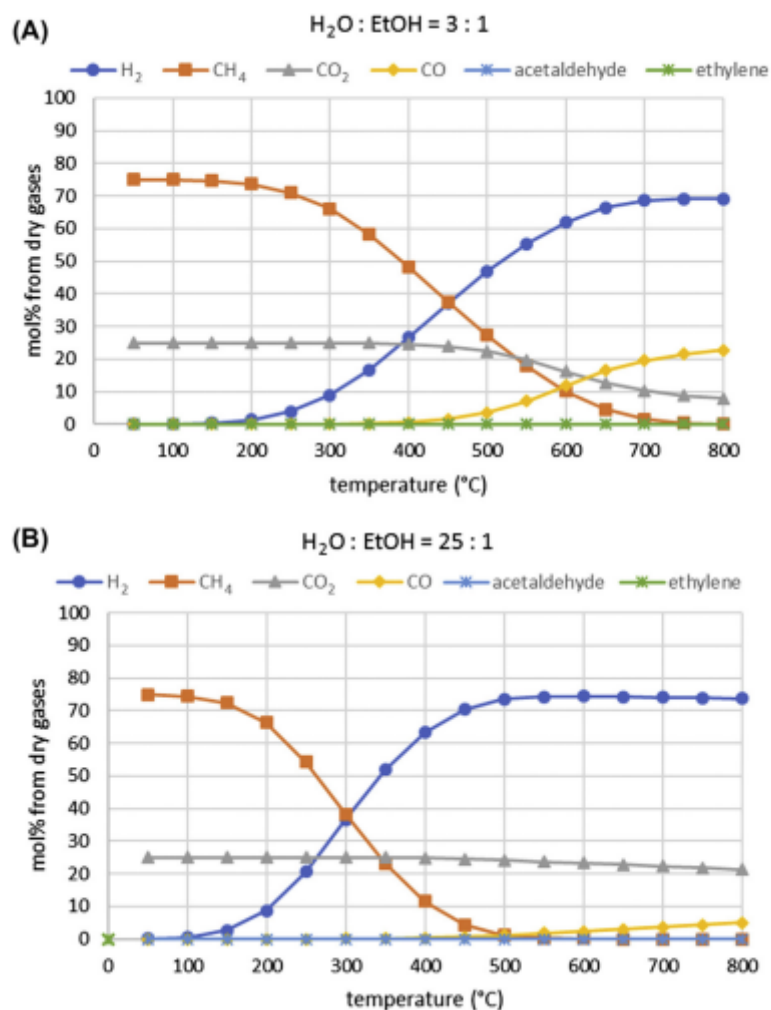


**Figure 1.4.** The ESR products concentration as obtained from thermodynamic analysis with 100 % ethanol conversion with different ethanol concentration in feed (A) stoichiometric ratio and (B) the ratio with similar proportion as presented in crude bioethanol [13].



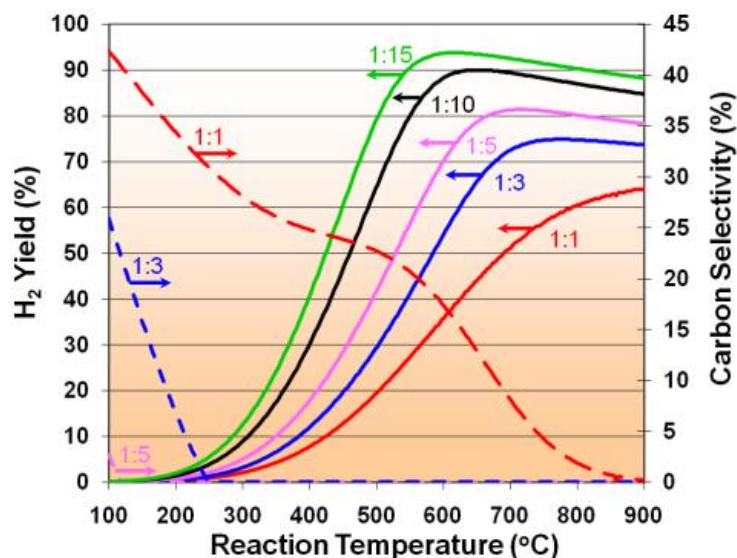


**Figure 1.5.** Effect of ethanol-to-water molar ratio on thermodynamic equilibrium of the products with no dilution [14].

Not only excess water, impurities from the fermentation reagents, bacteria, and various fermentation products are also presented in crude bioethanol. The non-complex method and low investment cost of separation can separate the inorganic compounds and fermentation bacteria. The remaining are the mixture of water, ethanol, several alcohols (C1, C3, and C4), aldehydes (C3 and C4), acetone, organic acids (acetic acid and lactic acid), amines, glycerol, and esters, which depends on the original source of fermentation. These impurities are organic substances that can engage in the catalytic reformation processes and potentially have both advantageous and detrimental effects on the reforming process. The beneficial aspect involves an augmented hydrogen output, whereas the main drawback is the accelerated deactivation of the catalyst caused by the accumulation of carbon. The presence of methanol increases the hydrogen yield from methanol reforming reaction. On the other hand, the presence of C3 and C4 alcohols leads to coke formation since they are not reforming but dehydrating to coke precursor. The presence of C3-amine and acetone deactivates the metal centers for reforming reaction, the high conversion is converted into the decomposition on the support instead. The presence of acetic acid, ethyl acetate, diethyl ether decreases the conversion and hydrogen yield due to coke formation. The presence of diethylamine and butanal increase ethanol conversion and hydrogen yield [13]. The purity of the ethanol feedstock is crucial to minimize impurities that could potentially affect catalyst performance or introduce unwanted reactions during the reforming process.

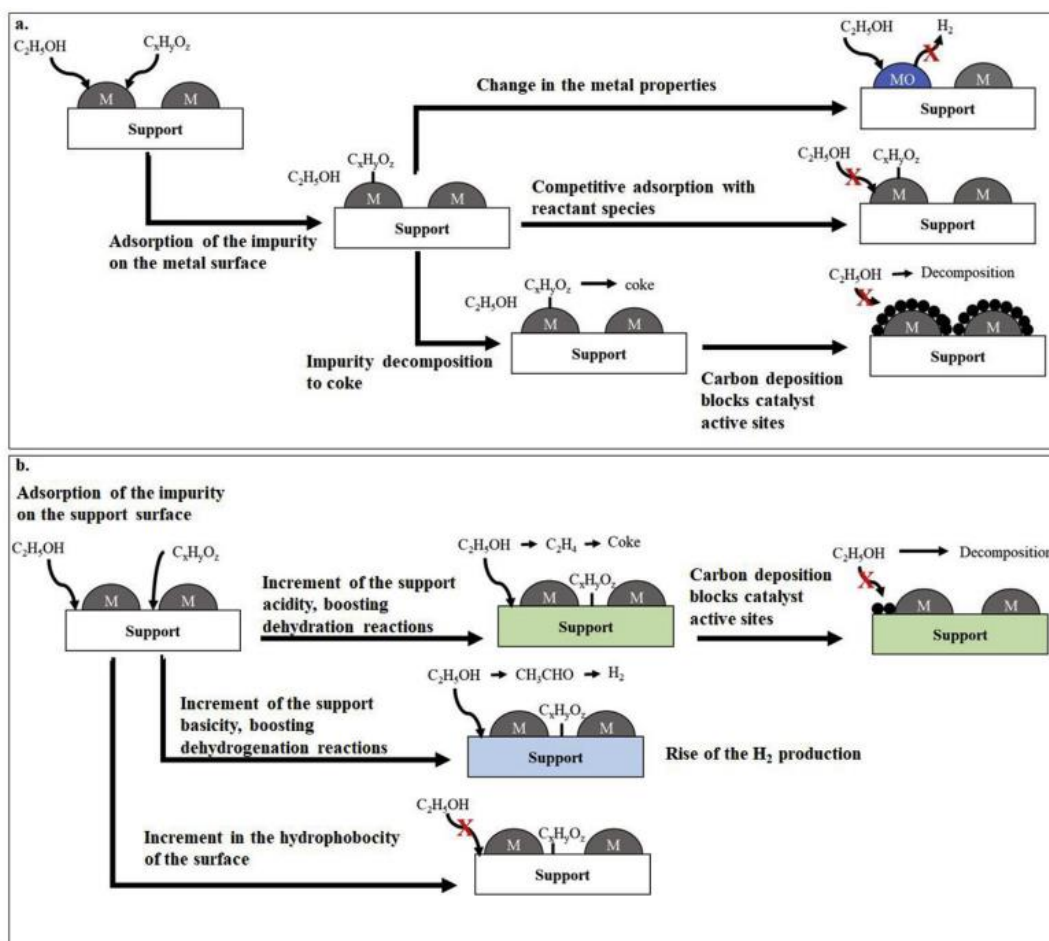


**Figure 1.6.** Effects of impurities in ESR: (a) associated with the active metal surface and (b) associated with the support surface [12].

| Impurity family  | Main components | Effect during ESR                                   | Produced during...                         | Strategy to control                        |
|------------------|-----------------|---|--|--|
| Alcohols         | Methanol        | Improve $H_2$ yield                                 | Fermentation/pectin degradation            | Pectin addition                            |
|                  | Glycerol        | Carbon deposits                                     | Fermentation/Glycolysis                    | Distillation                               |
|                  | Fusel alcohol   | Carbon deposits                                     | Fermentation/Amino acid biosynthesis       | $(NH_4)_2SO_4$ addition                    |
| Aldehydes        | Acetaldehyde    | Improve $H_2$ yield                                 | Glycolysis pathway                         | VHG fermentation                           |
|                  | Fusel aldehyde  |   | Ehrlich metabolic pathway                  | Metabolic engineering                      |
| Esters           | Ethyl acetate   | Carbon deposits                                     | Reaction between ethanol and acetic acid   | Low temperature<br>Pervaporation           |
| Carboxylic acids | Acetic acid     | Acidify the support.<br>Boost dehydration reactions | Lignocellulosic material decomposition     | Optimization<br>Distillation               |
| Sulfur compounds |                 |   | Acid hydrolysis when $H_2SO_4$ is employed | Use $HNO_3$ as catalyst                    |
| Amines           |                 | Increase support basicity                           | Decarboxylation of amino acid/amination    | Amino acid addition<br>Bacteria consortium |

**Figure 1.7.** Impurities in crude bioethanol: components, effects towards ESR reaction, the obtained products, and strategies to control their formation. (Yellow: increase in  $H_2$  yield; Orange: decrease in  $H_2$  yield; Gray: processes during fermentation; Green: processes during acid hydrolysis; Red: strategy thorough purification) [12]

## 2) Steam (H<sub>2</sub>O):

high temperature steam is introduced into the reaction system as one of the reactants. It provides the necessary oxygen for the reforming process, and also coke oxidation on the functioning catalyst. The most concern relating to steam is about the heat of vaporization of liquid water to steam, which requires a large amount of heat.

## 3) Catalyst:

As we know, the ESR reaction occurs at high reaction temperatures with the various side reaction pathways. With the help of using catalysts, the reaction is promoted towards the pathways with lower activation energy, and then easier to proceed. Catalysts enhance the breaking of chemical bonding in ethanol and water molecules to proceed steps of reaction yielding hydrogen and product gas. The steps of dissociation of ethanol and steam, allowing the rearrangement of atoms, and providing the ease of recombination to be hydrogen and carbon dioxide gas are crucial for ESR catalyst development and selection. The catalyst activity, stability, and resistance to deactivation are also required in consideration.

## 4) Reforming reaction and product formation:

the nature of reforming reaction is occurring on the catalyst surface. The reactants, ethanol and steam react, breakdown and recombine, into hydrogen and carbon dioxide (ideal/complete reaction). Hydrogen molecules (H<sub>2</sub>) are obtained from hydrogen in ethanol and water.

On the other hand, carbon dioxide comes from the carbon atom from ethanol and combining with oxygen atom from steam. Besides carbon dioxide as the complete/expected product, with the side reactions, carbon monoxide or other hydrocarbon or oxidative hydrocarbon species can be obtained, together with a coke formation. If consideration the ethanol steam reforming, the main purpose is hydrogen production. According to the reaction mechanism and pathway, the production of carbon monoxide can also be obtained. Normally, the H<sub>2</sub>/CO ratio obtained from ethanol steam reforming is relatively high due to the supply of H<sub>2</sub> from water in the reaction. Therefore, ESR condition can be adjusted to serve for syngas production, i.e., reduce the steam concentration in feed to reduce the hydrogen supply for the reformer, but this option is raised up the concern of heat utilization for water removal from crude bioethanol. Another way is to apply the proper purification and separation process that can utilize both pure hydrogens as renewable energy and the obtaining

syngas which is increased in  $H_2/CO$  ratio after the hydrogen separation, which become more suitable for syngas utilization at this stage.

Catalyst development is another strategy to achieve syngas with proper ratio for further utilization as low  $H_2/CO$  syngas. Mostly, the catalyst has been developed towards the highest hydrogen to feed fuel cell and improve selectivity towards water gas shift reaction converting  $CO$  to  $CO_2$ . The catalyst that has a property of maintaining or producing  $CO$  but not converting  $CO_2$  can be served for this purpose, limiting the activity towards WGS, for example the development of  $Ni/BEA$  zeolite by Rossetti et.,al. that they can obtain the  $H_2/CO = 2$  from ESR which are suitable for FT-reaction [15].

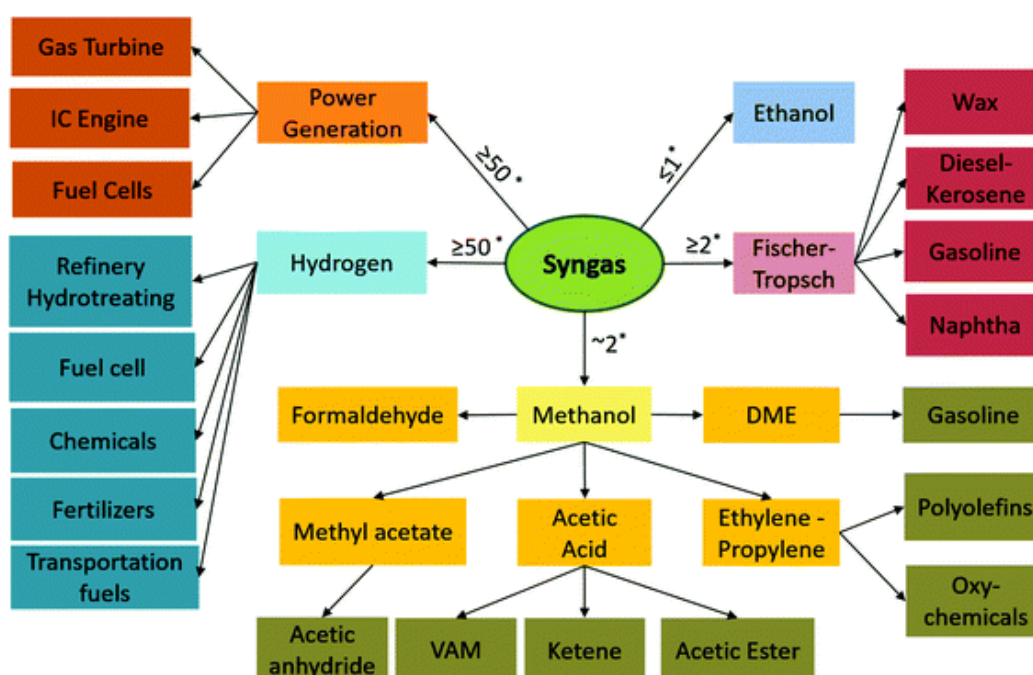


**Figure 1.8.** Syngas derivatives with reference to their composition (\* $H_2/CO$  molar ratio) [16].

The efficiency and selectivity of the reaction are also affected by operation temperature, operating condition, contact time (retention time), catalyst selection which affects catalyst activity and properties towards reactions. The parameter optimization is important to achieve the desired hydrogen yield with the minimization of undesirable byproducts.

- Temperature: The temperature plays a crucial role, as a significant influence on both the reaction rate and product selectivity. Elevated temperatures tend to accelerate the reaction speed, improve reactants conversion, and lower the coke formation for ESR but also raise the energy concerns. Low temperature is good in energy consideration,

but it is difficult to obtain a good reaction yield due to thermodynamic reasons and it is high in coke formation due to the reaction pathways producing C2 intermediates. It's crucial to pinpoint the ideal temperature range to maximize hydrogen production while keeping undesirable reactions at minimum as possible.

- Pressure: Pressure is a key factor impacting reaction speed and the composition of gases involved. Higher pressure can drive the equilibrium towards greater hydrogen output. Nevertheless, there exists an ideal pressure range where additional pressure may not significantly enhance hydrogen yield.
- Steam-to-carbon Ratio (S/C ratio): The proportion of steam ( $\text{H}_2\text{O}$ ) to ethanol ( $\text{C}_2\text{H}_5\text{OH}$ ) in the input influences the reforming procedure. It's important to optimize S/C ratio to transform ethanol into the expected products such as hydrogen and carbon dioxide. Excessive steam could result in an overproduction of  $\text{CO}_2$ .
- Residence Time: The duration that reactants spend inside the reactor impacts both the conversion level and the amount of hydrogen produced. This timeframe is shaped by the design of the reactor, flow rates, and dimensions. Attaining the right residence time is crucial for effective hydrogen production.
- Heat Management: Effective regulation and even distribution of thermal energy within the reactor are crucial for sustaining the intended temperature pattern. Skillful heat control contributes to attaining the ideal reaction temperature consistently across the catalyst bed.

The example of heat management and utilization within the system is the thermochemical recuperation (TCR), which is the system utilizing the waste heat from the exhausted gas to heat up the system for reforming to obtain the fuel with higher energy content, and then the obtaining fuel from reformer is utilized for process heating. The study of utilizing the TCR system in ethanol steam reforming mentioned that the maximum recovery (ratio of recuperated heat in TCR over exhaust heat) in the reformer is obtained at a steam-to-carbon ratio of 1. At the temperature of 900 K (approximately 627 °C), the system with steam-to-carbon ratio of 2 and 3, the gradually increase of recovery rate is still observed, but after this temperature, especially for the steam-to-carbon ratio of 3. The system with the temperature higher than 900K with higher steam-to-carbon ratio above 3 requires the supplied external heat [17].

Another example is the parameter optimization with heat integration system simulation study [18]. The study suggests the optimum operating pressure of 1 bar.

The optimum temperature of the moderate water-to-ethanol molar ratio 7.4:1 is about 755 °C. The heat integration by pinch technology heat exchanger network shows that the utilization of one heat-exchanger for heat integration can make the energy saving about 57.4% and can be further saved by the addition of another integration heat-exchanger.

Another concern of energy management in ESR is the regeneration of catalyst for coke removal, at least 700 °C [19], up to 1000 – 1200 °C [20] is required in coke combustion process. Figure 1.9. shows the coke oxidation temperature on the encapsulation catalyst in this study. To reduce this portion of energy consumption, the catalyst development for low carbon formation is indispensable.

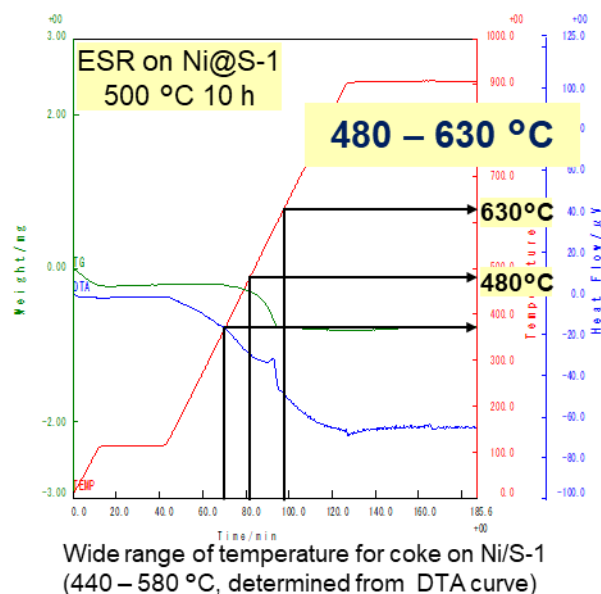


**Figure 1.9.** TGA and DTG curve of coke oxidation on Ni@Silicalite-1 in this study.

- Scale-up Considerations: When extending the application of the ESR process to an industrial scale, careful consideration of factors such as reactor size, heat and mass transfer, and overall system effectiveness is crucial to confirm the safety and efficiency for operations.
- Energy Efficiency and Sustainability: A detailed and careful assessment of process effectiveness and sustainability is also important. For example, evaluation of energy integration and various energy input and their source, evaluation of process components towards environmental impact, especially the source of process energy and effluent gas management.

- Safety: Safety measures, such as proper handling of flammable gases, reactor integrity, and emergency shutdown procedures, should be in place to ensure safe operation throughout the reaction process.

The reactor in the ESR process is the site where the catalytic reaction takes place, transforming ethanol into hydrogen, carbon monoxide, carbon dioxide, and other by-products. The good reactor design enhances the reaction in the operating condition to obtain hydrogen production efficiency. The reactor configuration may be varied based on application, targeted hydrogen yield, etc. Researchers and engineers put efforts to refine the reactor designs and processes, to improve efficiency, yield, and sustainability of ESR in real applications. In the context of ethanol steam reforming for hydrogen production. There are several key elements of ESR reactor to be considered as listed below.

- 1) Reactor Vessel: The reactor chamber serves as the primary containment where the ethanol steam reforming reaction occurs, offering a regulated setting for the reaction.
- 2) Catalyst Bed: The essential section within the reactor is the catalytic layer housing the catalyst material. Catalysts play crucial roles for facilitating the reaction, improving conversion and product selectivity, i.e., to hydrogen and carbon dioxide.
- 3) Heat Source: A heat source is required to maintain the necessary reaction temperature. This can be an external furnace or heating elements integrated into the reactor vessel.
- 4) Reactant Supply System:
  - a. Ethanol supply: an ethanol supply system ensures a steady and controlled flow of ethanol into the reactor.
  - b. Steam Supply: a system for supplying steam ( $H_2O$ ) is essential for the reaction, to initiate the reforming process.
- 5) Temperature and Pressure Controls: The reactor is outfitted with mechanisms to control and uphold the operating temperature and pressure within the designated range, aiming to optimize reaction kinetics.
- 6) Cooling System: In some reaction system, A cooling system could be implemented to manage any extra heat generated during the reaction, ensuring a controlled temperature inside the reactor.
- 7) Gas Collection and Purification System: The reactor is connected to a gas collection and purification system to collect the hydrogen-rich gas that is produced and separate it from any remaining reactants or byproducts to meet the utilization specification.

- 8) **Monitoring and Control Systems:** Monitoring and control systems, which encompass sensors, probes, and control units, are integrated to oversee diverse parameters like temperature, pressure, flow rates, and gas composition. By integrating these systems, safety and efficiency can be ensured during operation.
- 9) **Safety Measures:** Since the reaction system includes chemicals, high temperature, high pressure gas. Safety equipment and components, such as pressure relief valves, emergency shutdown systems and alarms are essential to ensure a safe operation and handle any unexpected events that might occur during operation.

There are some examples of reactor configuration suggestion for reforming of oxygenated hydrocarbon species, illustrated in Figure 1.10. for single reaction reactor, and Figure 1.11. for combined reforming.

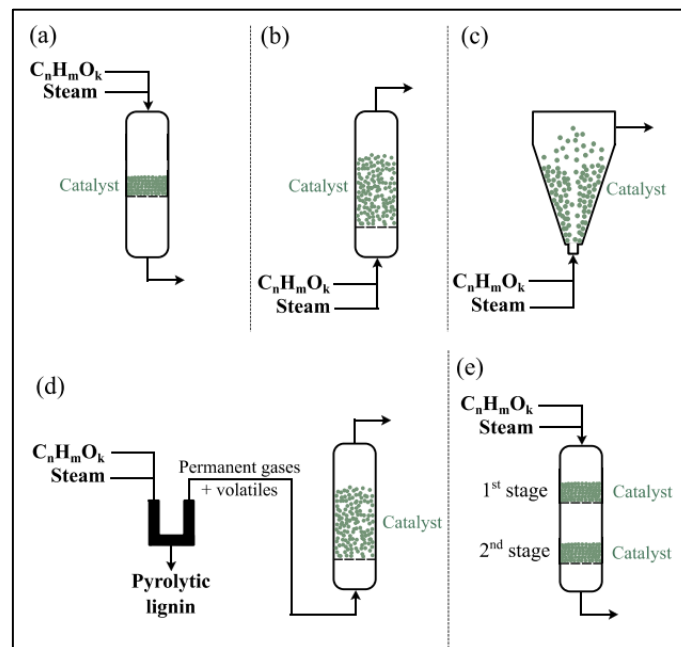


**Figure 1.10.** Reactor configurations for oxygenated biomass reforming [21].

There are possibilities of steam reforming to be combined with other types of hydrocarbon reforming to improve the product yield and selectivity. There are several reactor configurations summarized as in Figure 1.11.



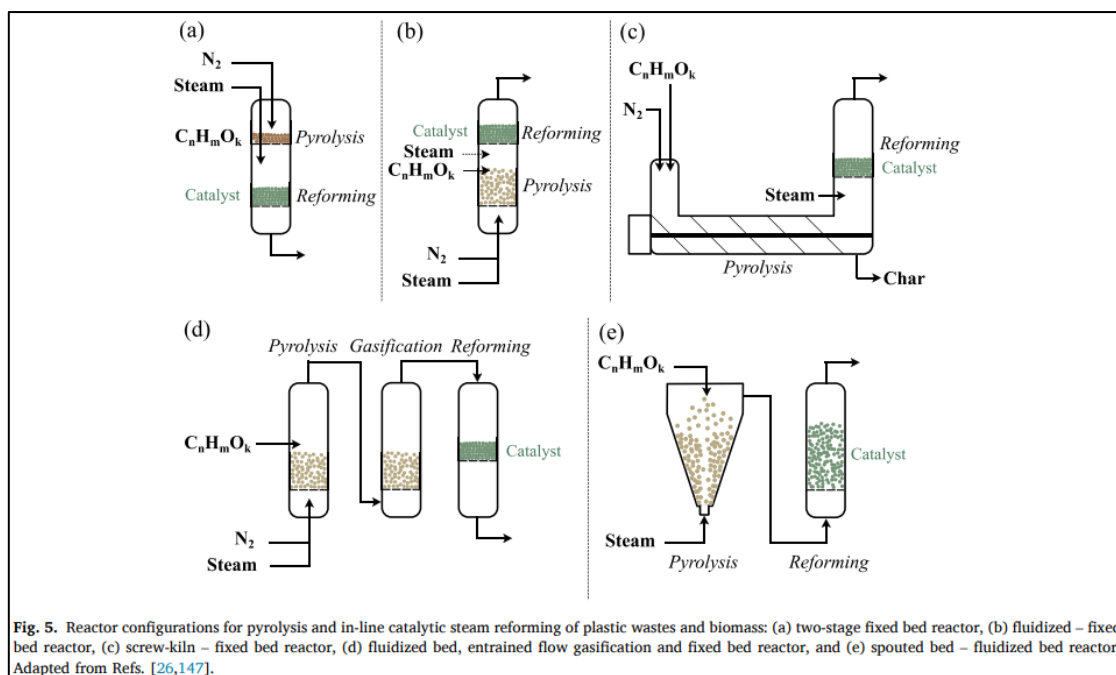


**Figure 1.11.** Reactor configurations for combined-oxygenated biomass reforming [21, 22].

In economics consideration, a major obstacle is the cost of the production process, together with the cost of the catalyst itself that utilizes the precious metals. According to the economic analysis studied in 2021 [23], it is found that among hydrogen production via ethanol steam reforming, dehydrogenation to ethyl acetate, and dehydrogenation to acetaldehyde, ethanol steam reforming required the lowest ethanol feed with the lowest fixed capital investment and manufacturing cost, which leads to the lowest cost of  $H_2$  production per kg (1.58 USD per kg  $H_2$ ). The challenge is the  $CO_2$  emission from the steam reforming process. The suggestion is to utilize those  $CO_2$  emission, for example, series the ethanol steam reforming with the methanol synthesis. The additional  $CO_2$  capture with steam reforming of ethanol increases the hydrogen manufacturing cost from 1.58 to 1.72 USD per kg. From this study, it is suggested that the dehydrogenation of ethanol into  $H_2$  and acetaldehyde exhibited the most promising potential when considering the cost competitiveness of  $H_2$  production compared to the steam reforming process. On the other hand, the dehydrogenation of ethanol into  $H_2$  and ethyl acetate was associated with the highest relative  $CO_2$  consumption among all the processes involved in  $H_2$  production and  $CO_2$  conversion into methanol.

## 1.2. Bio-ethanol reforming for hydrogen production

Scoping into this research which is the study of ethanol steam reforming reaction. Ethanol steam reforming is one of the thermochemical processes for hydrogen production. Standard reaction of ethanol steam reforming can be shown in Eq. (1.14). Bioethanol, the main reactant of this reaction, is a renewable source obtained from agricultural products or biomass residue fermentation. Consuming these materials and reducing fossil fuel consumption can help reduce the carbon footprint. Distillation might be done for concentrating the ethanol concentration and impurity separation. Moreover, bioethanol is a liquid fuel that is relatively easy to handle, transport, and store, due to its low toxicity.



Ethanol steam reforming has been selected for hydrogen production according to its renewable, environmentally friendly, non-toxic, and high energy content feedstocks as bioethanol. It is an option for lowering the carbon footprint of the hydrogen production process. It has been reported as the reaction that provides the highest amount of hydrogen production per mol of reactant (ethanol) [24]. It also has a potential in development since it can be compatible with the existing steam reforming reaction of other hydrocarbons, also the integration with an existing ethanol production for alongside hydrogen production without transportation of ethanol.

Apart from the advantages of ethanol steam reforming for hydrogen production, it also has some limitations. For the reactants, ethanol and water, feedstock availability and competition since the bioethanol production are relying on crops which could be affected by the weather and climate changes. Some of them are human foods, therefore, it may affect food safety if utilizing large amounts for ethanol production. The process requires steam as a reactant, the production plant may not be applicable in the area that faces water scarcity. The reaction itself required a high operating temperature. Without catalyst, the spontaneous reaction is occurred at 1000 – 1200 °C. and this could lead to an extreme energy supply of the process. The reaction itself produces carbon dioxide and carbon monoxide, which are greenhouse gases and raises the overall carbon footprint of the production process. These two concern contrasts to the goal of renewable energy. Therefore, research and development has been investigating to lower the operating temperature together with increase hydrogen yield through the use of catalysts but the impurity in ethanol feedstock such as sulfur could lead to catalyst poisoning. The additional process of ethanol purification or further developed catalyst to resist poisoning is required. Coke formation and catalyst degradation are the

drawbacks of catalyst development that scientists and engineers are trying to overcome. The carbonaceous species deposited on the catalyst surface affects the catalytic activity, stability, and can be a severe problem from temperature runaway and explosion if the formation is too high and porosity of catalyst material is completely destroyed. Therefore, the goal of the catalyst development is to enhance the reaction activity in a low reaction temperature, lower the coke formation, improve the tolerance toward impurities, and make the steam reforming of bioethanol to be a practical hydrogen production.

### 1.2.1. Ethanol reforming reaction pathways

Ethanol steam reforming (ESR) is a kind of thermochemical process to produce hydrogen. It involves the reaction of ethanol ( $C_2H_5OH$ ) and steam ( $H_2O$ ) at elevated reaction temperature. The product gases include hydrogen, carbon monoxide, and carbon dioxide, with some possible by-products. The overall equation is shown in Eq. (1.15).

Ethanol Steam Reforming:



Ethanol Decomposition:



Methane Steam Reforming:



Water-Gas shift reaction:



The reaction involved in the reaction system can be described in several steps, including ethanol decomposition, steam reforming, and water-gas shift reaction as shown above. Besides these proposed steps of reaction, there are a lot of possible reaction pathways which can occur due to the nature of reactant itself that consist of two carbon atoms, dissociation or combination of C-C bonds can occur during the reaction. The types of catalyst (active metal and type of supports) used and reaction conditions (operating temperature, reactants compositions, residence time, etc. can influence the product selectivity through enchanting of difference reaction pathways. The possible pathways and reaction mechanisms have been proposed by a lot of researchers [25–31] and can be summarized and mentioned in detail in section 3.1.

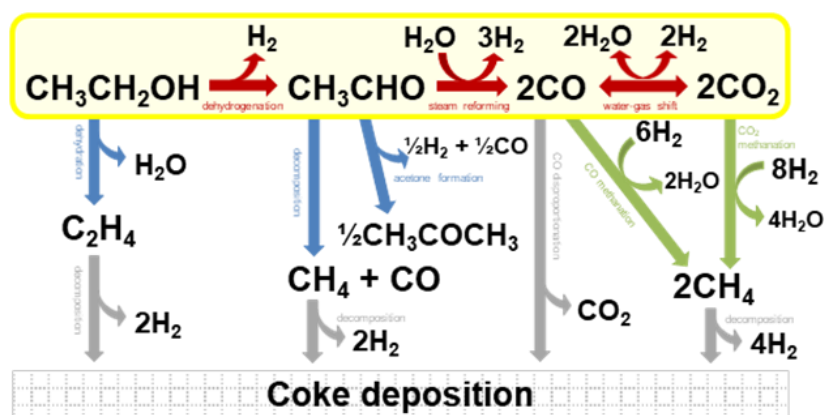


**Figure 1.12.** Reaction pathway of Ni catalyst [32].

### 1.2.2. Catalyst for ethanol steam reforming (ESR)

Numerous researchers have explored catalytic enhanced steam reforming (ESR) utilizing different catalysts in order to enhance feasibility and achieve the desired product selectivity for hydrogen energy production. The presence of a catalyst is essential as it helps reduce the reaction temperature, improving the conversion of both ethanol and water, and maximizing the yield and specificity of hydrogen. Catalysts effectively minimize the formation of undesirable intermediate compounds and lower carbon deposition, which lowers the chance of catalyst deactivation. The goal of ESR catalyst development is to achieve or fulfill those expected properties and be able to utilize the material in a real application. Various catalysts have been studied for ethanol steam reforming, utilizing various active metals, support materials, and promoters.

Active species for ESR catalysts have a duty to dissociate C-C bonds in ethanol. The enhanced activity of C-C bonds dissociation led to the easier reaction, i.e., lower the reaction temperature. Both noble and non-noble metals have been investigated. The noble metals show an excellent catalytic activity, which includes Rh, Ru, Pd, and Pt. Among these, Rhodium (Rh) has been identified as the most effective active metal for ESR. However, their high cost and limited availability make them less preferable. The chosen non-noble active metals for various studies include Ir, Cu, Co, and Ni [28, 33, 34]. These selections depend on the factors like cost-effectiveness, availability, and catalytic activities.

There are various support types which have been studied in ethanol steam reforming (ESR), including metal oxides, mixed metal oxides, hydrotalcites, zeolite, spinel, and perovskite. Among these, metal oxides like  $\text{Al}_2\text{O}_3$ ,  $\text{CeO}_2$ ,  $\text{ZrO}_2$ , and  $\text{MgO}$  have been mostly investigated as key supports. The choice of support significantly impacts the catalytic activity

and stability of the catalysts by stabilizing the metal active sites on the catalyst surface. Additionally, the support influences critical factors which affect the reaction mechanism. The factors include crystallite size of active metals, reducibility, electronic structure, metal-support interaction, and intermediates during ethanol conversion, consequently, influence hydrogen yield, the reaction pathway, and the deactivation due to carbon formation.

The deactivation, which is the gradual loss of catalytic activity over reaction time of ethanol steam reforming catalysts is contributed by several factors.

- 1) Carbon deposition: the primary cause of ESR catalyst deactivation. The carbon from several pathways is accumulated, blocking the active sites' accessibility, and hindering the catalytic activity of the catalyst. It is caused by the presence of coke precursor in the reaction media, which could be controlled by the catalytic activity of the catalyst and operating condition.
- 2) Sintering: the active metal is migrated and agglomerated to a large active site. In this case, the active surface area for a catalytic function is reduced, therefore, the catalytic activity of the catalyst is reduced. It is caused by the high operating temperature with the catalyst that has low sintering resistance properties.
- 3) Poisoning: impurities and contamination from the feedstock or within the system can adsorb on the active sites and inhibit the catalytic activity.
- 4) Oxidation and corrosion: High reaction temperatures together with a high level of reactive species, especially, the unbalanced oxidizing agent or reactive species in the reaction media can caused the oxidation of active sites and also corrosion.
- 5) Thermal degradation: high reaction temperatures and repetitive heating and cooling cycles can induce strain on the catalyst's structure, resulting in changing in its structure and reduced catalytic activity.

To make a high and stable catalytic activity at a specific level, various approaches in catalyst development have been studied and explored, including the study of various support materials, introducing dopants and/or promoters, and a range of preparation techniques to adjust the interaction between the metal and the support.

### **1.2.3. Ni-based catalyst for ESR: support and preparation techniques**

Various kinds of non-noble metals have been investigated in ESR due to its reliability in practical applications. The utilization of Ni-based catalysts in ESR is notable, as they are non-precious active metals chosen for their effectiveness, ready availability, cost-effectiveness, and thermal resilience at elevated temperatures. Ni exhibits the highest activity

among non-noble metals for ESR [34]. It exhibits significant proficiency in breaking C-C bonds and reforming CH<sub>4</sub> into syngas (CO and H<sub>2</sub>) [27]. Nevertheless, achieving robust catalytic activity necessitates elevated reaction temperatures (around 700–800 °C) to match the production levels achievable without a catalyst. Carbon deposition, a substantial challenge with Ni-based catalysts, results in catalyst deactivation. Hence, advancing Ni catalysts to achieve optimal metal dispersion, resistance to sintering, and minimized carbon formation under varying reaction conditions is imperative.

Extensive research has been conducted to explore a variety of supporting materials for catalysts with the goal of achieving Ni catalysts featuring finely dispersed, minute Ni particles. This aspect is vital because the size of the Ni particles holds significant importance in regulating activity, selectivity, and the tendency for carbon deposition. For Ni catalysts, diverse supports have been under investigation, including pure supports of Al<sub>2</sub>O<sub>3</sub>, SiO<sub>2</sub>, and CeO<sub>2</sub>, doped metal oxides support as doped-Al<sub>2</sub>O<sub>3</sub>, doped-SiO<sub>2</sub>, doped-CeO<sub>2</sub>, Sn-La<sub>2</sub>O<sub>3</sub>, K-ZrO<sub>2</sub>, MgAl<sub>2</sub>O<sub>4</sub>, Ce-MgAl<sub>2</sub>O<sub>4</sub>, zeolite (ZSM-5 and BEA), mesoporous silica (SBA-15), composite oxide materials such as perovskite and graphenedrotaelite, Ni-Mg-Al oxyhydride, as well as structured-carbon like activated carbon, carbon nanotubes, and graphene.

Zeolite is an attractive support material for ESR, from its high surface area and porosity which can enhance the interaction between the catalyst and reactants [35]. It provides thermal stability for the catalysts which are in a high reaction temperature. Zeolite has a well-defined pore structure that can selectively adsorb and accommodate smaller molecules, aiding in the separation and activation of reactant molecules like ethanol and water, as molecular sieve. Its acidic nature can help facilitate dehydrogenation and dehydration reactions, but too high acidity catalyst could lead to a high coke formation. In investigations utilizing zeolite supports for ESR, significant obstacles include the sintering of metals and the loss of the porous structure due to dealumination during reaction testing, ultimately leading to deactivation [36, 37]. Therefore, Silicalite-1, which is an MFI-type zeolite with pure silica composition in the structure, no aluminum atom as in traditional zeolite, is selected to avoid the effect of alumina and strong acidity towards ESR reaction.

The Ni-based catalysts, also Ni-zeolites catalyst in different preparation techniques used in the previous studies for ESR are summarized in Table 1.1.

**Table 1.1.** List of Ni-based catalysts for ethanol-steam reforming reaction (ESR) with reaction conditions [38].

| Catalyst                          | Catalyst Preparation Method | Reaction Condition |                |                                 | Ethanol Conversion (%) | Hydrogen Production (%) | Remark                                    | Ref. |
|-----------------------------------|-----------------------------|--------------------|----------------|---------------------------------|------------------------|-------------------------|---|------|
|                                   |                             | Temperature (°C)   | Pressure (atm) | H <sub>2</sub> O: Ethanol Ratio |                        |                         |   |      |
| 20 wt.% Ni/CeO <sub>2</sub>       | incipient wet impregnation  | 400–800            | 1              | 3.0                             | 90–100                 | 55–70                   | fixed bed U-shaped quartz tubular reactor | [28] |
| 10Ni/CeO <sub>2</sub>             | wet impregnation            | 300                | 1              | 3.0                             | 89                     | 25                      | Diluted condition                         | [39] |
| 20Ni/CeO <sub>2</sub>             |                             |                    |                |                                 | 80                     | 23                      |   |      |
| 3Pt/10Ni/CeO <sub>2</sub>         |                             |                    |                |                                 | 100                    | 43                      |   |      |
| 10Ni/3Pt/CeO <sub>2</sub>         |                             |                    |                |                                 | 100                    | 42                      |   |      |
| 3Pt-10Ni/CeO <sub>2</sub>         | coprecipitation             |                    |                |                                 | 100                    | 45                      |   |      |
| Ni/Al <sub>2</sub> O <sub>3</sub> | Impregnation                | 250 – 550          | 1              | 6.0                             | 100                    | ≤ 10                    | Ni loading is fixed at 10 wt %.           | [40] |
| Ni/Fe <sub>2</sub> O <sub>4</sub> | Citric Acid Complex Method  |                    |                |                                 | at 400 °C              | 0-40                    |   |      |
| Ni/Al <sub>2</sub> O <sub>4</sub> |                             |                    |                |                                 | 100                    | 0-41                    |   |      |
| Ni/Mn <sub>2</sub> O <sub>4</sub> |                             |                    |                |                                 | at 450 °C              | 0-30                    |   |      |

| Catalyst                                      | Catalyst Preparation Method                      | Reaction Condition |                |                                 | Ethanol Conversion (%) | Hydrogen Production (%) | Remark   | Ref. |
|---|--|--------------------|----------------|---------------------------------|------------------------|-------------------------|--|------|
|   |  | Temperature (°C)   | Pressure (atm) | H <sub>2</sub> O: Ethanol Ratio |                        |                         |  |      |
| 17.4Ni/Al <sub>2</sub> O <sub>3</sub>         | wet impregnation                                 | 400 / 550          | 1              | 3.0                             | 25–35                  | 5                       | quartz fixed-bed reactor                                       | [41] |
| 100   |  |                    |                |                                 | 15–20                  |                         |  |      |
| 10  |  |                    |                |                                 | 65–70                  |                         |  |      |
| 70–95   |  |                    |                |                                 | 45                     |                         |  |      |
| 8Ni/MgO                                       | wet impregnation                                 | 400 / 550          | 1              | 3.0                             | 80–95                  | 30–35                   | quartz fixed-bed reactor                                       | [41] |
| 100   |  |                    |                |                                 | 55                     |                         |  |      |
| 11.9Ni/SiO <sub>2</sub>                       |  |                    |                |                                 | 15–30                  | 30                      |  |      |
| 70–80   |  |                    |                |                                 | 35–40                  |                         |  |      |
| 11.8Ni/ZnO                                    | co-precipitation (support) wet impregnation (Ni) | 400–700            | 1              | 9.0                             | 90                     | 3 mol / mol             | Oxidative steam reforming ** stainless steel fixed-bed reactor | [42] |
| 15% Ni/CeO <sub>2</sub> -ZrO <sub>2</sub>     |  |                    |                |                                 | 91                     | 3.2 mol / mol           |  |      |
| 20% Ni/CeO <sub>2</sub> -ZrO <sub>2</sub>     |  |                    |                |                                 | 95                     | 3.5 mol / mol           |  |      |
| 30% Ni/CeO <sub>2</sub> -ZrO <sub>2</sub>     |  |                    |                |                                 | 100                    | 4.6 mol / mol           |  |      |
| 1%Rh-30%Ni/CeO <sub>2</sub> -ZrO <sub>2</sub> | impregnation                                     | 500                | 1              | 3.0                             | 99                     | 1.05 mol / mol          | 150 mg of catalyst fixed bed reactor (quartz)                  | [24] |
| 5Ni/Al(I)                                     |  |                    |                |                                 | 98                     | 1.32 mol / mol          |  |      |
| 5Ni/5Sr/Al(I)                                 |  |                    |                |                                 | 99                     | 1.11 mol / mol          |  |      |
| 5Ni/Al(C)                                     |  |                    |                |                                 | 89                     | 1.27 mol / mol          |  |      |
| 5Ni/5Sr/Al(C)                                 | co-precipitation                                 |                    |                |                                 |                        |                         |  |      |



| Catalyst                            | Catalyst Preparation Method                  | Reaction Condition |                |                                 | Ethanol Conversion (%) | Hydrogen Production (%) | Remark  | Ref. |
|-------------------------------------|--|--------------------|----------------|---------------------------------|------------------------|-------------------------|---|------|
|                                     |  | Temperature (°C)   | Pressure (atm) | H <sub>2</sub> O: Ethanol Ratio |                        |                         |   |      |
| 10Ni/Al                             | Sol-gel (support) dry impregnation (Ni)      | 600                | 1              | 3.0<br>6.0<br>10.0              | 100                    | 4.68–5.36               | 0.05 g catalyst diluted with 0.8 g of quartz                                    | [43] |
| 10Ni/Al-5Y                          |  |                    |                |                                 |                        | 4.69–5.20               |   |      |
| 10Ni/Al-10Y                         |  |                    |                |                                 |                        | 4.69–5.13               |   |      |
| 10Ni/Al-15Y                         |  |                    |                |                                 |                        | 5.04–5.55               |   |      |
| 20Ni/Al <sub>2</sub> O <sub>3</sub> | co-precipitation (support) Impregnation (Ni) | 300–500            | 1              | 13.0                            | 82–100                 | 22.5–27.0               | fixed bed micro-U-type stainless-steel flow reactor<br>0.15 g of fresh catalyst | [44] |
| 20Ni/Y <sub>2</sub> O <sub>3</sub>  |  |                    |                |                                 | 8–100                  | 30.0–37.0               |   |      |
| 20Ni/2Y-1Al                         |  |                    |                |                                 | 42–100                 | 27.0–35.5               |   |      |
| 20Ni/1Y-1Al                         |  |                    |                |                                 | 59–100                 | 29.5–36.0               |   |      |
| 20Ni/1Y-2Al                         |  |                    |                |                                 | 50–100                 | 26.5–33.0               |   |      |

There are four strategies to improve catalytic activity, provide metal sintering resistance, suppress the formation of coke precursors from side reactions, promote coke precursor removal reaction and lead to coke suppression.

- 1) Utilizing a support or promoter with basic properties: Ethylene typically originates from ethanol dehydration on a catalyst acidic site. Using a support or promoter with basic characteristics led to a reduction in acidity, reduction of ethylene, consequently, reduce coke formation.
- 2) Utilizing a support or promoter with redox activity: Metal oxides that display redox activity, such as  $\text{CeO}_2$ , known for their high oxygen mobility and storage capacity, can directly participate in the oxidation of coke and/or adsorbed coke precursors.
- 3) Fine-tuning particle size and oxidation state of the active metal: the highly dispersed small metal particles are advantageous for creating a coke-resistant active site. Particularly, coke formation occurs at metal terrace sites with high coordinate number. Having a small metal particle, the ratio of metal atom at terrace side decreased, therefore, coke formation decreased. Oxidation states of active metal affect the activity towards ethanol reforming and coke oxidation, for example, highly active and stable Co-based catalysts usually contain both metallic  $\text{Co}^0$  and  $\text{Co}^{2+}$  species and  $\text{Co}^{2+}$  could help in coke oxidation.
- 4) Bi- or Tri-metallic active metal: some metal provides benefits while staying adjacent to another metal for their redox properties. The addition of Cu, Co, or Au helps in water-gas shift reaction, reduce the formation of CO and coke formation from CO pathway. The addition of Fe helps in coke and  $\text{CH}_x$  gasification which benefits catalyst stability and coke suppression.

Various preparation methods, Ni precursors, and incorporation of dopants and/or promoters, have been studied to alter metal-support interaction [45, 46]. The catalyst preparation step can be generally separated into two parts, including the preparation of support materials and impregnation or deposition of active components. For support preparation, they are prepared by hydrothermal synthesis, sol-gel process, or precipitation. Subsequently, the active component is embedded in the catalyst via conventional methods of catalyst preparation, including impregnation, incipient wetness impregnation, precipitation, ion exchange, or deposition-precipitation. The development of ESR catalysts can be played with preparation steps, parameters in preparation, and techniques to achieve the goal of catalyst preparation as mentioned. The appropriate preparation methods and/or a suitable

catalyst support can be employed to govern the particle size and oxidation state of the active metal.

#### **1.2.4. Encapsulation structure of metal nanoparticles**

Encapsulation structure is the catalyst structure where metal particles are embedded or enclosed within a matrix or support material. This preparation technique can enhance the catalytic activity, selectivity, and stability of metal nanoparticles in various catalytic reactions. The general procedure of encapsulation starts with choosing the type of metal nanoparticles and the type of encapsulation material. After that, the metal nanoparticles are synthesized using chemical reduction, sol-gel preparation, or other techniques to obtain the well-dispersed particles with the specific size. The encapsulating material with stable and porous properties are also synthesized using a sol-gel, co-precipitation, hydrothermal synthesis, etc. Next, is the step that the metal nanoparticles incorporate with the prepared matrix or support using impregnation, deposition, or mixing. The final stage is the encapsulation process where the metal nanoparticles are covered and secured within the matrix. Techniques include calcination, deposition, or coating with additional layers.

The encapsulation of metal nanoparticles is a promising solution for ESR catalyst development since it provides several advantages towards catalytic reaction. The stabilized and maintained small size of metal nanoparticles function nicely in the catalytic reaction, i.e., they have sintering resistance properties, high dispersion, and active surface area for reaction. Reaction selectivity is enhanced due to the suppression of side reactions that produced the unwanted products, and this advantage is outgrowth of the encapsulation structure. Moreover, the encapsulation structure can help prevent catalyst deactivation. The encapsulation layer acts as a barrier protecting the metal particles from contamination or unwanted intermediates in the reaction media that reduce the catalytic activity.

There are several studies that mentioned the advantages of encapsulation structures toward hydrocarbon reforming reactions. In dry reforming of methane (DRM) reaction, yolk-shell structure of Ni-yolk@Ni@SiO<sub>2</sub> nanocomposite shows the advantages in the reaction. The encapsulation structure that traps the Ni metal inside exhibits higher catalytic activity than the Ni/SiO<sub>2</sub>@SiO<sub>2</sub> catalyst. The characterization results show the formation of Ni-phyllsilicate at the interface between Ni and SiO<sub>2</sub> that provides the strong interaction. After the decomposition of these Ni-phyllsilicate, the high dispersion of metal is obtained. But the value of specific surface area and Ni exposure is still considered as low for industrial use in lower reaction temperatures than 800 °C. Pretreatment with some reagents in a suitable

period of time can increase the surface exposure of Ni. The preparation method as hydrothermal treatment can increase the Ni accessibility. Moreover, the encapsulation structure that is a method to embed metal inside a highly crystalline structure could limit the space for coke formation [45, 47].

For the part of coke formation, there are several studies mentioned about the size of Ni nanoparticles that affect the coke formation behavior. For the case of Ni-alumina aero gel catalyst for dry reforming of methane, the Ni particle size less than 7 nm can prevent the severe coke formation from filamentous carbon [48].

With those ideas, our laboratory has been developing the encapsulation catalyst for DRM with the name of birdcage-type zeolite catalyst. The encapsulation of Pt nanoparticles in Silicalite-1 (Pt@Silicalite-1) was prepared with the preparation of amorphous-silica-coated metal NPs (Pt-SiO<sub>2</sub>) and nanocrystalline zeolite using a water-in-oil microemulsion. The encapsulated Pt NPs were found in the diameter less than 2 nm and well dispersed in the catalyst particles. By comparison to impregnation catalyst (Pt/Silicalite-1), the encapsulation catalyst exhibited a higher catalytic activity of DRM at 620 °C and provided a better stability over 24 h time on stream. But at the higher reaction temperature of 670 °C, severe deactivation occurred due to the collapse of zeolite structure. The collapse of catalyst structure led to the sintering of Pt NPs, then the deactivation proceeded. In this study, it is clear that the encapsulation structure inhibits sintering, but the thermal stability of zeolite, i.e., how strong of the protection matrix and divider between NPs, is the key factor in providing stability of the catalyst.

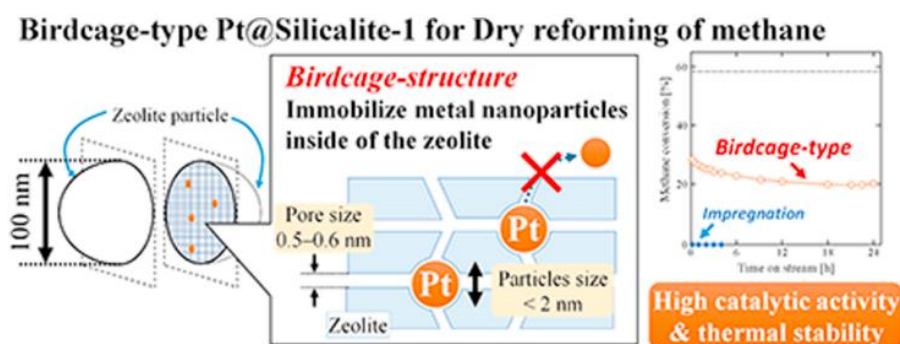


**Figure 1.13.** Birdcage-type Pt@Silicalite-1 for DRM [49].

In the next study [50], the encapsulation structure was studied with non-noble metal, Ni, in DRM reaction. The Ni encapsulated in Silicalite-1 (Ni@Silicalite-1) was synthesized by two-step method, including the Ni precursor prepared by microemulsion technique, obtained as an amorphous silica-encapsulated Ni-oxide nanoparticles (NiO<sub>x</sub>@SiO<sub>2</sub>). The precursor, uncalcined, was further used in hydrothermal synthesis for zeolite formation with

TPAOH and TEOS. It was found that, Ni-phyllsilicate structure was formed inside zeolite during hydrothermal synthesis and remains after calcination. After reduction, Ni-phyllsilicate decomposed into Ni metal active sites, which was highly dispersed, on the catalyst with the size of 4.5 nm. Both Ni@Silicalite-1 and Ni@SiO<sub>2</sub> precursor exhibited high and stable activity for DRM at 600 °C with negligible coke formation. The coke formation was slightly lower for Ni@Silicalite-1 (6.6 mg C/g cat). On the other hand, severe coke formation was found on impregnation catalyst (532 mg C/g cat). In thermal stability test at 850 °C 5 h, Ni@Silicalite-1 maintained its activity but the Ni@SiO<sub>2</sub> showed the decreasing activity due to the collapse of SiO<sub>2</sub> pore structures. In conclusion, Ni@Silicalite-1 for DRM showed a good performance in catalytic activity and stability, high sintering, and structure resistance towards an extreme condition as high reaction temperatures. It also provided coke formation resistance due to the encapsulation structure that protects the metal particle and does not let the coke form on their active metal surface.

Our recent study of the development of Ni@Silicalite-1 is the study on Silicalite-1 encapsulated Ni catalyst from Ni phyllosilicate for DRM by Zhang et al. [51]. The encapsulation catalysts prepared with Ni-PS precursors show an extremely low coke formation at 0.5 wt. % from DRM test at 600 °C 5 hours. In stability test at 850 °C for 24 hours, it exhibits high catalytic activity in a stable manner while maintaining the small size of Ni nanoparticle size of less than 7 nm in the reaction test. Compared to the conventional impregnation catalyst, the Ni/Silicalite-1 shows extremely high coke content at 40.9 wt.%. In this study, it is clear that utilizing an encapsulation structure for Ni-based catalyst in hydrocarbon reforming reaction can help reduce coke formation, which is the major drawback of this Ni catalyst utilization.

Ni@Silicalite-1 displays remarkable performance in DRM while effectively suppressing coke formation, Ni@Silicalite-1 could be an interesting option for ESR. The reaction mechanisms in both DRM and ESR involve similar reactions, like the oxidation of hydrocarbon species and the water-gas shift reaction. However, differences arise in the steps related to reactants, their activation, and the cleavage of C-C bonds. Furthermore, ESR carries a higher risk of coke formation due to a greater abundance of carbon species, allowing for a more extensive array of reaction pathways compared to DRM. Further exploration was conducted on advancing Ni@Silicalite-1 for hydrogen production through catalytic ESR in this study.

### 1.3. Problem statement

To realize hydrogen energy as an alternative energy in the first stage, or even the new main energy in the practical application. The development in hydrogen production is one of the key components. One of the hydrogen productions processes that is developing so far is through steam reforming of hydrocarbon. The steam reforming of hydrocarbon requires a high reaction temperature to proceed and produce an acceptable amount as mentioned in the introduction. Meanwhile, the utilization of a large amount of heat to produce another type of energy with a high surplus of energy consumption is also not applicable. The acceptable and worth-to-invest amount of hydrogen cannot be produced at a low reaction temperature. Therefore, to lower the total heat consumption of the process while obtaining the acceptable yield of hydrogen production, the development of active catalyst is introduced.

The drawbacks of most catalysts used is the low activity, severe coke formation, loss activity due to active site sintering, blockage by coke formation, and structure collapse from the severe reaction condition (high temperature, and steam atmosphere). To overcome those drawbacks and obtain sufficient production of hydrogen for further application. Scientists and engineers are investigating and developing various kinds of catalysts. Various kinds of active metals, catalyst supports, preparation techniques, and different catalyst structures have been investigated.

Our group, in this study, the development of Ni-zeolite catalysts with encapsulation structure prepared by hydrothermal synthesis is introduced. The various preparation conditions during hydrothermal synthesis that could affect the catalyst morphology are investigated. The consideration of reaction pathway and comparison to equilibrium are investigated to understand the reaction behavior. The catalytic activity, along with catalyst properties are evaluated to illustrate the benefits of encapsulation structure of Ni nanoparticles for ESR in different reaction condition.

### 1.4. Objectives

The purpose of this study is to develop the Ni-based zeolite catalyst for ethanol steam reforming. The catalyst was prepared by hydrothermal synthesis to obtain the encapsulation structure of Ni nanoparticles inside Silicalite-1 MFI zeolite (Ni@Silicalite-1). The objectives of this study are listed below:

1. To investigate the effect of preparation condition to improve the morphology, catalytic properties, and steam tolerance of Ni@Silicalite-1
2. To study the reaction pathways of Silicalite-1 and Ni-Silicalite-1 catalysts, the role of Ni sites, and the effect of reaction temperature on reaction activity, comparing to the thermodynamic equilibrium condition.
3. To Investigate the catalytic activity, coke formation, sintering resistance, and stability of Ni@Silicalite-1, compared to Ni/Silicalite-1.

### 1.5. Scope of the study

This study is focusing on the development of zeolite-encapsulated Ni catalyst for bioethanol steam reforming. The study is divided into the preparation of catalysts, then study of reaction activity, including reaction pathway and stability.

For preparation and characterization. 1 wt % of Ni catalysts were prepared in this study. Ni@Silicalite-1 was prepared with hydrothermal synthesis with the addition of Ni-PS precursor. 3 wt% expected of Ni loading Ni-PS were prepared in different conditions and used in Ni@Silicalite-1 preparation. The different zeolite preparation conditions were also investigated, including different H<sub>2</sub>O:Si ratio and hydrothermal synthesis temperature. Ni/Silicalite-1 was prepared with an incipient wetness impregnation of Ni-water solution onto the highly crystalline house-synthesized Silicalite-1. The surface morphology of the catalyst was evaluated by XRD, N<sub>2</sub> physisorption, and SEM. Properties of Ni were investigated using N<sub>2</sub>O pulse chemisorption, TEM, XRF, and H<sub>2</sub>-TPR.

Catalytic activity of bioethanol steam reforming was investigated in quartz tubular reactor at reaction temperature of 500 – 800 °C, at atmospheric flow condition. The product yield and selectivity comparison were investigated on Silicalite-1 (support without Ni), Ni/Silicalite-1 (Ni on the catalyst surface), and Ni@Silicalite-1 (encapsulation structure of Ni), together with catalyst properties after the reaction test. Coke formation on the spent catalysts were evaluated by TG-DTA analysis, and SEM. Stability tests were investigated at 500 °C as a low reaction temperature to illustrate the performance of different catalyst in reaction activity and coke resistance, and at 800 °C as high reaction temperature to illustrate the performance on Ni sintering resistance and structure tolerance towards severe reaction condition (temperature and steam atmosphere).

According to the objectives and scope of this study, the outline of this study will be portrayed into three chapters of experiments, calculations, and investigation on catalyst preparation, reaction pathway, and utilization.

In chapter 2 the preparation of Ni@Silicalite-1 was studied. In this chapter, the details in encapsulation catalysts preparation parameters were studied. Starting with the preparation with and without Ni-PS precursor, different precursors preparation that were used in catalyst preparation, the behavior of different dissolution time in mother liquor preparation, the effect of hydrothermal synthesis parameters, including, different H<sub>2</sub>O:Si ratio, and hydrolysis temperature. The criteria for judgement of the preferred catalyst catalytic activity including coke formation, surface morphology, in terms of changing in surface area and micropore volume as the structure thermal stability. The phenomena during the preparation procedure on each condition are illustrated based on the observations on appearance, general knowledge, and prediction.

In chapter 3, ethanol steam reforming reaction mechanism and possible pathway on Ni over Silicalite-1 catalysts were studied. The literature will mention the possible pathway on Ni-based catalysts. The calculation of thermodynamic equilibrium composition is portrayed, and compare with the phenomena on Silicalite-1, and Ni@Silicalite-1 synthesized. The calculation and experimental data were further used in reaction temperature judgement on catalytic activity test, together with the understanding for the catalytic behavior of the catalyst utilization in the next chapter.

In chapter 4, the investigation of catalytic activity of Ni@Silicalite-1 was studied. Ethanol steam reforming reaction tests were conducted in different reaction temperatures from 500 – 800 °C. The ethanol conversion, product selectivity, and coke formation were investigated. The catalyst properties were evaluated with various characterization techniques before and after the reaction tests to understand the phenomena during the reaction test, including the data of surface morphology and Ni properties. The comparison was evaluated on Silicalite-1 (support material without active site Ni), conventional Ni/Silicalite-1 (prepared by incipient wetness impregnation), and our developed Ni@Silicalite-1 (encapsulation structure). The different operating conditions, such as, steam-to-carbon ratio in feed was also investigated. The stability of the prepared catalysts was investigated at low temperature in long reaction time, to evaluate the performance of encapsulation catalyst in kinetic control condition which product selectivity and coke formation can be obviously investigated, and high temperature to evaluate the thermal stability of the Ni active sites and zeolite morphology.



## Chapter 2 : Preparation of Ni@Silicalite-1 with Ni-Phyllosilicate precursor

### 2.1. Introduction

#### 2.1.1. Goal and criteria for “ESR ideal catalyst”

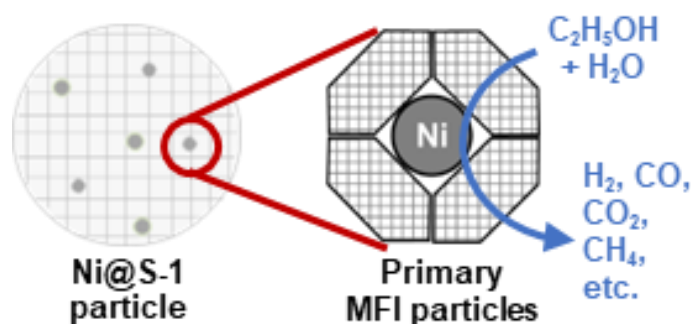


**Figure 2.1.** Scheme of Ni@Silicalite-1 catalyst.

The goal in development of ESR catalyst is to obtain the catalyst properties that help the reaction proceeded to obtain the high hydrogen production yield with the low cost, in catalytic material cost, and operating cost. The selection of Ni as an active metal can make the cost of catalytic material cheaper. Weak points of using Ni are the requirement of high reaction temperatures to obtain the hydrogen yield as in the noble metal, also catalyst deactivation from severe coke formation and metal sintering. The high operating temperature and feed pretreatment, distillation for specific ethanol concentration and remove impurities, relies on the cost of operation, which is another part of ESR to be still far from a practical application. The development of ESR catalysts aim for several properties and characteristics, which benefits to the reaction and operations:

- 1) High activity and selectivity towards the desired reaction pathways and products which are hydrogen and carbon dioxide. In other words, minimize the formation of undesired products through unwanted pathways.
- 2) Maintaining a good dispersion and a high surface area of the active site is a crucial property to maximize the catalytic activity.
- 3) Provide stability and durability under ESR operating conditions which consists of pretreatment, reaction temperature, high temperature steam, impurity presented in reactants, etc. which leads to catalyst deactivation by structure collapse, active metal oxidation and poisoning. The compatible catalyst towards the different condition with a long catalytic lifetime without significant deactivation or structural deformation realizes the lower cost in maintenance and operation.

- 4) Coke resistance property is one of crucial points of ESR catalyst development. The coke formation leads to catalyst deactivation, the severe coke formation can drastically shorten the catalyst activity and its lifetime, and also possible to cause the uneven distribution of pressure and temperature in the reactor causing an accident in operations.

## 2.2.2. Zeolite formation mechanism via hydrothermal synthesis: General knowledge

### 2.2.2.1. Hydrothermal synthesis of zeolites

Hydrothermal synthesis is an autogenous pressure, sol-gel process [52]. In hydrothermal synthesis for zeolites, it includes several times of hydrolysis and condensation process all along the formation. The formation timeline can be divided into induction period and growth period of zeolite. Induction period is the period that monomers and oligomers combine to form an unstable gel which has a possibility to rearrange its shape and structure all the time. At this stage, the zeolite templates are surrounded by silicon particle clusters. This unstable gel is transformed, rearrange, and agglomerate to be a structure with more ordered, into amorphous gel and metastable gel, respectively. The obtained metastable gel is a crucial point for further condensation, the starting point of zeolite formation, called as “nucleation” since it is the stage which critical size of zeolite ring is obtained. If the condition is not suitable, zeolite is not able to form.

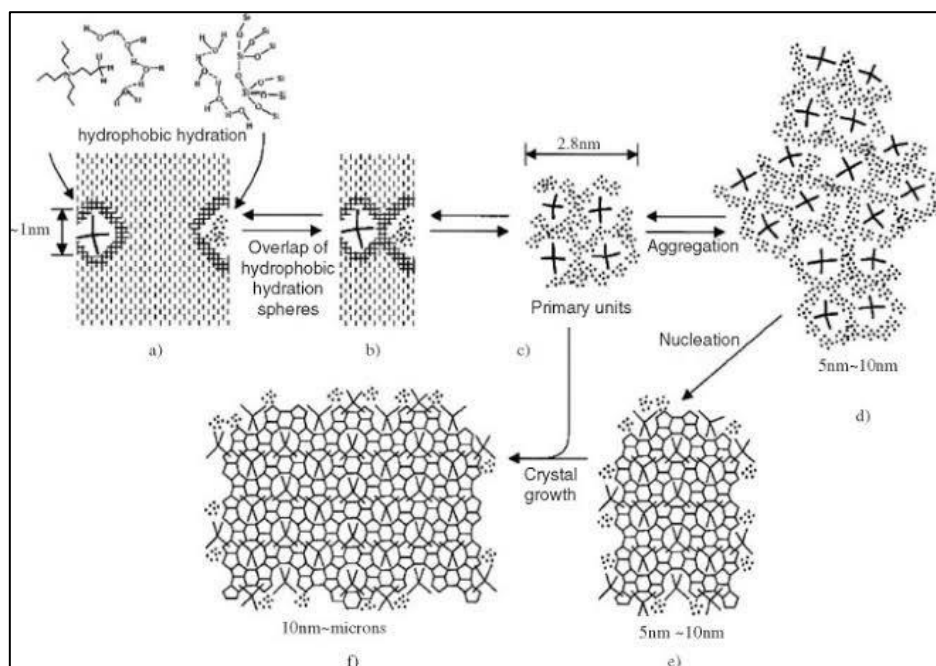


**Figure 2.2.** Formation of zeolite: metastable gel, nucleation, and crystallization [53].

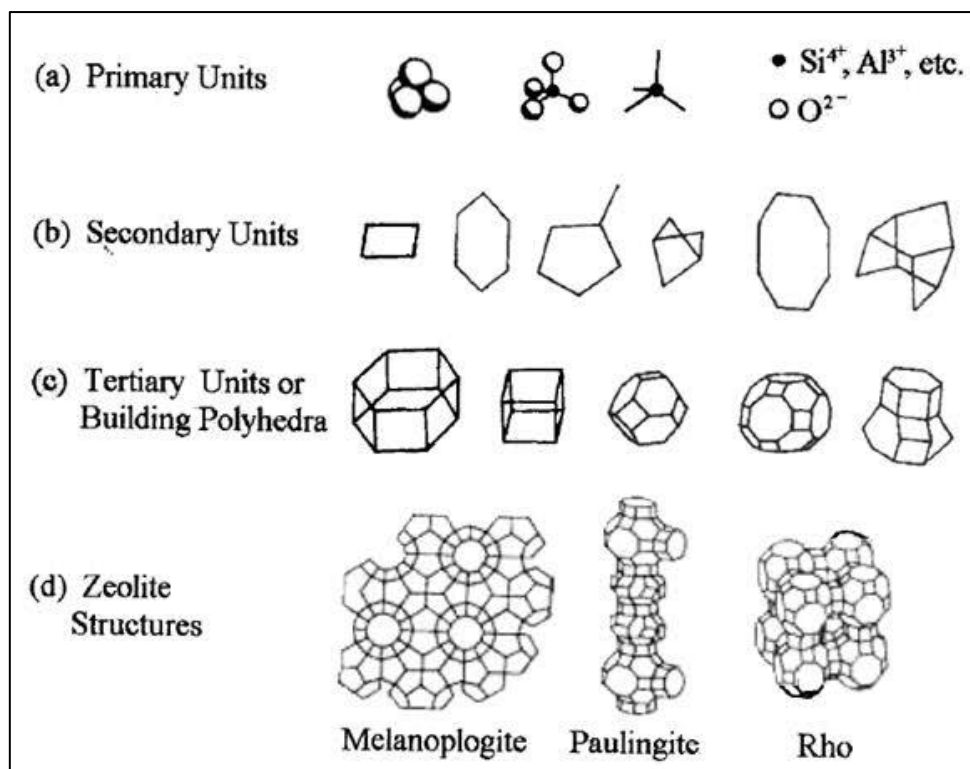


**Figure 2.3.** types of zeolites building units [54].

After obtaining the metastable gel which is a supersaturated solution of primary building units (PBUs) of zeolites with critical size, hydrolysis and condensation is proceeded to turn the PBUs into second building units (SBUs), one closed-ring structure in zeolite, then tertiary building units, and small structure of zeolites. These steps are in a nucleation process of zeolite and the structure of obtained zeolites are defined since here. The intermediates in the dissolution of silica sources affect crystallization, also particle sizes and zeolite morphology. Unstable nuclei will hydrolyze back into sol-gel stage. The high pressure and temperature can affect the solubility of different species in the solution, make a faster saturated solution, shorter the induction period, and faster nucleation is occurred. By the way, too fast formation can lead to some drawbacks of repelling alien species presenting in a solution.

After passing the induction period, nucleation was triggered, then become “growth period”, which is the stage that the nuclei with critical size make a fast crystal growth. The rate of both nucleation and crystallization depends on the stage of the precursor presents in the solution. The suitable condition is no nucleation during crystal growth, the faster crystal growth, the more uniform crystal size is obtained from the synthesis. On the other hand, in the slow crystal growth, nucleation of the new particle can occur at the same time, then the various size of zeolite can be obtained. These various zeolite sizes within one batch can

reflect the different properties of the obtained zeolite particles, especially zeolite with alien atoms inside or designed pore-structured zeolite.

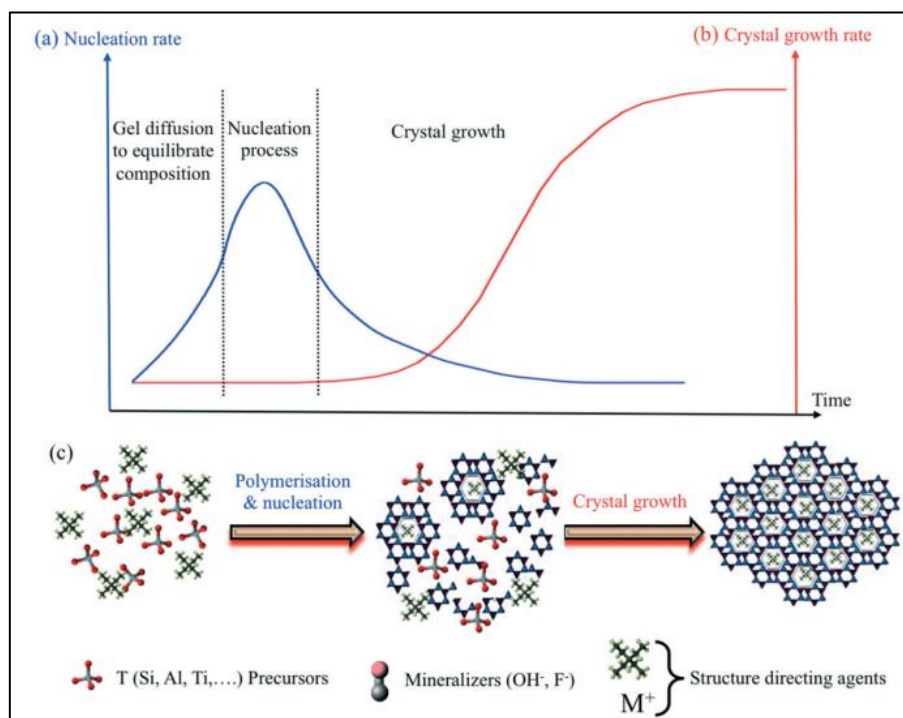


**Figure 2.4.** Schematic representation of the (a) nucleation rate and (b) crystal growth rate of zeolites described with a typical S-shaped curve, and (c) related rearrangements from amorphous particles into crystalline zeolite during the synthesis [55].

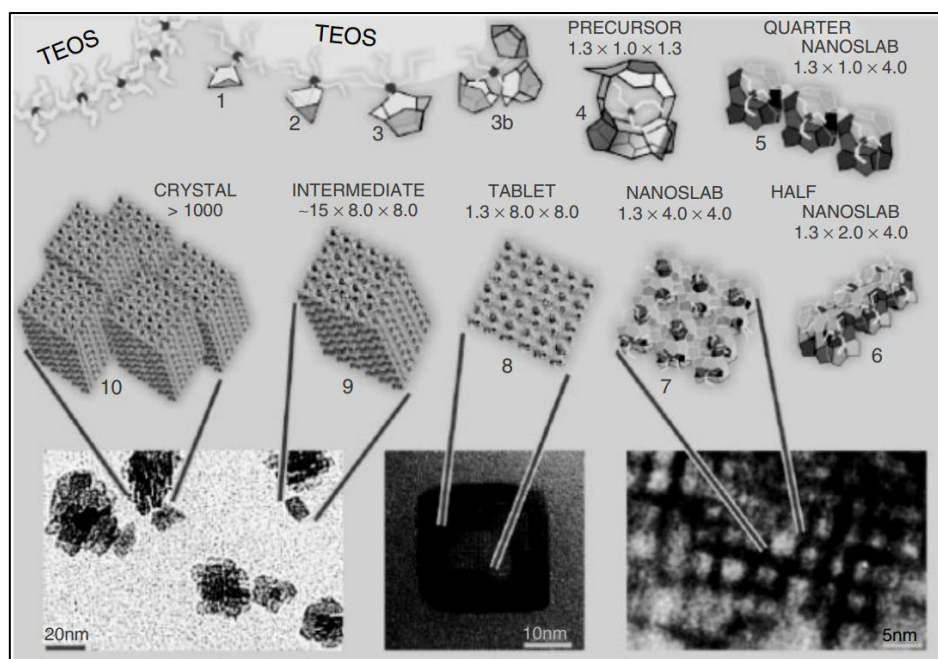


**Figure 2.5.** Formation of Silicalite-1 zeolite from clear solution [56].

### 2.2.2.2. *Hydrothermal synthesis parameters that effect the properties of zeolites*

The optimum condition is required to obtain the ideal design zeolite in individual applications. There are several parameters to consider in zeolite synthesis.

#### 1) Molar composition (concentration) of ions and precursors

The composition of the starting materials, including the type and ratio of silicon and aluminum sources, affects the final zeolite structure and properties. The phenomenon in consideration is how the silica species arrange around the template. The other atoms added into the solution system are considered as one obstacle for normal crystallization, and each type of obstacle has its own characteristic for existing in a solution. Therefore, this is the reason why the addition of ions can control the structure of zeolite since it can influence nucleation and crystallization kinetics, frameworks composition, crystal size and morphology can be altered. For example, the low Si/Al leads to a cage-like structure, but the high Si/Al leads to a channel structure.

#### 2) Alkalinity and pH

The pH levels in the hydrothermal solution play a role in both the creation of distinct zeolite phases, since meta stable phase formation, and the crystallization process. In general, the pH is between 9 and 13. The dissolution of gel (hydrolysis, induction period) is catalyzed by  $\text{OH}^-$  and the hydroxide ions are used, so that the pH of the solution in this stage is lowered. Then, the condensation occurs and release  $\text{OH}^-$  into the solution, at this stage, the pH is drastically increased. In a high pH system, faster nucleation (shorter the induction period) and faster crystal growth can be obtained. At a high pH also causes the difficulty for further condensation reaction, so the crystals stop their growth. Typically, alkali metal hydroxides are used to regulate alkalinity of the solution. The type of metal or non-metal alkali hydroxides are used specifically since it can alter the properties of obtained zeolite. There is a study that mentioned the pH might change the shape of the Silicalite-1 crystal, in width and length but not the thickness. The system with low pH, the obtained Silicalite-1 tends to be a longer in length than the high pH system that yields the short one. [ref]

#### 3) Solvent of the system

The selection of the solvent or the inclusion of extra ions in the hydrothermal blend can impact both the growth of crystals and the purity of the zeolite.

#### 4) Pressure

Hydrothermal synthesis is conducted under high-pressure conditions, typically ranging from a few atmospheres to several hundred atmospheres. Pressure affects the phase stability and crystal growth kinetics of zeolites.

#### 5) Temperature

In each system, the certain temperature limit shows a positive influence in zeolite formation. Increasing temperature tends to shorter crystallization time of the zeolite, from making a denser phase under hydrothermal synthesis condition. In the system that utilizes water as a solvent, at elevated temperature, the fraction of water in liquid phase decreases. The water has its duty to stabilize the pores in the structure formation. There is an upper limit temperature of the system that is the water release out and the pore is not yet stabilized, therefore, the porous structure cannot be form. If the high temperature is required for the system, the type of solvent is reconsidered.

#### 6) Hydrothermal synthesis time

The duration of the hydrothermal synthesis process impacts the crystallinity, crystal size, and morphology of the zeolite. In a solution pool, the solid products consist of the zeolites, unreacted amorphous silica, the part that partially transformed into precursor. According to Ostwald ripening phenomena, the smaller particles or crystals dissolve and then redeposit on larger particles or crystals, leading to an increase in the average size of the larger particles and a decrease in the number of smaller particles.

#### 7) Stirring and mixing

Proper agitation and mixing of the hydrothermal mixture are crucial to ensure uniformity and homogeneity, which can affect crystal growth and phase distribution.

#### 8) Autoclave type/size/design

The design and materials of the autoclave (reactor vessel) used for the hydrothermal synthesis can influence temperature and pressure uniformity, affecting the synthesis process.

#### 9) Template molecules (referred as structure directing agents, SDA)

Organic molecules (templates) added to the synthesis mixture can influence gelation, precursor formation, nucleation, and crystal growth. The same inorganic concentration in the mother liquor with the different type of OSDA leads to the different in crystallization behavior [57]. There are two types of SDA, either structure

stabilization or structure blocking agent. Therefore, the zeolite framework structure and pore size distribution change when using the different SDA molecules.

#### 10) Seed crystal

The addition of small amounts of pre-formed zeolite crystals (seeds) can influence the crystallization process, enhancing the formation of desired zeolite phases and improving crystallinity.

#### 11) Aging and pretreatment

Aging of the mother liquor solution by mixing in low temperature for a long time could help metastable gel formation from the enhancement of dissolution of PBUs. It shortens the induction period of crystallization process; the larger number of nuclei is obtained. Smaller zeolite crystal size is obtained when the aging period is long.

#### 2.2.2.3. Zeolite preparation with seed utilization (seeding)

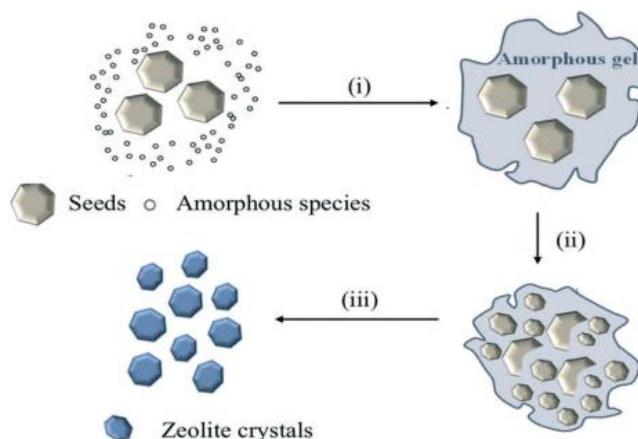


**Figure 2.6.** zeolite preparation with crystal seeds induction [55].

There is another method of zeolite preparation, which is the nucleation and crystallization of zeolite with a suspension of crystal seeding without the utilization of SDA molecules. In this preparation procedure, nucleation and crystallization deviate from the usual nucleation route. It shows the effectiveness towards the crystal size control [58]. It acts as a nucleation site for a desired product, initiate crystallization, and growth. The phenomena are in the sequence as follows.

- (i) The amorphous silica-alumina species dissolve, resulting in a blend that is partially laid down onto the seed crystal surfaces.
- (ii) Nucleation and growth of crystals take place within the gel structure, influenced by the existence of seed crystals.

- (iii) Complete utilization of the initial amorphous gel results in the production of a fully crystallized zeolite material.

Since the seed crystal is a key to initiate crystallization, it must provide a sufficient surface area for the desired product to be grown on. Some researchers proposed the growth mode as a core-shell growth mechanism [59, 60]. The number of seeds used is also a factor to control the number and size of the zeolite formation. In general, zeolite seeds with 0.1 – 10 wt% were used as nuclei for further crystallization, but also depends on the nature of the system to has its own kick-off number. This technique promotes the formation of nuclei, increases the synthesis rates, and is able to reduce the impurities formation in the solution system.

With the combination ideas in the literatures, taking consideration with our study. Our solution system has both seeding and SDA molecules. Seeding in our case is not a crystalline material but amorphous silica in an ordered structure. Therefore, their dissolution behavior might directly affect the nucleation and crystallization process. And their effects are studied through the different conditions, which will be mentioned and discussed in Section 2.3.

### 2.2.3. Ni-phyllsilicate: structure and advantages

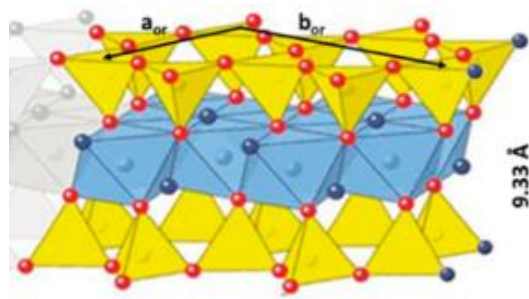


**Figure 2.7.** 2:1 phyllosilicate structure [61].

In this study, Ni-PS precursor is a composite oxide containing Ni and amorphous silica (Ni-PS/SiO<sub>2</sub>) and used as Ni solid precursor. The obtained precursor contains Ni-phyllsilicate structure inside the silica structure. Phyllosilicate is a structure that is formed with a building block of silica tetrahedral, a central silicon surrounded by four oxygen atoms as a tetrahedral structure. It forms in a sheet-like or layered structure. Ni atoms are incorporated into the crystal layers during the preparation process. There are two possibilities of formation structure, which are 1:1 and 2:1 Ni-phyllsilicate structure. The 2:1 Ni-PS are formed as Ni<sub>3</sub>Si<sub>4</sub>O<sub>12</sub>H<sub>2</sub>) consists of ~36 wt % Ni and 1:1 Ni-PS are formed as Ni<sub>3</sub>Si<sub>2</sub>O<sub>9</sub>H<sub>4</sub>) consists of ~46 wt % Ni. The formation of 1:1 or 2:1 Ni phyllosilicate can be controlled by changing the pH value of the solution. Ni that is stayed inside the specific structure as



phyllosilicate are higher in metal-support interaction, compared to the normal impregnation. In order to decompose this structure, it particularly required higher energy, therefore, the decomposition temperature of 2:1 Ni-PS is higher than 1:1 Ni-PS. In catalytic field, the decomposition of Ni phyllosilicate that functions as an active species in the catalyst might refer to a reduction temperature.

My preliminary study, Ni@Silicalite-1 was prepared by Ni@SiO<sub>2</sub> precursor prepared by microemulsion technique. The characterization results show that the obtained catalysts consist of a high content of amorphous silica. The Ni nanoparticles are found to be agglomerated 8 -12 nm after reduction at 700 °C before the reaction test in different batches of preparation with the same hydrothermal synthesis condition. Those catalysts had been investigated in ethanol steam reforming. It was found that very high carbon formation was obtained together with the structure collapse after the reaction test at 500 °C for 4 hours. With the unsuccessful results, the choice of precursor had reconsidered to be Ni-phyllosilicate prepared by hydrothermal synthesis. This precursor had tested in the preparation then catalytic reaction test at 700 °C, the observation on coke formation on the catalysts beds was shown in Figure 2.8. The appearance of catalyst bed at the top part of Ni@Silicalite-1 prepared with NiSiO<sub>2</sub> are likely to Ni/Silicalite-1 and it was found to be 11 wt % of carbon. On the other hand, Ni@SiO<sub>2</sub> and Ni@Silicalite-1 prepared with Ni-PS precursor showed a difference on observation. Coke formation on Ni@Silicalite-1 prepared with Ni-PS precursor was found to be 5 wt %, which is less than the case of utilizing Ni@SiO<sub>2</sub> as a precursor. At that point, the decision making of changing the type of precursor to Ni-PS was drawn. Together with the result as mentioned in Zhang's study in DRM reaction. It is even emphasized that the precursor changes proves the benefits towards catalytic properties of Ni@Silicalite-1.

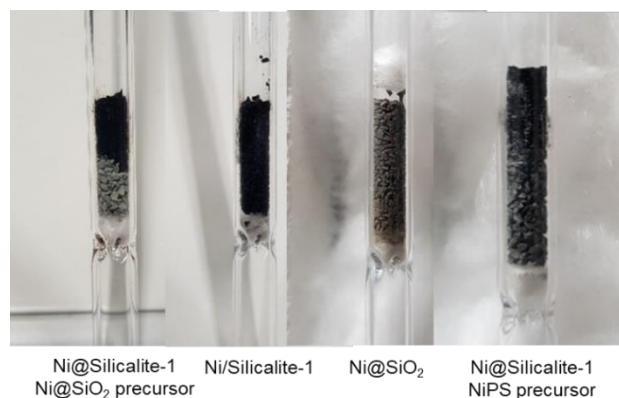


**Figure 2.8.** Coke formation behavior on spent catalyst after the reaction test at 700 °C.

## 2.2. Experimental

In this study, the preparation of materials is divided into 3 groups:

- (1) Preparation of Ni-phyllsilicate precursor (Ni-PS) which are further used as a Ni precursor in the encapsulation catalyst. The variation of preparation condition will be mentioned in section 2.2.1. and discussed in section 2.3.2.
- (2) Preparation of Ni@Silicalite-1: the encapsulation catalyst which is our main material in this study. The different preparation conditions are investigated to obtain the higher and better catalytic properties for the reaction. The effects of different preparation conditions (from both precursor and hydrothermal synthesis) will be shown in section 2.2.2. and discuss in section 2.3.3.
- (3) Preparation of Ni/Silicalite-1: the conventional preparation method of impregnation. The preparation of Silicalite-1 and preparation of Ni/Silicalite-1 will be mentioned in 2.2.3. and the result will be mentioned as a comparison to Ni@Silicalite-1 in later chapters.

Various of chemicals are used in this study, as listed in

Table 2.1. All chemicals were purchased from FUJIFILM Wako Pure Chemical Industries, Ltd., Japan. and used without any further purification.

**Table 2.1.** List of chemicals in this study.

| Chemical Name   | Purity/ Concentration   | Purpose  |
|---|-------------------------|--|
| Tetrapropyl ammonium hydroxide (TPAOH)  | 10 wt% aqueous solution | Zeolite synthesis                                |
| Tetraethyl orthosilicate (TEOS)   | 95 % purity             | Ni-PS, zeolite synthesis                         |
| Nickel nitrate hexahydrate ( $\text{Ni}(\text{NO}_3)_2 \cdot 6\text{H}_2\text{O}$ ) | 99.9 % purity           | Ni-PS preparation<br>Ni/Silicalite-1 preparation |
| Nitric Acid ( $\text{HNO}_3$ )  | 35 % v/v                | pH adjustment<br>(zeolite recovery)              |
| ammonia aqueous solution ( $\text{NH}_3$ )  | 28 wt%                  | Ni-PS preparation                                |
| Ethanol ( $\text{C}_2\text{H}_5\text{OH}$ )   | 99.5 % purity           | Reactant in reaction test                        |
| Distilled water   | -                       | Reactant in reaction test<br>Ni-PS washing       |

### 2.2.1. Preparation of Ni-PS precursors

Ni-phyllsilicate precursors were prepared by hydrothermal synthesis of the solution containing  $\text{Ni}(\text{NO}_3)_2$  as a nickel source,  $\text{NH}_3$  solution, and TEOS as a silicon source. The amount of each component were calculated according to  $\text{H}_2\text{O}:\text{Si}$  molar ratio,  $\text{NH}_3:\text{Ni}$  molar ratio based on the total solution volume used in hydrothermal synthesis. DI water and 1 M Ni solution, prepared with  $\text{Ni}(\text{NO}_3)_2 \cdot 6\text{H}_2\text{O}$  in water were firstly mixed for 20 mins. After that, the calculated amount of TEOS was added to the solution and continued stirring for 2 h. The mixed solution was transferred to Teflon autoclaves for hydrothermal synthesis. The hydrothermal synthesis was performed at  $100\text{ }^\circ\text{C}$  for 72 h. After hydrothermal synthesis, the sample was centrifuged to separate the solid part from the solution, washed with DI water (no pH adjustment), for 3 cycles, and then dried in a hot air oven overnight. The obtained Ni-PS was further calcined in a muffle furnace at  $550\text{ }^\circ\text{C}$  for 12 h (for the one which are further used as calcined Ni-PS). At this stage, the Ni-PS obtained was ready for further use in a synthesis of Ni@Silicalite-1.

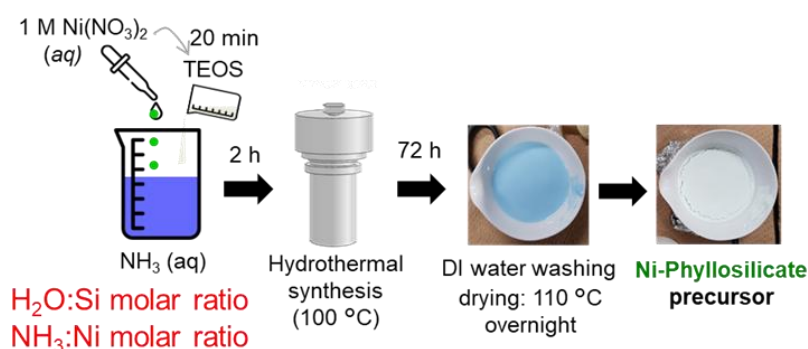


**Figure 2.9.** Preparation procedure of Ni-phyllsilicate precursor.

The Ni-PS samples that are further investigated in section 2.3.2, the different conditions of Ni-PS used in Ni@Silicalite-1 synthesis, as listed in Table 2.2. All the samples were prepared with expected Ni loading of 3 wt% (obtaining 2.1 – 2.7 wt% due to the Ni loss during preparation and variation between different batches).

**Table 2.2.** Ni-PS used in the Ni@Silicalite-1 preparation

| Ni-PS sample            | $\text{H}_2\text{O}:\text{Si}$<br>molar ratio | $\text{NH}_3:\text{Ni}$<br>molar ratio | Calcination | Ni loading<br>(wt %) |
|-------------------------|---|--|-------------|----------------------|
| 3 Ni-PS (non-porous, C) | 34  | 60                                     | Yes         | 2.35                 |
| 3 Ni-PS (porous, NC)    | 100   | 120                                    | No          | 2.19                 |
| 3 Ni-PS (porous, C)     | 100   | 120                                    | Yes         | 2.20                 |

### 2.2.2. Preparation of Ni@Silicalite-1

In this study, there are 2 main categories of Ni@Silicalite-1 preparation which are 1-step and 2-step preparation. The difference outcome of the usage of Ni-PS precursor will be discussed in section 2.3.1. The procedures for both ways of preparation are shown in the following figures.

Figure 2.10 shows the preparation of 1-step Ni@Silicalite-1. Starting with the preparation of TPAOH-TEOS solution of specific H<sub>2</sub>O:Si ratio. After mixing overnight, a calculated amount of Ni solution for 1 wt % Ni loading in Ni@Silicalite-1 was added to the solution, then continue mixing for 2 h. The solution was transferred to a Teflon autoclave for hydrothermal synthesis at study temperature for 72 h. pH adjustment of the obtained solution after hydrothermal synthesis was performed for zeolite recovery. The sample was centrifuged and washed with DI water for 3 washing cycles. The solid part was transferred to the crucible for drying in 110 °C hot air oven overnight and calcined in the muffle furnace 550 °C 12 h. The obtained Ni@Silicalite-1 was ready for characterization and activity test.

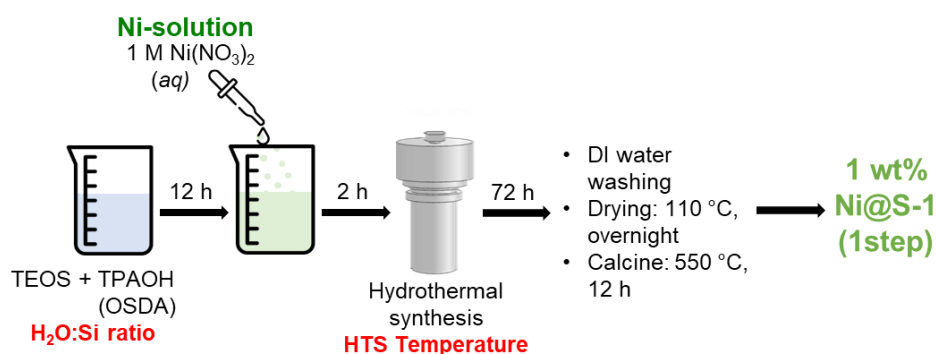


**Figure 2.10.** Preparation procedure of 1-step Ni@Silicalite-1.

The next part is the preparation of 2-step Ni@Silicalite-1. The catalysts were prepared with hydrothermal synthesis method as shown in Figure 2.11. Preparation of Ni@Silicalite-1, with Ni-PS addition as a last step.. A calculated amount of 10 wt % TPAOH, DI water, and TEOS were mixed in a Teflon beaker at room temperature. The Si:OSDA were kept at 3:1. The hydrolysis of TEOS was performed by this mixing step for 6 h. After that, add the calcined precursor into the mixture, and continue stirring for a specific time of 18 h. The amount of solid Ni-PS addition is according to its Ni loading and calculated for 1 wt % of Ni@Silicalite-1. After the mixing time ended, the solution was transferred to Teflon autoclave for hydrothermal synthesis. The hydrothermal synthesis of Ni@Silicalite-1 were investigated at 100 and 150 °C for 72 h with 10 rpm of rotational speed. After the completion of hydrothermal synthesis, a pH adjustment, wash, and centrifuge for three cycles were

performed for zeolite recovery. The same drying condition of 110 °C overnight and calcination at 550 °C 12 h were applied for all prepared Ni@Silicalite-1.

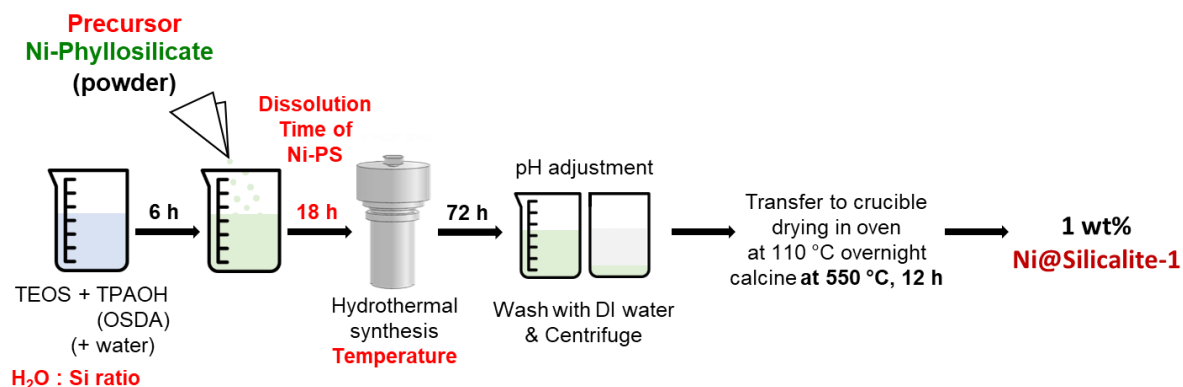


**Figure 2.11.** Preparation of Ni@Silicalite-1, with Ni-PS addition as a last step.

In mother liquor preparation, the dissolution time of Ni-PS addition were investigated for the different catalyst properties, which expected to be the influence towards dissolution of Ni-PS, which controls the species in a solution for hydrothermal synthesis, then the phenomena in recrystallization for zeolite formation will be different, therefore, the different catalyst properties will be obtained.

Besides Ni@Silicalite-1, which is the main material in this study, the conventional catalyst as Ni/Silicalite-1 was also prepared for comparison. The Silicalite-1 support was prepared as a procedure illustrated in Figure 2.12. The mother liquor of TPAOH and TEOS was prepared by mixing overnight, then transferred to Teflon autoclave for hydrothermal synthesis. The hydrothermal synthesis was performed at 200 °C 72 h, the high temperature is used to confirm the high crystallinity of synthesized Silicalite-1. After 72 h of hydrothermal synthesis, the sample was cooled down in ice bath, pH adjustment, washed with DI water, and centrifuge for zeolite recovery. The sample was dried at 110 °C overnight and calcined at 550 °C 12 h.

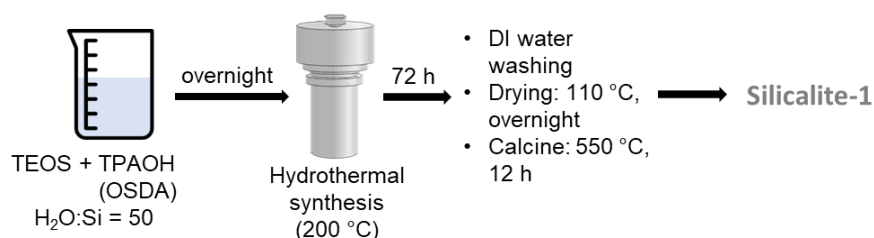


**Figure 2.12.** Preparation of Silicalite-1.

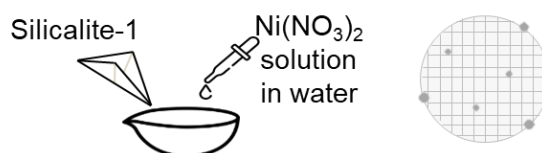


**Figure 2.13.** Preparation of Ni/Silicalite-1.

The obtained Silicalite-1 after calcination was further used for 1 wt % in Ni/Silicalite-1 preparation. 0.1 M Ni solution was prepared from  $\text{Ni}(\text{NO}_3)_2 \cdot 6\text{H}_2\text{O}$  in water as Ni source. The diluted Ni solution helps the dispersion of the metal in support material [62]. The solution was drop-wise impregnated onto Silicalite-1 as an incipient wetness impregnation. The amount of solution addition is quantified from Silicalite-1 adsorption ability test prior to the catalyst preparation. The wet-sand-like slurry of Ni/Silicalite-1 was dried in 110 °C hot air oven overnight, and further calcined in a muffle furnace at the same zeolite calcination condition, 550 °C for 12 h.

### 2.2.3. Materials Characterization (before reaction tests)

The properties of prepared Ni-PS, Silicalite-1, Ni/Silicalite-1 and Ni@Silicalite-1 were investigated before the reaction test to collect the information about morphology, surface, and active sites properties, and then compare the data with the characterization after the reaction test. The properties changes before and after the reaction test will be discussed for pros and cons of each material. The characterization techniques/equipment that is used to evaluate the material properties before the reaction test are listed as follows.

#### 1. X-ray Diffraction (XRD)

Ni-PS precursor, support, and catalysts' surface morphology, including crystal structure, silica/zeolite type, metal species, were investigated with SmartLab-XRD, Rigaku Co., Ltd., Japan. The settings of equipment are Cu  $K\alpha 1$ , radiation at 40 kV/15 mA, 5° - 90° 2-theta, 0.02° step size, and 10° per min.

#### 2. N<sub>2</sub> physisorption

The N<sub>2</sub> adsorption was performed at -196 °C (77 K) using a high precision volumetric gas adsorption analyzer BELSORP mini II, MicrotracBEL, Japan. Specific surface area, micropore volume, and crystallinity implementation can be verified by the adsorption isotherms, Brunauer- Emmett-and-Teller (BET) calculation for BET surface area, and t-plot calculation for micropore volume.

#### 3. Scanning electron microscopy (SEM)

Zeolite crystal size and surface morphology appearance of Ni-PS, Silicalite-1, Ni over Silicalite-1 catalysts were observed using a scanning electron microscope (S-5200, Hitachi High-Tech Corp., Japan) with accelerated voltage of 1.5 – 2.0 kV. The samples were magnified from 10,000x – 120000x for surface observation. The size measurement of materials in photos taken from SEM was evaluated by ImageJ software.

#### 4. Transmission Electron Microscopy (TEM)

Transmitted morphology of Ni catalysts was illustrated by the transmission electron microscope (TEM; H-7650, Hitachi High-Tech Corp., Japan) with accelerated voltage of 120 kV. The catalyst sample was reduced at 700 °C in H<sub>2</sub>/N<sub>2</sub> stream before the characterization. The Ni size on the catalysts were investigated and then calculated from the measurement using ImageJ software.

#### 5. N<sub>2</sub>O pulse chemisorption

Ni dispersion on the catalysts were evaluated by N<sub>2</sub>O titration (5% N<sub>2</sub>O in He balance) performed with Chemisorption Catalyst Analyzer (BELCAT II, Microtrac BEL Japan). The sample was reduced in-situ with 50 % H<sub>2</sub> in He at 850 °C for 1 h and purged with He prior to the pulse chemisorption performed at 50 °C.

#### 6. X-ray fluorescence (XRF)

Ni loading on the samples was measured by XRF (Super Mini, Rigaku Co., Ltd., Japan). The measured value is correlated and calculated with the Fe/Si calibration to obtain the actual value of Ni contents of each sample.

#### 7. Hydrogen temperature-programmed reduction (H<sub>2</sub>-TPR)

Temperature-programmed reduction was performed using a fixed-bed reactor equipped with Mass spectrometer (BELMASS, Microtrac BEL Japan). The sample was oxidized in air at 850 °C for 1 h and purged with Ar prior to the measurement. The reduction process was performed using 5% H<sub>2</sub> in Ar. The consumed hydrogen (m/z = 2) at different temperature was recorded from 100 – 900 °C with a ramping rate of 10 °C/min.

## 2.3. Results and discussion

### 2.3.1. Explanation of Ni@Silicalite-1 formation mechanism

In our study, there are two steps of material synthesis, including the synthesis of Ni-PS precursor and use that precursor in zeolite synthesis. Figure 2.14 illustrates the formation mechanism in Ni-PS precursor preparation.

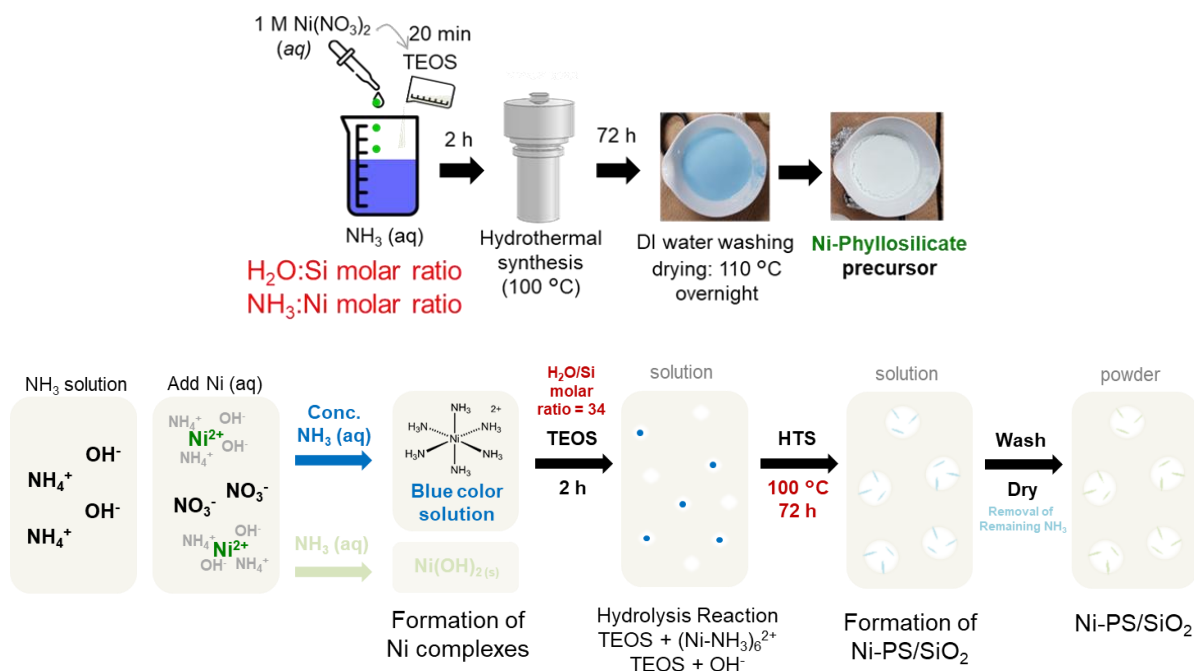
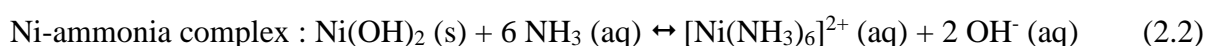
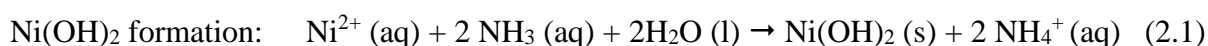


**Figure 2.14.** Formation mechanism in Ni-PS precursor preparation.

The solution is starting with the mixture of ammonia solution and the addition of Ni(NO<sub>3</sub>) solution in water a solvent. The green color of Ni(NO<sub>3</sub>) solution in water is the formation of Hexaaquonickel (II) ion, [Ni(H<sub>2</sub>O)<sub>6</sub>]<sup>2+</sup>. Adding this green solution into ammonia solution, the color of the mixed solution changes to royal blue color. At this stage, there are two possibilities of formation, which are the Ni-NH<sub>3</sub> complex ions, and nickel(II) hydroxide, Ni(OH)<sub>2</sub>, precipitates as shown in Eq.(2.1) and (2.2). The excess ammonia in the solution can further dissolve Ni(OH)<sub>2</sub> to complete formation of Hexaamminenickel (II) ion, [Ni(NH<sub>3</sub>)<sub>6</sub>]<sup>2+</sup> [63, 64].





The solution consists of  $\text{H}_2\text{O}$  as solvent, excess  $\text{OH}^-$ ,  $[\text{Ni}(\text{NH}_3)_6]^{2+}$ , and  $\text{NO}_3^-$  ions. TEOS was used as a silica source. It was added into this basic solution for kick-off the hydrolysis. The reason for adding  $\text{NH}_3$  with a much larger amount than the Ni: $\text{NH}_3$  ratio of 1:6 is for this purpose, the hydrolysis of TEOS to form the structure of amorphous silica containing Ni-phyllsilicate inside the structure while hydrothermal synthesis [65]. The gel of silica containing Ni-complex was formed. The formation might be in the configuration of the Ni-complex surrounded by tetrahydroxy silane, together with the region of pure silica and solely Ni species. This solution was transferred to the autoclave for hydrothermal synthesis. The gel was transformed into an amorphous silica containing the Ni-complex inside the structure. After drying the sample, Ni-PS precursor was obtained in powder in green color, which implies the change of Ni state existed in the material. With the drying temperature, ammonia is evaporated and released from the silica material. It might be existing in  $\text{Ni}^{2+}$  as on the same species as prepared incipient wetness impregnation, but with the different location in/on the material. The yield obtained was around 97% and the nickel loading was found to be 2.3 – 2.4 wt% (from ideal loading of 3 wt%), therefore, there is a small loss of both silica and nickel in this preparation. During the silica recovery process, there is no pH adjustment of the process since it can affect the structure of the Ni- $\text{NH}_3$  complex that stays in the material. The remaining silica can dissolve in an alkaline solution. For the liquid part, the solution is still in the light color of  $[\text{Ni}(\text{NH}_3)_6]^{2+}$ , which means that the Ni loss during the silica synthesis. The remaining of both unreacted silica and Ni complex ions exist and dissolve in an alkaline solution, therefore, there is a chance that Ni stay on the outer surface of this porous silica precursor. This precursor will be utilized in the preparation of Ni@Silicalite-1. The difference in properties of precursor porosity, calcination stage, and dissolution time of the precursor will be studied in detail for the proper precursor selection, together with proper dissolution conditions.

The next part is the zeolite formation with solid Ni-PS precursor utilization by hydrothermal synthesis which is illustrated in Figure 2.15. The preparation started with the preparation of mother liquor including the hydrolysis of TEOS with the presence of TPAOH as OSDA. The addition of Ni-PS precursor as a solid precursor is considered as both Ni source and Si source. The precursor is not fully dissolved during mother liquor preparation, presenting as solid remaining during hydrothermal synthesis. The use of different precursors shows slightly different in the appearance of the solution with a different pH value, implies the different states of solid or ions presence at the mother liquor state. These differences would lead to the difference in the formation of metastable phase, consequently, nucleation

and crystallization, and the properties of obtained Ni@Silicalite-1. Moreover, the hydrothermal synthesis condition also affects the zeolite formation. These parameters will be further discussed in detail in section 2.3.2 – 2.3.3.

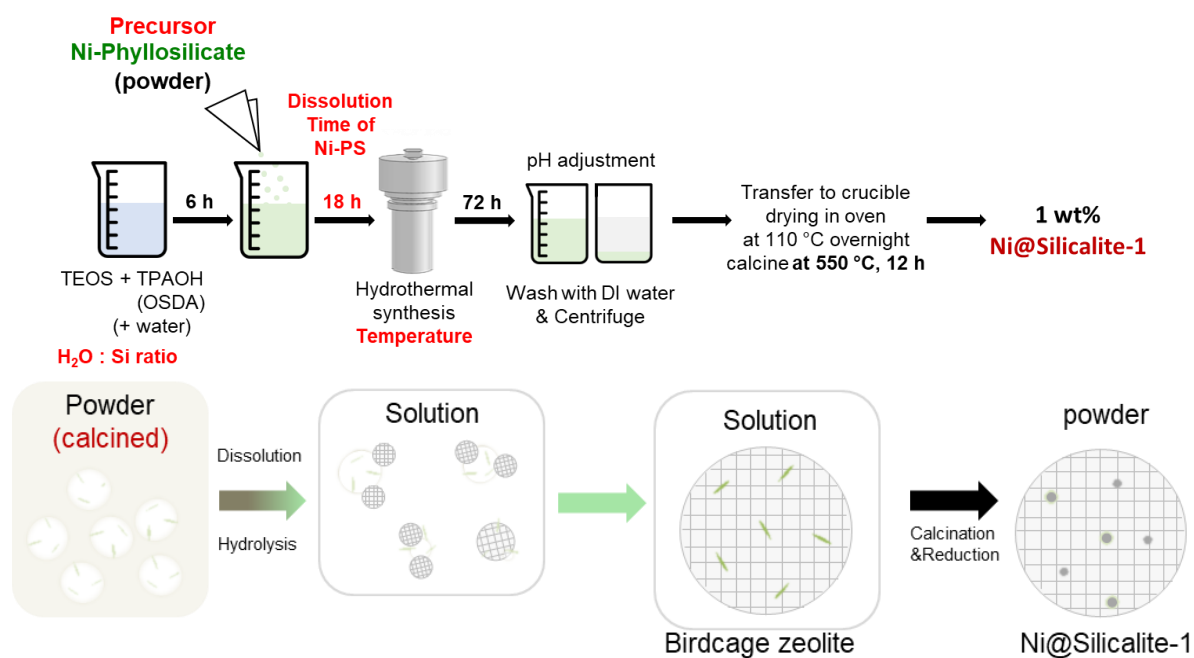


**Figure 2.15.** Formation of Ni@Silicalite-1 with two steps preparation using Ni-PS precursor.

### 2.3.2. Effect of Ni-phyllsilicate condition

In this section, the discussion of each condition will be mentioned with related to two parts, the observation of the solution phase with the appearance, pH changes, and obtained yield of the prepared Ni@Silicalite-1, and then the utilization of the material in catalytic ESR with the result of conversion, selectivity, coke formation, and morphology of the catalyst.

#### 2.3.2.1. Effect of the use of precursor in the preparation of Ni@Silicalite-1 (1-step vs 2-step preparation)

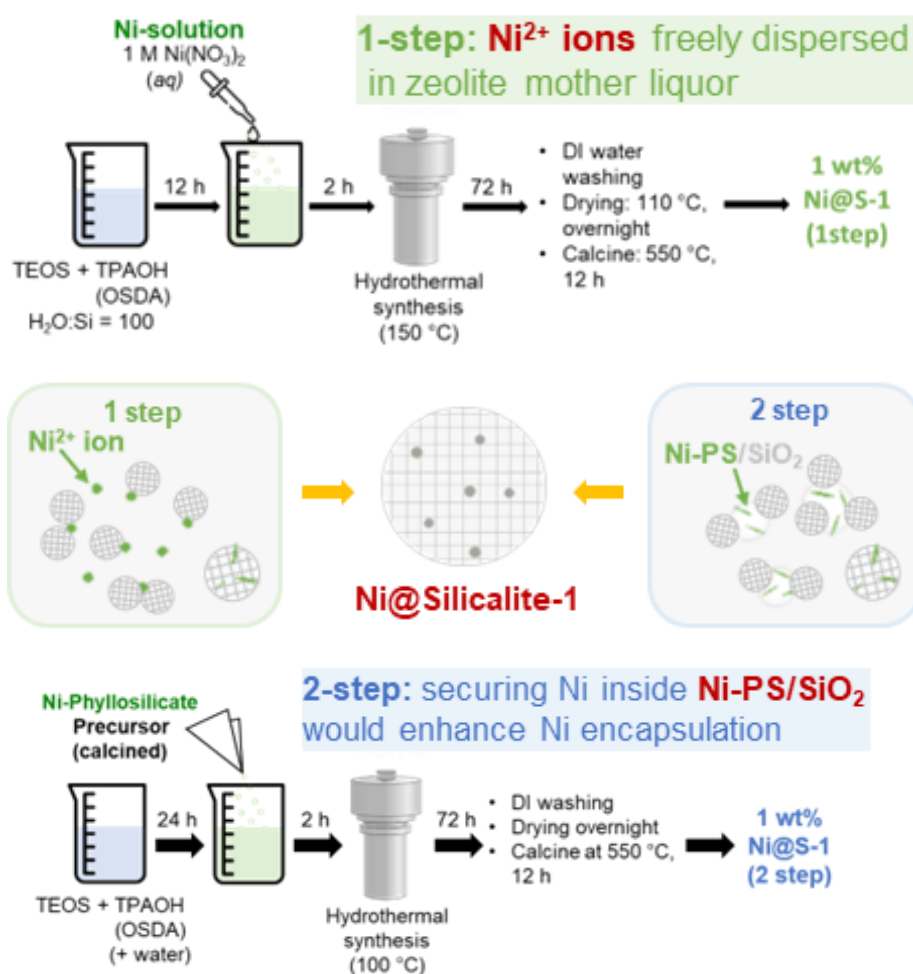


**Figure 2.16.** Schematics describe the formation of Ni@Silicalite-1 in 1-step vs 2-step preparation.

The obtained catalysts were used in the ESR catalytic reaction test to evaluate the catalytic performance at 500 °C for 10 h. This reaction temperature was selected for the investigation since it combines the effect of Ni sizes and locations towards reaction activity and coke formation and the clear phenomena can be observed after the long reaction time of

10 hours. The reactivity results are illustrated in Figure 2.17. The kick-off ethanol conversion at first hour for both catalysts are high at almost the same value, but for the 1-step Ni@Silicalite-1, the activity drops very fast and remains only half of the starting performance at time on stream 10 hours.

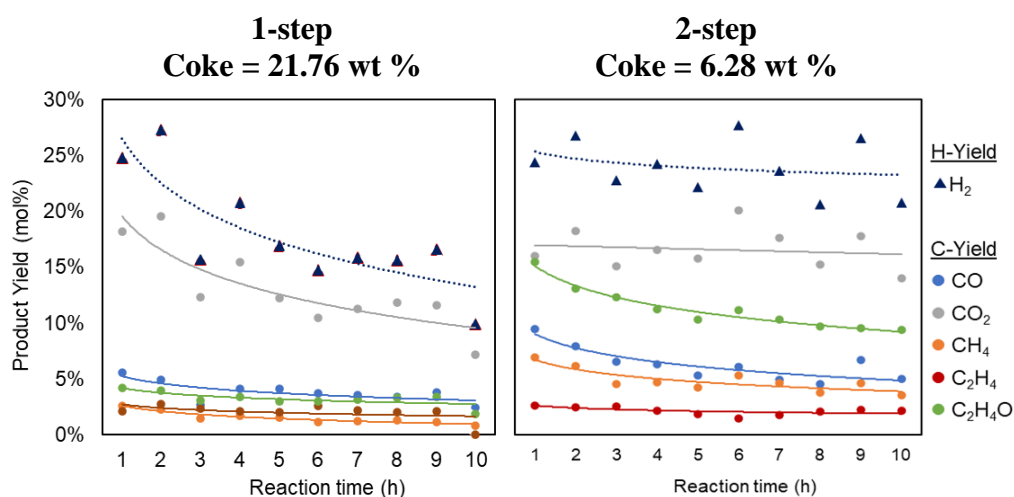


**Figure 2.17.** Catalytic activity of 1-step vs 2-step Ni@Silicalite-1 evaluated at 500 °C 10 h.

The coke formation on 1-step catalyst is a lot higher than those of 2-step catalysts, about three times higher. But the average Ni particle size remains very close to each other even after 10 hours of reaction test. In this case, the activity difference and coke formation originated from the different location of Ni that stay in the catalyst. The higher coke formation in 1-step preparation is the phenomena of unencapsulated Ni which coke is easy to grow from those sites.

**Table 2.3.** Ni properties of 1-step vs 2-step Ni@Silicalite-1.

| Sample            |                      | 1-step          | 2-step          |
|-------------------|----------------------|-----------------|-----------------|
| Ni loading (wt%)  |                      | 1.33            | 0.91            |
| Ni Dispersion (%) |                      | 1.99            | 6.54            |
| Ni particle size  | Before Reaction Test | $3.62 \pm 1.24$ | $3.76 \pm 0.56$ |
|                   | After 10 h reaction  | $4.36 \pm 1.05$ | $4.38 \pm 0.99$ |

The morphology changes of surface area and micropore volume can support the hypothesis that Ni on 1-step Ni@Silicalite-1 are more on the surface of the catalyst. Since the severe coke formation is usually formed on the outer surface of the catalyst, after calcination of coke, the crystalline material is not affected and remains high in surface area and

micropore volume. These phenomena arise from the formation mechanism during zeolite synthesis. The use of Ni solution added dropwise into the mother liquor and then transfer to autoclave for zeolite synthesis by hydrothermal synthesis. At the stage of mother liquor preparation, some precipitates form which might be the  $\text{Ni}(\text{OH})_2$  from the precipitation reaction, even the alkalinity of the solution is high, but they might not be dissolved well during the hydrothermal synthesis. Also, in the hydrothermal synthesis, the nucleation process in zeolite formation is not guaranteed to include Ni(II) ions in the metastable gel. The trace amount of Ni(II) ions can be repelled out of the gel formation around the SDAs, the outside-stay phenomena lead to the deposition of Ni on the outer surface, not encapsulate inside zeolite, even the size of particle is not large but severe coke formation can be occurred.

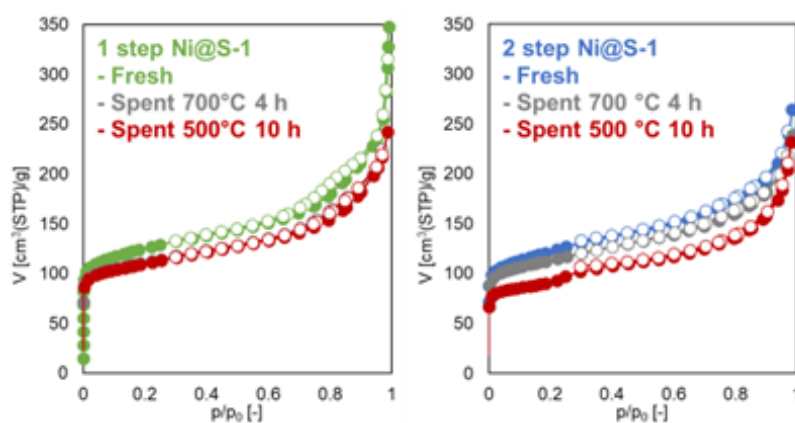


**Figure 2.18.**  $\text{N}_2$  physisorption of 1-step vs 2-step Ni@Silicalite-1 in different conditions.

**Table 2.4.** surface area and micropore volume change after ESR reaction at 500 °C 10 hours.

| Sample       | Surface area                              | Micropore Volume                       |
|--------------|---|--|
| Fresh / 10 h | ( $\text{m}^2/\text{g}_{\text{sample}}$ ) | ( $\text{cm}^3(\text{STP})/\text{g}$ ) |
| 1-step       | 458.93 / 413.49                           | 0.1335 / 0.1212                        |
| 2-step       | 447.33 / 428.06                           | 0.1396 / 0.1117                        |

### 2.3.2.2. Precursor calcination and porosity

Since the route of Ni@Silicalite-1 synthesis is chosen to be 2 steps of preparation. From the results in the previous section, the utilization of solid precursor can help secure Ni sites encapsulated inside zeolite particles. In this section, the different conditions of precursor used in the preparation were investigated to elucidate the proper choice of precursor used in zeolite preparation. There are three precursor conditions for this evaluation, the preparation condition of each precursor was listed in Table 2.5. The same condition of zeolite

hydrothermal synthesis was utilized as a control parameter,  $H_2O:Si = 50$ , hydrothermal synthesis temperature of  $100\text{ }^\circ\text{C}$ , and hydrothermal synthesis time of 72 hours.

**Table 2.5.** Catalysts preparation conditions of the catalyst used in this experiment.

| Ni@Silicalite-1 catalyst                             |             | P_NC         | P_C      | NP_C       |
|--|-------------|--------------|----------|------------|
| NiPS   | porosity    | porous       | porous   | Non-porous |
|  | calcination | non-calcined | calcined | calcined   |
| Ni loading (wt %)                                    |             | 1.0          | 1.15     | 0.96       |
| Coke formation after $700\text{ }^\circ\text{C}$ ESR |             | 14.00        | 6.00     | 5.15       |

The obtained catalysts were used in the ESR catalytic reaction test to evaluate the catalytic performance at  $700\text{ }^\circ\text{C}$  for 4 h. This reaction temperature was selected for the investigation since it is the temperature that can almost cut out the complexity of reaction pathways in kinetic conditions. The coke formation can be a criterion, with the thermal stability of the zeolite. The activity results were reported as shown in Figure 2.19 with the weight of coke formation on these spent catalysts.

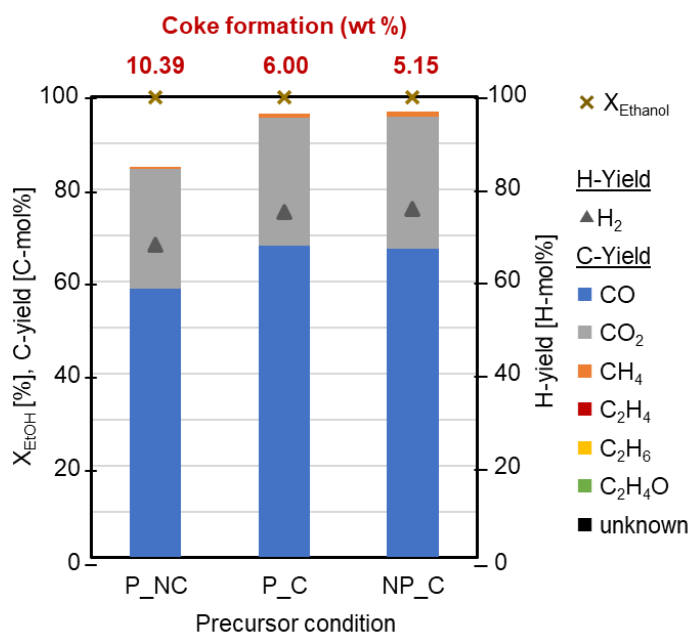


**Figure 2.19.** ESR activity of Ni@Silicalite-1 prepared with different precursor with the amount of coke formation.

From the results, it is clearly observed that the utilization of non-calcined Ni-PS precursors provide the least Ni activity towards ESR with the highest amount of coke formation among three catalysts. Meaning that, the non-calcined precursor cannot stabilize the Ni in the zeolite framework during the hydrothermal synthesis, which might dissolve well

in alkali solution, yielding non encapsulation Ni particles. Calcination of precursors can help retain Ni to stay inside the zeolite structure, reaction activity and coke formation is not far from each other, so other properties should be verified to confirm the suitable precursors in the preparation. Zeolite morphology, including TEM images (Figure 2.20) and N<sub>2</sub> physisorption (Figure 2.21 and Table 2.6) are investigated for this purpose. The unincorporated NiPS precursor is clearly observed on the zeolite surface. This formation is also observed on the N<sub>2</sub> physisorption isotherm as shown in Figure 2.21.

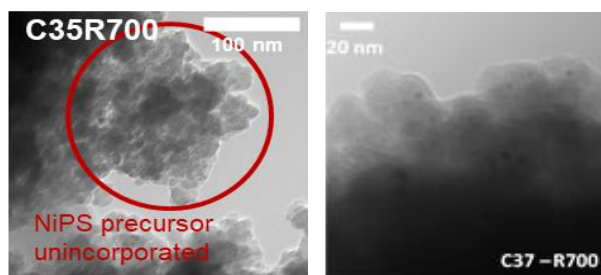


**Figure 2.20.** TEM images of Ni@Silicalite-1 prepared with calcined Ni-PS precursors

Left – porous precursor, Right – non-calcined precursor.

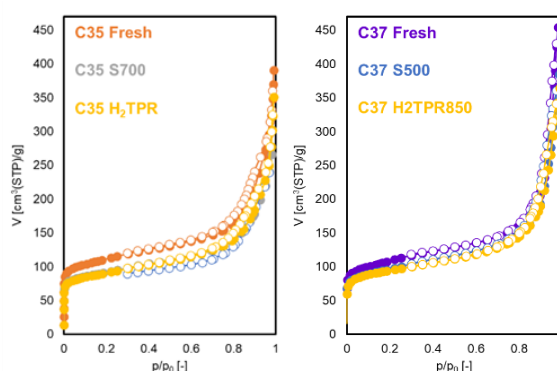


**Figure 2.21.** N<sub>2</sub> physisorption of Ni@Silicalite-1 prepared with calcined Ni-PS precursors

Left – porous precursor, Right – non-calcined precursor.

This silica portion presence in Ni@Silicalite-1 affects the thermal stability of the zeolite. The calcined porous precursor used in the synthesis of Ni@Silicalite-1 leads to the presence of amorphous silica which leads to higher in both coke formation and structure deterioration.

**Table 2.6.** Surface area and micropore volume change after ESR reaction at 700 °C 4 hours.

| Sample List  | Surface area<br>(cm <sup>2</sup> /g <sub>sample</sub> ) |              | Micropore Volume<br>(cm <sup>3</sup> (STP)/g) |              |
|--------------|---|--------------|---|--------------|
|              | Fresh   | Spent 700 °C | Fresh   | Spent 700 °C |
| Ni@S-1_P_C   | 409.075   | 308.910      | 0.1143  | 0.1015       |
| Ni@S-1:_NP_C | 393.844   | 340.354      | 0.1037  | 0.0812       |

### 2.3.2.3. Precursor dissolution: dissolution time

The solubility of Ni-PS precursor is a critical parameter to control the location of Ni in the hydrothermal synthesis of zeolite and also crystallinity of the sample. Too much dissolution of precursor, from its low stability in the mother liquor which is an alkaline solution are verified. The precursor that cannot dissolve properly also presents the portion of amorphous silica, which also affects the catalyst morphology and thermal stability.

Ni-PS precursor used in the preparation of Ni@Silicalite-1 is considered as both Ni and Si source of the catalyst, the dissolution affects the species in a solution for hydrothermal synthesis, then the zeolite nucleation and recrystallization. The difference in nucleation and crystallization yields the different zeolite formation, therefore, the different catalyst properties will be obtained. In this section, the dissolubility of calcine Ni-PS precursor was tasted as shown in Figure 2.22.

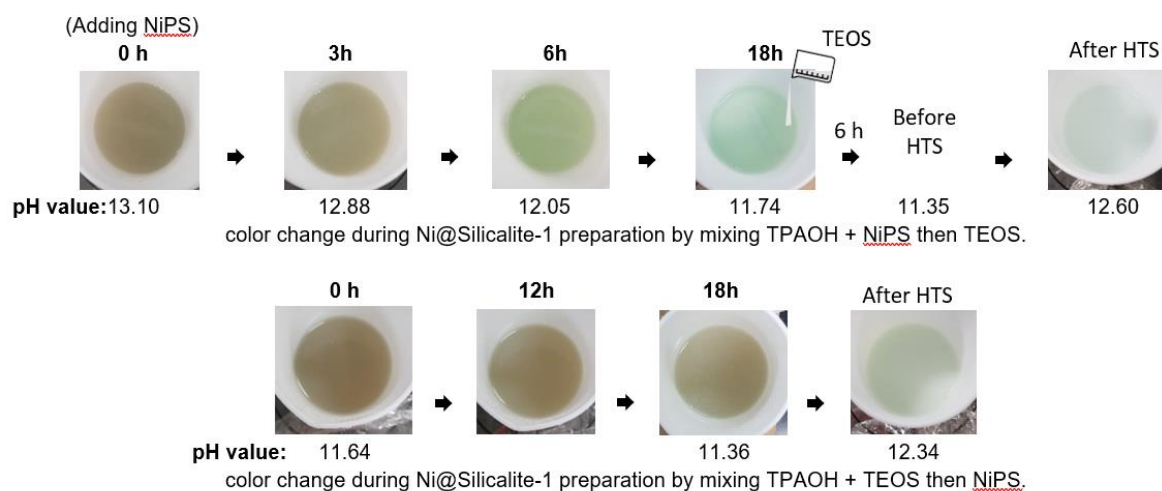


**Figure 2.22.** The mother liquor solution appearance in the observation on dissolution time of precursor.

From the dissolution time experiment, there are 2 possibilities of the Ni-PS dissolution since in the mother liquor state of preparation which are (1) partial dissolution as we still observed the green-gray color of the solution and (2) complete dissolution as observed in a clear green solution, which is the same appearance as the case of 1-step Ni@Silicalite-1. After hydrothermal synthesis, the zeolite can form but a slight difference is observed, including the pH after HTS which could reflect the degree of crystallization. Compared with the 1-step Ni@Silicalite-1, the partial dissolution of Ni-PS is preferable in 2-step Ni@Silicalite-1 preparation in order to secure more Ni inside zeolite structure are an encapsulation structure. The optimization of dissolution time is a crucial parameter for further study.



### 2.3.3. Effect of hydrothermal synthesis condition towards zeolite formation

#### 2.3.3.1. Effect of $H_2O:Si$ ratio

Besides the state of precursor use in the Ni@Silicalite-1 preparation that affects the zeolite formation, then obtained catalyst properties. Hydrothermal synthesis condition directly affects the zeolite formation mechanism. In this section, the difference in  $H_2O:Si$  ratio in mother liquor preparation was studied towards the obtained catalyst properties. The preliminary results, not shown here, suggest that the high alkalinity with less water in the system leads to the production of catalyst with more non-encapsulated Ni. The ratio of 50 and 100 was investigated. The obtained catalysts were investigated in ESR reaction at 700 °C for activity evaluation. The results suggest that the diluted system could provide a better encapsulation of Ni inside zeolite, with better crystallinity (lower structure deterioration). This can be the effect from the lower alkalinity controlling the dissolution of precursor, the speed of nucleation and crystallization, the role of water in gel stabilization during zeolite formation.

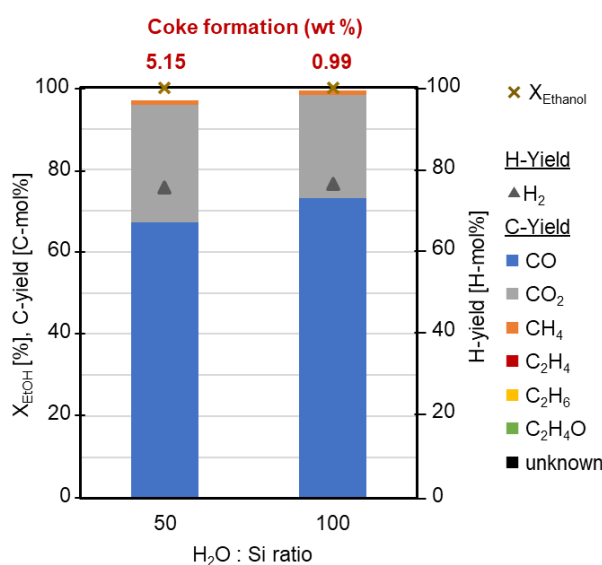


**Figure 2.23.** ESR activity of Ni@Silicalite-1 prepared with different  $H_2O:Si$  ratio of mother liquor with the amount of coke formation

**Table 2.7.** Surface area and micropore volume change after ESR reaction at 700 °C 4 hours.

| Sample List | Surface area<br>(cm <sup>2</sup> /g <sub>sample</sub> ) |              | Micropore Volume<br>(cm <sup>3</sup> (STP)/g) |              |
|-------------|---|--------------|---|--------------|
|             | Fresh   | Spent 700 °C | Fresh   | Spent 700 °C |
| Ni@S-1_50   | 393.844   | 340.354      | 0.1037  | 0.0812       |
| Ni@S-1_100  | 447.330   | 421.064      | 0.1396  | 0.1321       |

### 2.3.3.2. Effect of hydrothermal synthesis temperature

The hydrothermal synthesis temperature also makes a greater effect towards nucleation and crystallization. The impact of hydrothermal synthesis temperature on the catalyst's properties was investigated. With general knowledge of zeolite synthesis, the higher hydrothermal synthesis shortens crystallization time of the zeolite, from making a denser phase under hydrothermal synthesis condition. But this system utilized water as a solvent, the critical point of structure stabilization with the temperature needed to be combined consideration. The study explored the temperature of 100 and 150 °C. Subsequently, the catalysts produced were assessed for activity in the ESR reaction at 700 °C.

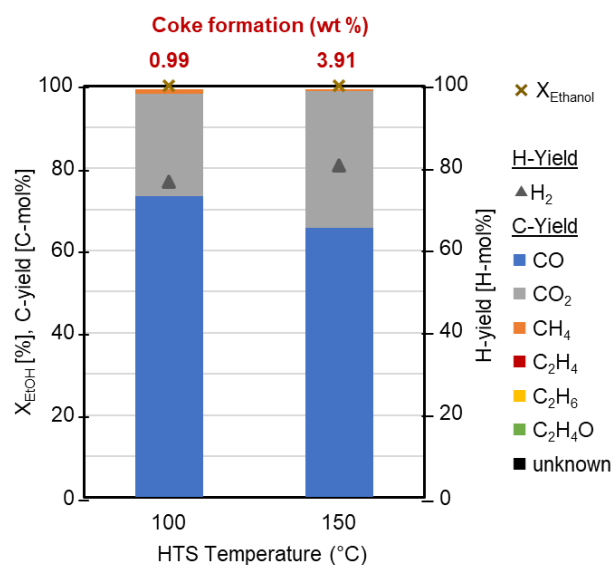


**Figure 2.24.** ESR activity of Ni@Silicalite-1 prepared with different hydrothermal synthesis temperature with the amount of coke formation.

Considering the ESR activity of the prepared catalysts, the hydrothermal synthesis temperature has a weaker effect towards the hydrothermal synthesis of 2-step Ni@Silicalite-1 comparing to the  $\text{H}_2\text{O}:\text{Si}$  ratio since the small difference of activity and coke formation were obtained. The high hydrothermal synthesis temperature also leads to the less active Ni with the configuration of outside instead of encapsulating inside zeolite structure. The effect of high temperature that affects the crystallization speed might be too fast. Some parts are repelled out of the structure, but it is still fast enough to keep some part of Ni inside. This high thermal synthesis might be used, but the hydrothermal synthesis time should be shortened.

In the summary of this chapter, Ni encapsulated Silicalite-1 catalyst (Ni@Silicalite-1) can be prepared with hydrothermal synthesis. The expected properties of the Ni nanoparticles encapsulated inside zeolite, including small size, well-dispersed, and being encapsulated within the high crystallinity zeolite. The properties to be avoided are the large Ni particles which are prone to agglomeration and ease of coke formation, Ni that stays on the zeolite surface, and the amorphous silica that still remains after hydrothermal synthesis which lowers the crystallinity of zeolite.

There are a lot of parameters that affect the formation to obtain encapsulated catalyst. The preparation can be prepared with several Ni precursors, such as, liquid precursor as Ni solution, and solid precursor as Ni-PS/SiO<sub>2</sub>. The preparation using solid precursor helps securing Ni active sites to be encapsulated within zeolite structures than the system using free Ni ions in the mother liquor solution. The state of Ni precursor present in the solution is crucial for encapsulating Ni since it determines the solid and ion concentration of both Si and Ni, which affects the formation of zeolite since the stage of nucleation, then crystallization. The comparison of porosity and calcination of the precursor were investigated. Calcination of the precursor provides a stronger structure for securing Ni to be crystallized within zeolite particles, furthermore, the non-porous precursor can further secure the Ni with the less coexistence of amorphous silica in the obtained zeolite. Too much dissolution of precursors leads to free Ni<sup>2+</sup> ions which are repelled to the outside of the zeolite structure. So far, the encapsulation catalyst prepared with calcined non-porous precursor is the best condition within this study. However, the optimum dissolution of Ni-PS precursor is needed to be verified in the future to obtain the better encapsulation structure of Ni, which can increase the catalytic activity, lower coke formation and can tolerate the severe steam and temperature conditions from its high crystallinity.

Besides the precursor condition, which is the determination of species in mother liquor, the next section was the investigation of hydrothermal synthesis condition, including H<sub>2</sub>O:Si ratio (concentration of species and alkalinity of the mother liquor), and hydrothermal synthesis temperature which are directly affected how fast of the solution for equilibrating themselves and nucleation is triggered, and crystals are grown. The lower driving force, i.e., slower nucleation and crystallization rate, from the more diluted system with lower alkalinity and lower hydrolysis temperature helps the Ni to be more embraced within zeolite crystal, either or both of solid precursors as core-shell growth and free nickel and silicon ions in the mother liquor solution. It can also improve the crystallinity of the sample from the observed higher surface area and micropore volume of the synthesized zeolite and maintain its

structure well after the reaction test. On the other hand, the increasing of hydrothermal synthesis temperature to 150 °C, can provide a good crystallinity of zeolite. But it might lead to redissolution and crystallization that make some part of Ni to be on the surface of the good crystalline zeolite, leading to good activity with the presence of coke formation.

In conclusion, various parameters in the synthesis procedure are all affected toward the properties of encapsulation structure of Ni inside Silicalite-1, in terms of how well Ni is encapsulated, and how high of the sample crystallinity. The condition optimization in zeolite mother liquor preparation (for the dissolution of Ni-PS precursor; concentration as solid and ions), and proper hydrothermal synthesis (of the mother liquor solution obtained after dissolution) must be validated, to achieve the perfect encapsulation structure of Ni nanoparticles inside zeolite.

## Chapter 3 : Study of reaction mechanism and pathway of ethanol steam reforming on Ni over Silicalite-1

### 3.1. Introduction

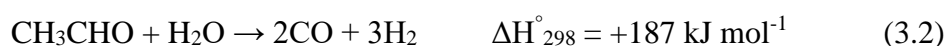
#### 3.1.1. Ethanol steam reforming reaction pathway

To design and select the proper catalyst in ESR, the understanding of reaction mechanism and pathway is very important to know all the possibilities of the reactions that occur in the reaction system. Combining with the knowledge in physical and chemical properties of the material, we can select and design the catalysts that intensify the desired reaction pathway of ethanol steam reforming and reduce the possibility of the unwanted by-products formation. The research has outlined the routes of reactions involved in ethanol steam reforming using transition metals that are non-noble [32]. The expected sequence of reactions on the catalysts during steam reforming consists of several stages: ethanol dehydrogenation leading to acetaldehyde formation, followed by acetaldehyde steam reforming and subsequently the water-gas shift reaction. At lower reaction temperatures, ethanol dehydrogenation predominantly yields acetaldehyde. As the temperature increases, all reactions along the steam reforming pathway are enhanced. Ethanol steam reforming pathways start to proceed at the temperature higher than 500 °C [66].

Dehydrogenation:



Acetaldehyde steam reforming:

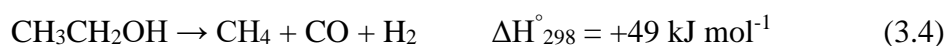


Water gas shift reaction:



In addition to the described reaction mechanism, several chemical reactions may take place during this process. Ethanol breakdown and ethanol removal are two common reactions. Ethanol breakdown results in the production of methane, carbon monoxide, and hydrogen. On the other hand, ethanol dehydration, which tends to favor acidic sites on the catalyst, leads to the formation of ethylene, a precursor to coke, and water. A part of acetaldehyde obtained from ethanol dehydrogenation can be either further decomposed to methane and carbon monoxide or combined to form acetone in a reaction system.

Ethanol decomposition:



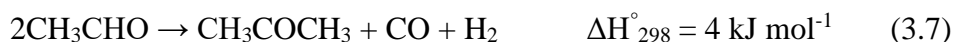
Ethanol dehydration:



Acetaldehyde decomposition:



Acetone formation:



The main issue of ESR catalysts is the deactivation, primarily by coke formation on the catalyst, which controls by the reaction mechanism and pathway. Carbon monoxide (CO), methane (CH<sub>4</sub>), and assorted hydrocarbon species (C<sub>x</sub>H<sub>y</sub>) within the reaction media are recognized as coke precursors, ultimately leading to catalyst deactivation. Moreover, specific reactions involving hydrogen gas can reduce the hydrogen yield, as seen in the methanation reaction. The coke formation can be formed from ethylene decomposition, Boudouard reaction, and methane decomposition. Boudouard reaction is dominant at temperature 400–700 °C. On the other hand, methane decomposition is dominant at temperatures above 600 °C.

Methanation of CO:



Methanation of CO<sub>2</sub>:



Ethylene decomposition:



Boudouard reaction (CO disproportionation):



Methane decomposition:



Ethylene polymerization



Ethylene steam reforming



An alternative pathway for highly active metals like Ni as their strong C-C bond cleavage ability, it primarily involves ethanol decomposition, with a minor ethanol dehydrogenation and subsequent acetaldehyde decomposition. This pathway results in the

formation of CH<sub>4</sub>, CO, and H<sub>2</sub> species. CH<sub>4</sub> is then subject to further reactions through methane steam reforming, while CO undergoes the water-gas shift reaction. The activation of stable CH<sub>4</sub> is more challenging than that of C<sub>2</sub> species, requiring higher reaction temperatures. Consequently, at lower reaction temperatures, the produced CH<sub>4</sub> remains in the reaction medium.

Aside from the coke formation pathway, some catalysts provide oxygen mobility on the surface. The operating condition that dilutes the coke precursors in the reaction media or providing more oxidation possibilities, for example, the condition with high oxygen or steam. The coke reduction pathways as coke gasification can be proceeded.

Coke gasification:



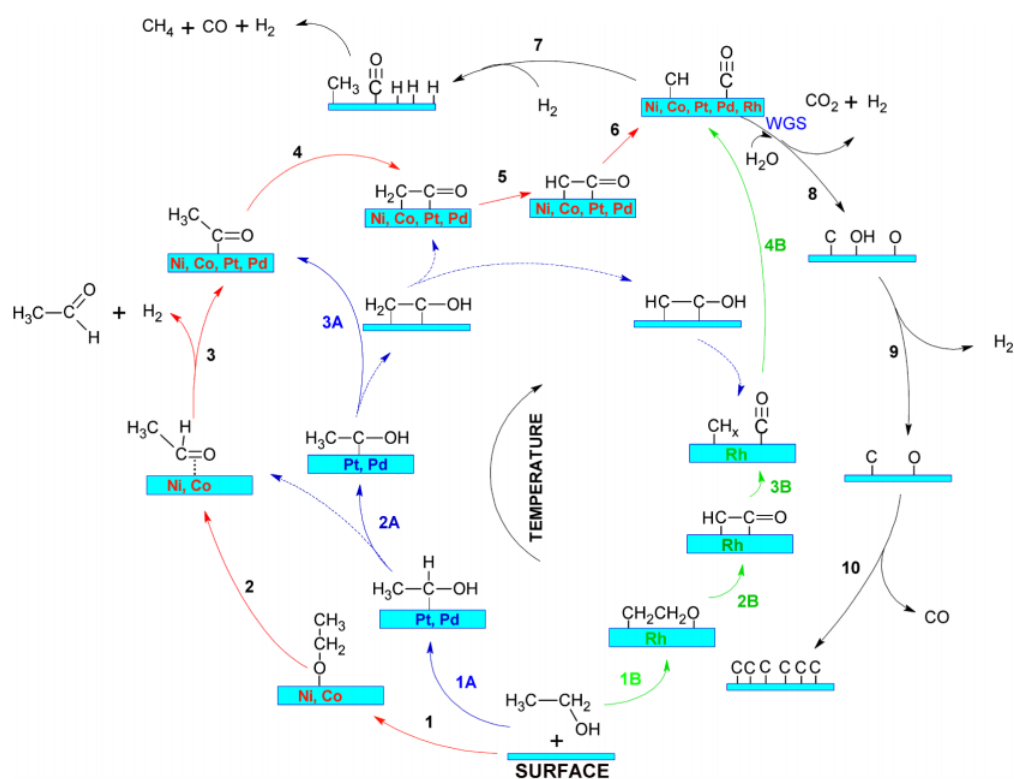
### 3.1.2. Ethanol steam reforming reaction mechanism on Ni-zeolite catalyst

Zanchet et al. summarize the reaction pathways on different metal active sites. Taking a scope on the Ni active sites, starting with ethanol activation by the cleavage of OH bond at hydroxyl group of ethanol, absorbed on the Ni surface. With the increasing in temperature, dehydrogenation proceeds forming intermediates including acetaldehyde (CH<sub>3</sub>CHO\*), acetyl (CH<sub>3</sub>C\*O), ketene (\*CH<sub>2</sub>C\*O), and ketenyl (\*CHC\*O), respectively. The C-C bond cleavage is occurred at the stage of ketenyl (highly dehydrogenated species) adsorbed on Ni surface, then hydrogenation/dehydrogenation of CH<sub>x</sub>\*, water activation taking into the account of WGS, and then oxidization of C\* species, which is a coke precursor. The critical step for a stable catalyst is to form a single-C intermediate, CH<sub>x</sub>\*, which can further react or transform into CH<sub>4</sub> or C\*. For the case of Ni, the formation of CH<sub>4</sub> from CH<sub>x</sub>\* occurs at lower temperatures than decomposition to C\* species, due to the lower reactivity towards oxygen. Another important property of the ESR catalyst is the activation of water to oxidize the C\* to CO or CO<sub>2</sub>. These critical steps are both favored at a low-coordinated active site, i.e., a smaller metal particle site [67]. That is the reason why the size of the active metal needs to be considered in catalyst design.

Tripodi et al. studied the simulation of reaction mechanism of ethanol steam reforming on 9wt% K<sub>2</sub>O/10wt%Ni/ZrO<sub>2</sub> using ASPEN and MATLAB [68]. The study suggests that the concentration of water in ethanol mixture (EtOH:H<sub>2</sub>O up to 1:5) enhances the reforming of both ethanol and coke. The higher reaction temperature favor acetaldehyde reforming with less effective towards ethylene reforming. The last point is about the basic

promoter towards the reaction sequence. The basicity affects the reaction sequence of ethanol-to-ethylene-to-coke but interferes less with acetaldehyde reforming.

Hua Song also summarizes the catalytic hydrogen production from bioethanol in several points. When ethanol and water are dissociative adsorbed, they form ethoxide elements and hydroxyl groups, respectively. The active metal helps catalyze the breaking of C-C bonds and the creation of individual carbon species. Bioethanol steam reforming reaction might occur at the metal-support interface, where the active metal meets the oxide support, potentially involving the oxide support in supplying lattice oxygen to aid in oxidizing the carbon species. The oxygen vacancies are automatically refilled by the hydroxyl group from the adsorbed water. The higher metal dispersion in the catalyst favors ethanol adsorption and creates additional metal/oxide interaction points along with breaking C-C bonds to enhance accessibility.



“Red, blue, and green colors indicate main routes on Ni or Co, Pt or Pd, and Rh, respectively; dashed lines are secondary routes.

**Figure 3.1.** ESR reaction pathways as a function of temperature for different metal surfaces [67].



### 3.2. Experimental

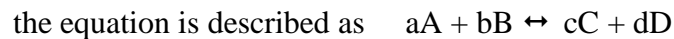
In this section, the different product composition in the reaction media is the main parameters that are observed and discussed. The study is divided into the composition obtained from calculation and from experiments. Thermodynamic equilibrium is referred to a state in which a system has reached a stable and unchanging condition with respect to its macroscopic properties, i.e., no net change observed in temperature, pressure, density, composition, or other thermodynamic variables.

For thermodynamic equilibrium composition calculation in each reaction temperature, the constant chemical composition of each species is assumed, and no net chemical reaction occurred. As we known from the literature that, ethanol steam reforming reaction system consists of various reaction pathways, and each reaction has its own equilibrium constant. The reaction system is assumed to follow these conditions.

- (1) In real experiments, we also know that equilibrium is obtained generally at high temperatures. Therefore, the situation in a high temperature is assumed for the ease of understanding and calculation.
- (2) Assuming that all ethanol and steam are converted into CO<sub>2</sub> and H<sub>2</sub> as in the total ESR reaction, therefore, the starting composition in thermodynamic calculation is assumed to be 1:3 of CO<sub>2</sub>:H<sub>2</sub>. Assuming the partial pressure of CO<sub>2</sub> is 0.25 and H<sub>2</sub> is 0.75.
- (3) The possible reactions of CO<sub>2</sub> and H<sub>2</sub> in equilibrium are listed as these two following equations:



The equilibrium constant is to calculate using the series of equations:



The equilibrium constant, K, can be expressed as partial pressure or Gibbs free energy expression.

$$K = \frac{\left(\frac{P_C}{P^\circ}\right)^c \left(\frac{P_D}{P^\circ}\right)^d}{\left(\frac{P_A}{P^\circ}\right)^a \left(\frac{P_B}{P^\circ}\right)^b} = \exp\left(-\frac{\Delta G_R}{RT}\right) \quad (3.18)$$

With Gibbs Free Energy expression in a relation with reaction's entropy and enthalpy, we can rewrite the expression and determine equilibrium constant,  $K$ , in step (i) and (ii).

$$\begin{aligned} \Delta G_R &= \Delta H_R - T\Delta S_R, \quad dG = -SdT + Vdp \\ \frac{d}{dT} \left( \frac{\Delta G_R}{RT} \right) &= \frac{T \frac{d\Delta G_R}{dT} - \Delta G_R}{RT^2} = \frac{-T\Delta S_R - (\Delta H_R - T\Delta S_R)}{RT^2} = -\frac{\Delta H_R}{RT^2} \\ \ln K &= \ln K^{\circ} + \int_{T_0}^T \frac{\Delta H_R}{RT^2} dT = \ln K^{\circ} + \frac{(\Delta H_R^{\circ} - \Delta C_{pR,A}T_0 - \Delta C_{pR,B}T_0^2/2 - \Delta C_{pR,C}T_0^3/3 - \Delta C_{pR,D}T_0^4/4)}{R} \left( -\frac{1}{T} + \frac{1}{T_0} \right) + \frac{\Delta C_{pR,A}}{R} \ln \left( \frac{T}{T_0} \right) + \frac{\Delta C_{pR,B}}{2R} (T - T_0) + \frac{\Delta C_{pR,C}}{6R} (T^2 - T_0^2) + \frac{\Delta C_{pR,D}}{12R} (T^3 - T_0^3) \end{aligned} \quad (3.19)$$

### 3.3. Results and discussion

By Searching for physical property values of each substance, stoichiometric relations and Standard reaction enthalpy, Gibbs energy, entropy, specific heat capacity, substitutes the values, then equilibrium constant can be further used in thermodynamic equilibrium composition calculation, and these obtained values can be compared between two methods of calculation.

The reaction extent can be calculated for forecast the composition at equilibrium. For example, the reaction extent for  $\text{CO}_2$  can be written as the following relation:

$$K_{(ii)} = \frac{p_{\text{H}_2\text{O}}^{eq} \cdot p_{\text{CO}}^{eq}}{p_{\text{H}_2}^{eq} \cdot p_{\text{CO}_2}^{eq}} = \frac{(0.25\xi_{eq})^2}{0.25(1-\xi_{eq}) \times (0.75-0.25\xi_{eq})} \quad (3.20)$$

At particular temperatures, the calculated equilibrium constant is obtained from the mathematical relation as mentioned above. With a given initial composition, the extent of reaction in equilibrium can be calculated at that reaction temperature. The obtained extent of reaction is further used to evaluate the composition of species in thermodynamic equilibrium at the particular temperature.

$$n_{eq,i} = \xi_{eq} \nu_i + n_{initial,i} \quad (3.21)$$

This reaction extent can be utilized in the calculation of equilibrium partial pressure with the given initial partial pressure of the system. The obtained equilibrium partial pressure of  $\text{CH}_4$ ,  $\text{CO}_2$ ,  $\text{CO}$ ,  $\text{H}_2\text{O}$ , and  $\text{H}_2$  from calculation are the values which will be mentioned and discussed in section 3.3.1.

### 3.3.1. Calculation of chemical equilibrium concentration of ESR

The calculated partial pressure under thermodynamic equilibrium conditions with the assumption of ideal ESR from reaction temperature of 450 – 850 °C was shown in Figure 3.2. From the calculation, the reaction is in kinetic mode, the state of the reaction that the composition in the reaction media keep changing due to the various reaction pathway. These gradually increase or decrease are starting to a flat, i.e., no change of the composition or partial pressure in the reaction system, at the temperature above 650 °C. The species including hydrogen in the structure are easier to be in an equilibrium state than carbon monoxide and carbon dioxide. With the change of inert gas flow in the system, the concentration of the system might differ, but they will be in the same manner of equilibrate their pressure through different pathways and be back at the equilibrium concentration of the individual system at the same reaction temperature. This information is utilized to help judge the proper temperature for the purpose of catalytic investigation for ESR. The clear difference in reaction pathway should be evaluated in a kinetic region, the performance will be deviated between catalyst in the region that the large change (high slope of the concentration change) is observed. On the other hand, to evaluate the stability of the catalyst as a sole effect, it should be done in a temperature that reach thermodynamic equilibrium, so that the results can be clearly determined without confusion of changes obtained by the too many pathways existing in the reaction media.

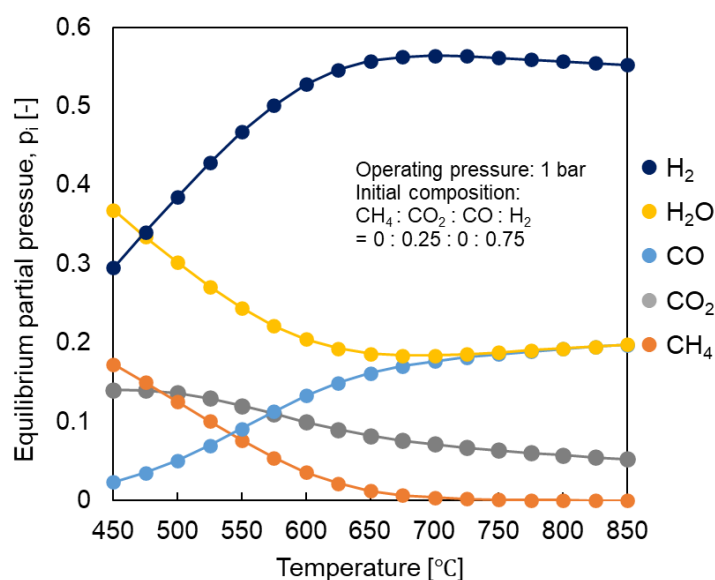


**Figure 3.2.** Calculated equilibrium partial pressure of ESR with the assumption of 1:3 molar ratio of CO<sub>2</sub>:H<sub>2</sub> product obtained.

To compare experimental outcomes within the temperature range of 500 to 800 °C to the calculation values, assuming complete conversion of reactants. The equilibrium state of the reaction environment reflects a balance between two concurrent reactions, steam reforming and water-gas shift, both achieving 100% carbon recovery without the formation of coke. The thermodynamic equilibrium composition of our system can be calculated and represented as in Figure 3.3. with the condition that 100 % ethanol conversion. This calculated data can be suitable for comparison in the case of full conversion only. Therefore, this data might be suitable for comparison in the high reaction temperature of 700 – 800 °C. For the case that reaction is still under kinetic control conditions, variation in kinetic parameter affects the chemical kinetics of the reaction, different conversion and product selectivity are obtained. Therefore, for the case of the low reaction temperature that ethanol conversion is not reached 100%, the comparison might be made in the ratio of product selectivity, etc.

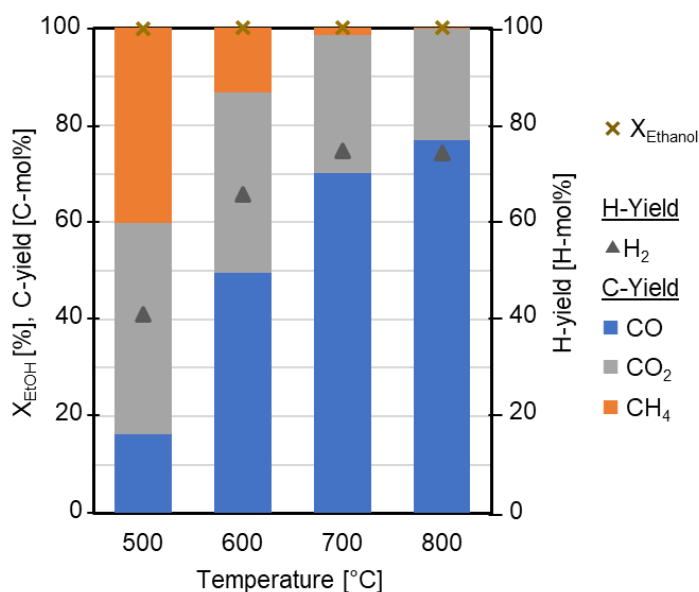


**Figure 3.3.** Calculated thermodynamic equilibrium composition of C1 species with hydrogen yield at temperature of 500 – 800 °C.

### 3.3.2. Effect of different reaction temperature towards ESR reaction mechanism on Ni over Silicalite-1 catalyst

Reaction temperature plays an important role in the reaction mechanism of ethanol steam reforming reaction. The consideration on reaction activity must be considered on both thermodynamic (mainly the effect of temperature) and kinetic (with the consideration of catalyst active site) perspectives. Figure 3.4 shows the catalytic activity results on Silicalite-1 and Ni over Silicalite-1 (Ni@Silicalite-1 as a representative)

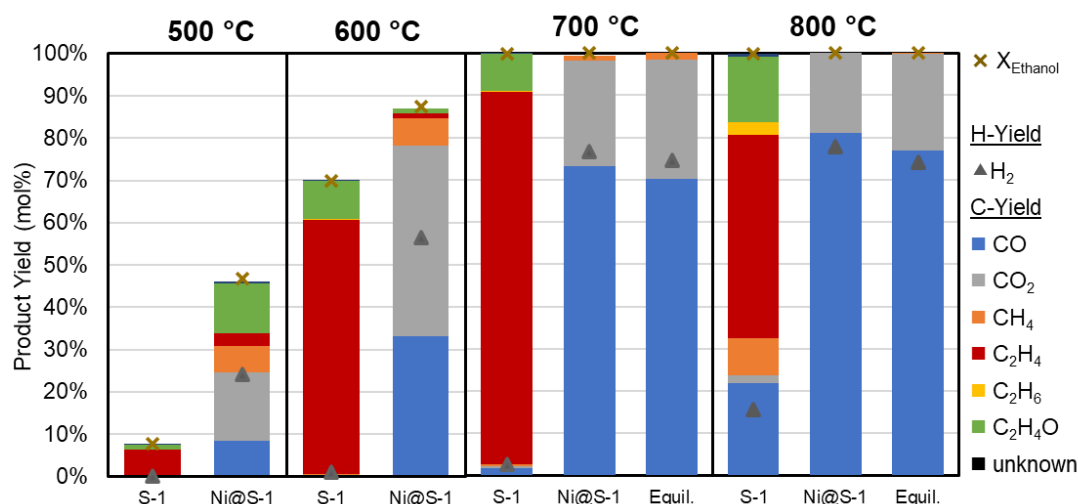


**Figure 3.4.** The catalytic activity results on Silicalite-1 and Ni over Silicalite-1 (Ni@Silicalite-1 as a representative) in the different reaction temperature.

At 500 °C, it is quite low temperature to thermodynamically activate all of the reactants in ethanol steam reforming reaction, moreover, our active metal is Nickel which requires a high temperature to proceed the catalytic function. Consider the case of the Silicalite-1 support without Ni active sites, conversion of ethanol is less than 10% and mainly converted to ethylene, and some acetaldehyde. These two products indicate the dehydration of ethanol to ethylene, where C-O bonds in ethanol are being cleavage, which can be catalyzed on the weak acidity of Si-OH on the Silicalite-1 surface. The minor pathway is dehydrogenation of ethanol to form acetaldehyde, but this pathway is a very small fraction since the production of hydrogen is extremely unnoticeable. With the presence of Ni active sites, as in a kinetic control condition, ethanol and water molecules are both activated for the reaction. Ethanol can be converted into different products, including carbon monoxide, carbon dioxide, methane, ethylene, acetaldehyde, with coke formation. Ethanol goes through dehydrogenation pathway to form acetaldehyde, with the ability to activate water molecules, therefore, C-C bonds cleavage via the steam reforming with subsequent water-gas shift reaction can occur and obtain CO<sub>2</sub> and H<sub>2</sub>. The remaining part of CH<sub>x</sub>\* produced is reacted

with hydrogen and obtained  $\text{CH}_4$ . The capability of Ni at this temperature is still limited, therefore, some C2 species remain. At this temperature, it is very active for coke precursors to form solid carbon since there is a lack of oxidative species in the reaction system. The remains C2, ethylene might go through adsorption and polymerization to form coke or dissociation to diffuse C and precipitation to filamentous coke.

At 600 °C, the temperature is sufficient to activate most reactants, ethanol, and water, thermodynamically since without the presence of Ni active sites, as the high ethanol conversion are obtained. The conversion at this temperature is not far different from the result at 700 °C since it is near to thermodynamic equilibrium of the reaction. The reaction mechanism is in the same manner as in the pure support at 500 °C. The difference is observed in the case with Ni active site. The conversion does not increase that much compared to the reaction on pure Silicalite-1, but the conversion to C1 product portion is a lot higher than the reaction in 500 °C. There is no coke formation even with the high concentration of C2 in the reaction media. It is confirmed that coke formation occurs in the condition of Ni exist. The higher reaction temperature accelerates the dehydrogenation of ethanol to form acetaldehyde until the completion of C-C bonds dissociation, and water-gas shift reaction. At this temperature, the coke formation is observed on the spent catalyst, but the pathway of coke formation might be different from the lower reaction temperature from the different coke precursor in the reaction media that are higher in C1 than C2 species.

For 700 °C, Complete ethanol is obtained on the pure support, without Ni active site. This implies a high enough temperature for ethanol activation. They change to ethylene through dehydration and acetaldehyde by dehydrogenation. Auto Steam reforming pathways are also enhanced in this temperature, a small portion of C1 product is obtained for pure Silicalite-1. Ethanol can undergo thermal decomposition to form  $\text{CH}_4$  and CO. Since the ethanol are all activated with the effect of temperature, with the presence of Ni, all of the activated reactants can convert into C1, therefore, there is an absence of C2 species. In this case, the obtained coke formation is produced by Boudouard reaction, where CO is consumed to produce  $\text{CO}_2$  along with coke. More hydrogen was generated than predicted by the equilibrium composition calculation, primarily because coke was formed through the decomposition of ethylene or methane pathways.

For 800 °C, the temperature is high enough to activate reactant and promote various reaction pathways, including thermal decomposition and auto steam reforming of ethanol and also C2 intermediates, so that a larger portion of C1 products is obtained. Thermal ethanol dehydrogenation is intensified more than dehydration; therefore, the acetaldehyde portion

becomes larger at this reaction temperature. Thermal decomposition of acetaldehyde is also possible to occur, according to the observation of  $\text{CH}_4$  and  $\text{CO}$  production. There is no coke formation occur on the spent catalyst, which is the result of enhanced steam reforming, water-gas shift, and coke gasification pathways (lower coke precursor and coke elimination).

### 3.3.3. Proposed reaction mechanism on Ni@Silicalite-1

In order to propose the reaction mechanism on Ni@Silicalite-1, the catalytic component of the catalyst must be listed and identified. Mostly, the catalyst material contains active sites, and the supports. The active sites are normally the active metals used for improving catalytic activity by enhancing reactants adsorption and conversion. For the supports, metal oxides are normally used with inert properties towards the reaction. But there are a lot of studies that the support materials help improving the catalytic activity by metal-support effects, improving the metal-support interaction, improving redox properties, or providing oxygen mobility on the supports promoting the oxidation of the unwanted species. In our case, Ni@Silicalite-1 catalyst, the main active metal function in the reaction is Ni. The active Ni in ESR reaction is in the form of Ni metal ( $\text{Ni}^0$ ). Silicalite-1, Pure Silica MFI-type zeolite is used as a support material. Therefore, in this section, the proposed mechanism will be discussed on the Ni active metal, Silicalite-1 support, and their surface properties which affect the reaction. In ethanol steam reforming, Ni active sites have a role as C-C bond cleavage, enhance steam reforming pathway, and coke formation site. For Silicalite-1, ethanol and water molecules can be absorbed on the defect sites. The following discussion will be about these phenomena.

#### 3.3.3.1. Ethanol adsorption and its surface reaction

##### *Surface defect sites of Silicalite-1*

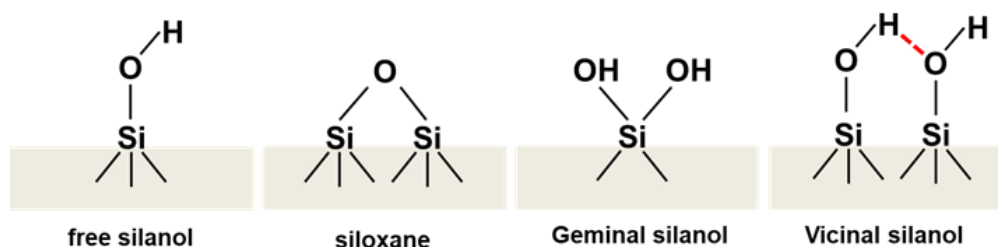


**Figure 3.5.** Possible defect silanol on zeolite surface.

On the surface of zeolite or amorphous silica, it contains the defect sites which is a position of non-perfect crystalline structure. The electronic structure of these defect sites can

be absorbed or reacted with attached species. On zeolite or amorphous silica surface, there are four types of general defects found, including free silanol, siloxane, geminal silanol, and vicinal silanol, the defect site structure is shown in Figure 3.5. All of the defect sites contain Si-OH (silanol bond), Si with hydroxyl (-OH) and Siloxane (Si-O-Si). The hydroxyl functional group is reactive as Bronsted acid site (H donor) or providing a H-bond towards other polar molecules. The lone-pair electrons on Siloxane can also interact with the incoming molecules with high polarity and make it possible to break the Si-O bonds. In our study, the reactants, ethanol, and water are both polar molecules, therefore, some interactions occur and affect the reaction. In crystallization process of zeolite formation, hydrolysis and condensation is simultaneously occurring at this site, connecting to form a structure, releasing water as a product. The small alkane also has a small interaction with this Bronsted acid sites and with the increasing of molecular weight, the interaction increase [69].

#### *Ethanol adsorption on free Silanol*

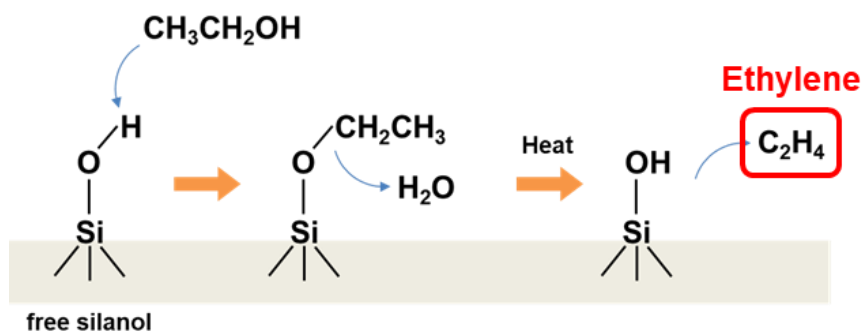


**Figure 3.6.** Ethanol adsorption mechanism on free Silanol and its proceeding reaction.

Ethanol can adsorb on Silica surface at free silanol on the surface. The adsorption occurs by protonation and subsequent cleavage of Si-OH to form ethoxide (CH<sub>3</sub>CH<sub>2</sub>O-) on Si atom. This interaction usually occurs in high temperature conditions. This is the main pathway for alcohol adsorption on zeolite/silica surface (than on Siloxane) [70, 71]. The behavior as shown in Figure 3.6. With the activation by increasing temperature, it is considered as ethanol dehydration to ethylene on free silanol. This is considered as a main reaction pathway of reaction on pure silica without metal active site, producing a large amount of C<sub>2</sub> intermediates which is ready for the coke formation mechanisms.



### Ethanol adsorption on Siloxane

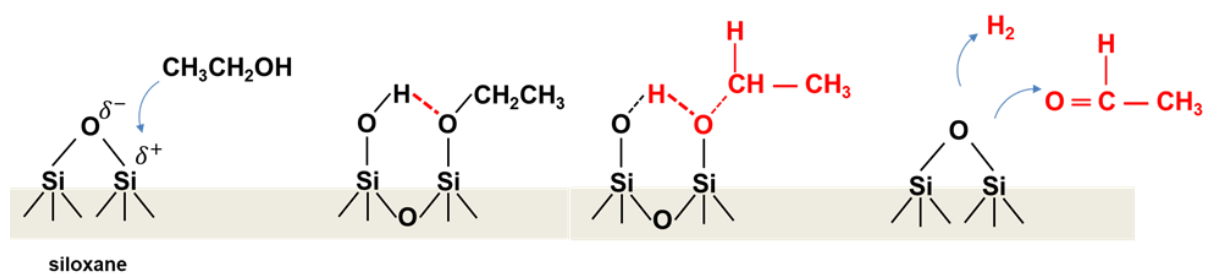


**Figure 3.7.** Ethanol adsorption mechanism on Siloxane and its possible proceeding reaction.

Ethanol can also adsorb on Silica surface at siloxane position on the surface. The adsorption occurs as shown in Figure 3.7. It starts by attacking the positive dipole moment Si which is connected to O-position, which has negative dipole moment of electron localization. The adsorption yields one free silanol and one ethoxide attaching Si. The free silanol can further react with reactants in the reaction media which is the same route of producing  $C_2H_4$  as mentioned in Figure 3.6. This is considered as an indirect ethylene formation from ethanol alkoxylation. Desorption can also occur as acetaldehyde and hydrogen gas but as a minor pathway of desorption. By the way, this reaction pathway is occurred only with alcohol, the situation with only water or steam is difficult to affect this position [72].

### Ethanol adsorption on Ni active sites

Ethanol adsorption is a very important step to initiate ethanol steam reforming reaction. The study on adsorption position of ethanol on active metal sites has been investigated. The most stable adsorption of ethanol occurs at O atom as Ni — O (average distance of 2.05 Å) [73]. After adsorption, the bond breaking order of ethanol is considered. The breaking order had been verified by several studies [74, 75], after adsorbed on metal surface, the bonds start to break from O-H, C-H of the C connected to O, C-C bond cleavage, and C-H bonds. The order was written in Figure 3.8 as ①→②→③→④.

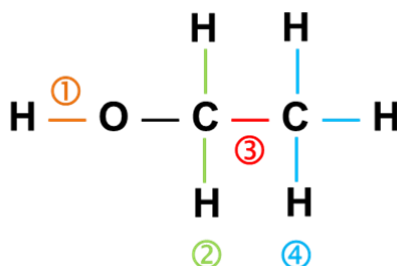


**Figure 3.8.** Activation order of bonding in Ethanol on Ni active sites.

### *Ethanol and its surface reaction mechanism on Ni active sites of Ni@Silicalite-1*

With consideration of reaction conversion and selectivity, together with literatures [10, 26, 82, 66, 67, 76–81], The possible reaction of ethanol on the Ni@Silicalite-1 has two possibilities as illustrated in Figure 3.9. The first one is the dehydration of the ethanol to ethylene catalyzed by acidic site of the support as mentioned in the previous section of ethanol adsorption on Silicalite-1. The second one is the main pathway on Ni active sites which is the dehydrogenation of ethanol to acetaldehyde. This reaction pathway is preferable for steam reforming reaction. The adsorption occurs at O position on ethanol released two active surface hydrogen, then combines into hydrogen gas. At this stage, the adsorbed acetaldehyde can desorb as gaseous species to the reaction environment. If not, it is continued to the next step of the reaction mechanism, either steam reforming route or coke formation route.

In steam reforming route, hydrogen atoms are further released from  $\text{CH}_3\text{CO}$  to  $\text{CH}_2\text{CO}$ , and  $\text{CHCO}$ , with the formation of  $\text{H}^*$  on the catalyst surface. C-C bond cleavage occurs at the stage of  $\text{CH-CO}$  to  $\text{CH}$  and  $\text{CO}$  on two separated sites. There are another two possible reaction pathways, involving the adsorption of either water or hydrogen gas. The acetaldehyde steam reforming route involves the adsorption of water, either on the zeolite surface or Ni active site, which depends on the properties of active sites and support surface. The high reactivity Ni enhances the water adsorption on the Ni surface, especially the small Ni size (low coordinate site) and step site of Ni. The activation of water requires a high temperature. The oxidation of CO depends on the dissociation of OH from water molecules adsorbed on the catalyst surface, which also depends on the metal active sites. With the activation of water, water-gas shift (WGS) reaction proceeds releasing  $\text{CO}_2$  and  $\text{H}_2$  as products. The nature of WGS also requires a high temperature to proceed, at least above  $347\text{ }^\circ\text{C}$ . The remaining adsorbed C, O, and OH on the surface can further form coke by releasing CO and  $\text{H}_2$ .

Methane formation via acetaldehyde decomposition route can also proceed after the C-C bond cleavage. It starts proceeding in a lower temperature below  $427\text{ }^\circ\text{C}$  yielding  $\text{CH}_4$ , CO, and  $\text{H}_2$ . This reaction route has a possibility to lower the hydrogen yield of the reaction since it utilizes hydrogen within the reaction.

Apart from the desirable steam reforming route, coke formation routes can also be proceeded in this reaction system. Hydrogen does not release from  $\text{CH}_3\text{CO}$ , but C-C bond cleavage proceeds at this stage, yielding  $\text{CH}_3^*$  and  $\text{CO}^*$ . This reaction route is called acetaldehyde decomposition. There are two possible reaction routes for coke formation



Towards all types of surfaces silanol groups, they increase the hydrophilicity of the surface enhancing the possibility to adsorb water on the surface. With the enhanced hydrophilicity of the surface, the surface has higher possibility of attacked sites for hydrolysis in the structure, especially the free silanol group. In order to verify the density of each type of silanol can be verified by DRIFT technique (wave number of  $3738\text{ cm}^{-1}$ ).

The role of water towards free Silanol (Si-OH), water bonds with hydroxyl group by hydrogen bond between the lone pair on water and hydrogen on Si-OH position. The activated (protonated) water molecules or cluster can participate in reaction with reactants to obtain some products [83]. In the system consisting of both alcohol and water, alcohol can compete with water in adsorption on silanol group.

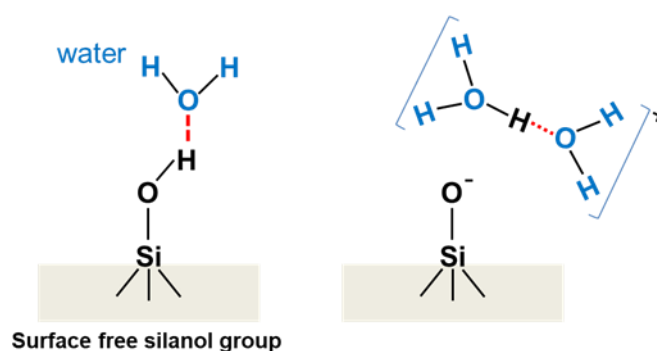


**Figure 3.10.** Adsorption of water on free silanol.

Only water cannot adsorb or react with the surface of zeolite or silica at Siloxane Position (Si-O-Si). The adsorption is enhanced by specific conditions. In gaseous phase reaction, the high reaction temperature enhances the adsorption and proceed surface reaction. On the other hand, in the solution system, the strong acidity or basicity can enhance the surface reaction, i.e., Desilication (hydrolysis) of structure making the deterioration. The phenomena of desilication are illustrated stepwise in Figure 3.11. There is the study of the effect of steam on the structure deterioration of Silicalite-1, it is reported that the presence of internal silanol (Si-OH) defects inside the zeolite structure leads to the loss of crystallinity after steaming at  $200\text{ }^{\circ}\text{C}$ ,  $18.6\text{ atm}$  [84]. Water increases the number of Si-O-Si on the surface but reduces the crystallinity drastically. Therefore, the reduction of surface silanol group presence in zeolite is necessary to improve the tolerance in severe conditions. Examples of surface treatment to reduce free Silanol are organosilane,  $\text{SiCl}_4$  treatment, and F treatment.

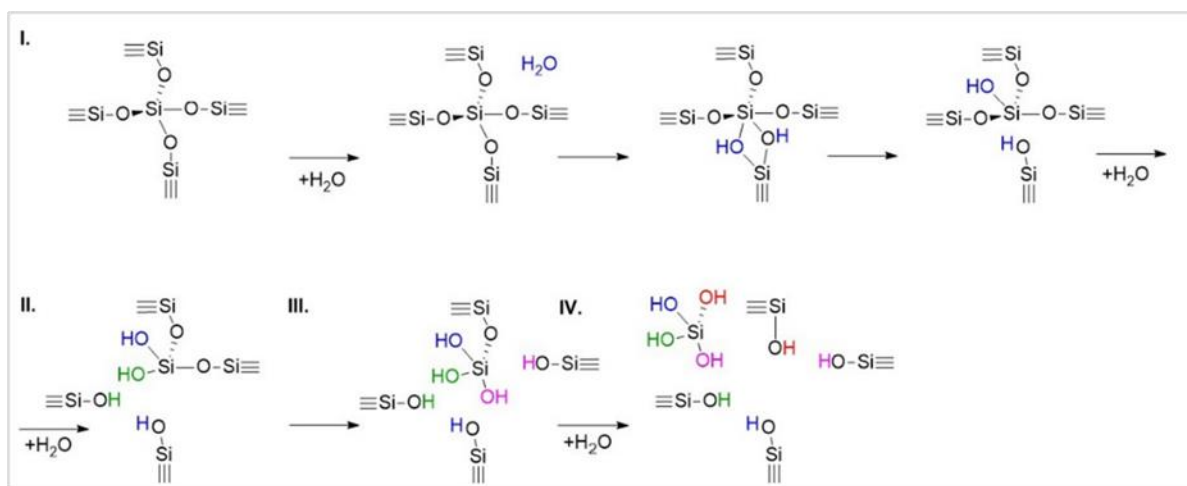


**Figure 3.11.** Desilication phenomena at Siloxane position [85].

In summary for chapter 3, the reaction mechanism and possible pathways has been studied from the literature review, thermodynamic equilibrium calculation, and catalytic activity tasting experiment, to compare the phenomena with previous study. For ethanol steam reforming, the thermodynamic equilibrium of the reaction system is reached at the reaction temperature around 700 °C. At thermodynamic equilibrium condition, the gas products are H<sub>2</sub>, CO, CO<sub>2</sub>, and CH<sub>4</sub>, and the increasing in temperature, hydrocarbon products reduce. This information can be further utilized in catalytic experiments design for validation of catalytic properties of the prepared catalysts. The reaction pathways are studied in the experiment of ESR investigation in 500 – 800 °C, on Silicalite-1, and Ni@Silicalite-1.

Without the presence of Ni active sites, the major reaction pathway on Silicalite-1 is the ethanol dehydration to ethylene, with the minor of ethanol dehydrogenation to acetaldehyde. The production of ethylene is being catalyzed by weak acidity of Silanol surface functional group. With the presence of Ni active sites, ethanol adsorbed and activate to proceed dehydrogenation to acetaldehyde, followed by acetaldehyde reforming produced H<sub>2</sub>, CO, and CO<sub>2</sub>. Coke formation occurs due to the presence of coke precursor in reaction media, and their concentration is the control parameter of the coke formation amount. The increasing of temperature enhances steam reforming pathway from water activation, together with the reaction of coke precursors to the oxygenated species.

The conversion towards complete products for ethanol steam reforming are obtained with the presence of Ni active sites only. The properties of Ni sites are an important parameter to control the catalyst activity, and its properties can be affected by size of metals and location in the catalyst, which are studied in the next chapter.

## Chapter 4 : Investigation of Catalytic activity of Ni@Silicalite-1

### 4.1. Introduction

Besides of the reaction mechanism and pathways that alters the product yield and selectivity of ESR reaction, which is mainly discussed in the last chapter, metal sintering and coke formation pathways are also playing roles to control product selectivity and catalyst deactivation which is one of the main drawbacks of ESR catalyst development. In this introduction section, the coke formation mechanism with the relation to reaction pathways and metal size will be researched and summarized. With the knowledge of the coke formation and the relationship towards the metal particle size, we can draw a better understanding of the advantage of encapsulation structure.

Considering the reaction pathway, there are a lot of side reactions that lowers hydrogen yield. And these reactions are involved in the coke precursor formation, and then coke formation occurs. The pathways include decomposition of ethanol, decomposition of acetaldehyde producing methane, methanation of CO and CO<sub>2</sub>, the direct coke formation pathways, including ethylene decomposition, Boudouard reaction, and methane decomposition.

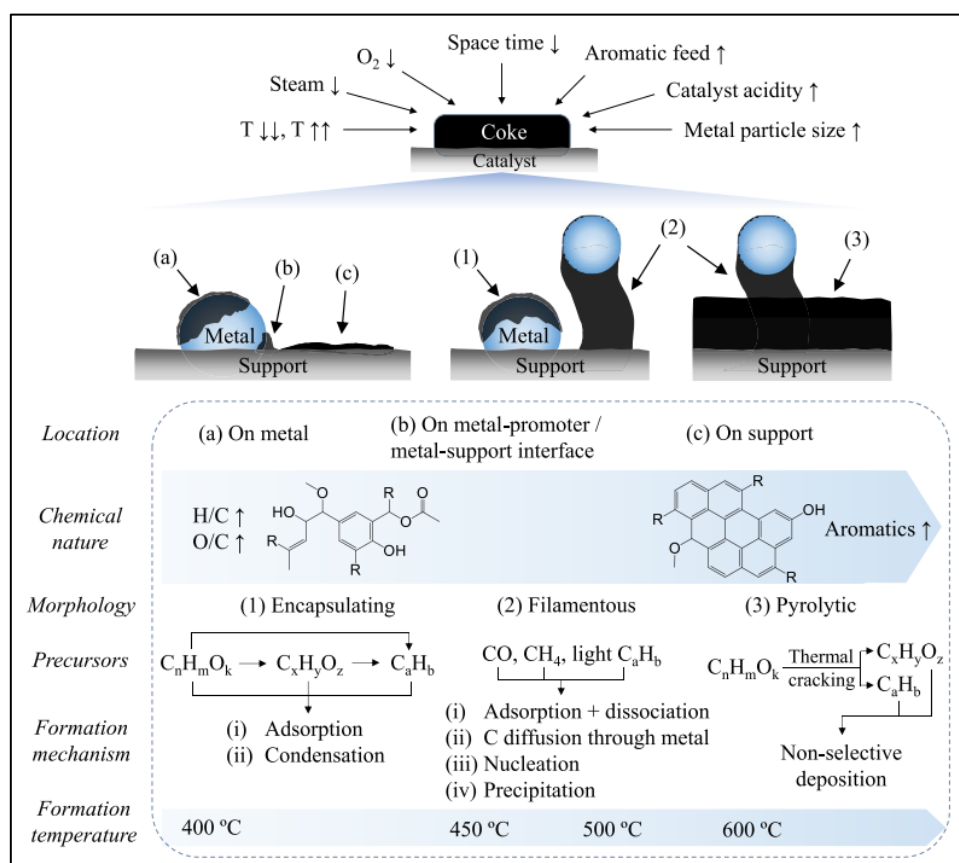


**Figure 4.1.** Main features of coke deposited on catalyst in reforming reactions [86].

The coke formation starts with the monolayer chemisorption of carbon species to form metal carbide or physical adsorption in multilayer to block the active site accessibility. Then, the active sites are encapsulated with coke, also the micro/mesopore are plugged with the coke, therefore, the active sites in the inner pore are fully hindered. The final and severe stage is the changes in crystal structure and reactor plugging. To overcome the coke formation problems, the catalyst design to minimize the formation of coke, the optimum operating conditions for coke minimization, and reactor design with regeneration strategies are very important for a real application.

Figure 4.1 summarizes the coke formation on reforming catalyst. Coke formation is affected by the operating conditions of the reaction system. The condition that makes coke formation increases are including the low reaction temperature that tends to produce reactive coke intermediates, low in steam and oxygen which are the reactants in coke gasification, short space time can increase both amorphous and filamentous coke since there is not enough time for the active metal to convert the coke precursors into other products. The larger size of the reactant as the increasing amount of carbon in the molecule can increase the chances of coke formation. Increasing catalyst acidity can increase the chances of coke formation due to the enhancement of ethanol dehydration to ethylene in ESR, and the larger particle size are prone to coke formation.

Consider our study reaction, ESR, to the coke formation information in Figure 4.1. As its chemical nature of ethanol that is a straight chain oxygenated hydrocarbon, the coke precursor obtained from the reactions falls into two groups: (1) ethoxy ions, acetaldehyde, acetone, and ethylene can be further adsorbed and condensed to form encapsulating coke, then filamentous coke, and (2) carbon monoxide, methane, and also ethylene are undergo the adsorption, dissociation, carbon diffusion, nucleation, and precipitation to form filamentous coke. These coke forms on the metal or at metal-support interface.

Gohier et al. studied the carbon nanotube growth mechanism on different metal types and size in catalyst film. The investigation included Ni with an average diameter of 5 and 15 nm. The results revealed that the smaller size of Ni at 5 nm, the coke formation was a base growth mode, metal is always at the base of coke filament. The obtained coke is single-wall or few-wall carbon nanotubes (SWCNTs or FWCNTs) with a diameter smaller than 5 nm. On the other hand, the large Ni particle size of 15 nm, filamentous coke forms in a tip-growth mode, Ni sites always at the tip of coke filaments. The obtained coke from the larger Ni is a multi-wall carbon nanotube with the average diameter larger than the size of the Ni sites.

The reason for this difference in growth mode is the interaction between Ni and silicon in the support material towards the formation of carbon patches in CNTs nucleation, on the metal surface. In the case of large particle size that the tip-growth mode is found, the larger surface area in one particle allows carbon patches diffuse all over area. The most stabilized carbon patches which are ready for nucleation are those in the area of catalyst/substrate interface, not the complete formation of the hemispherical cap on the metal surface. At the tip, the top surface of metal sites is exposed to carbon adsorption, therefore, the phenomena are called tip-growth mode. The tip-growth mode of filamentous coke can lead to the loss of active sites from catalyst surface as illustrated in Figure 4.2.

In contrast, the base growth mode is generally observed in the case with strong interaction. The smaller metal size is more reactive and provides a stronger interaction with the carbon patches. The hemispherical cap on the surface of the metal is successfully formed but leaves the metal/substrate interface available for adsorption and decomposition of reactants. In this case, the refill supply of carbon is coming in at the base, therefore, this phenomenon is called base-growth mode of filamentous carbon. While carbon is forming, the active sites are still functioning and stayed on the substrate, i.e., support materials, therefore, the active sites are still functioning as an active metal in the catalytic reaction without losing from the surface.

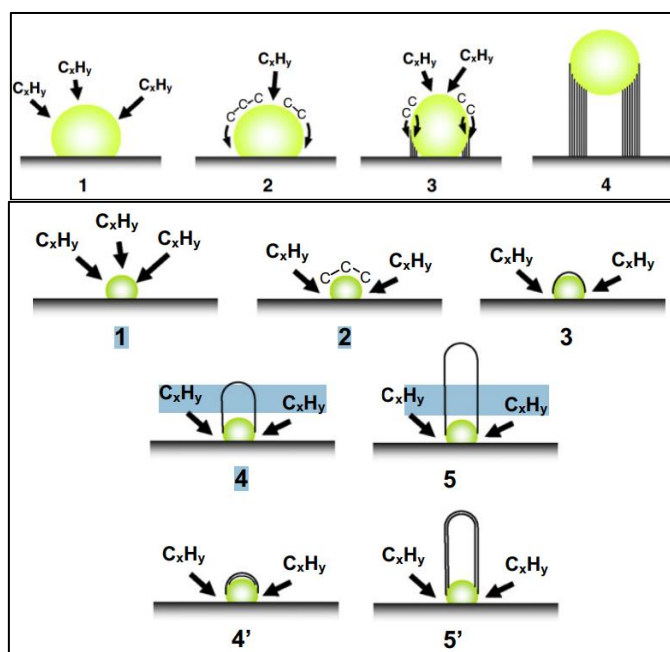


**Figure 4.2.** Filamentous carbon growth phenomena on different metal particles sizes.

Top – MWCNTs growth in tip-growth mode in a large metal particle.

Bottom – SWCNTs and FWCNTs growth in base-growth mode in a small particle [87].



### Coke formation from ethylene

The important coke precursor in the reaction system of ethanol steam reforming is C<sub>2</sub> hydrocarbon and oxygenated hydrocarbons. Ethylene has been reported as a carbon precursor in preparation of CNTs and CNFs [88, 89]. It is a potential coke precursor in ESR since it can involve in ethylene decomposition which is considered as hydrogen transfer reaction promoting coke formation (H extraction from deposited) [90] (Eq.(4.1)) and ethylene polymerization to form carbon (Eq.(4.2)). It might proceed in ethylene steam reforming (Eq.(4.3)) but not selective at high reaction temperatures. Reactions involving ethylene in ESR are listed below.

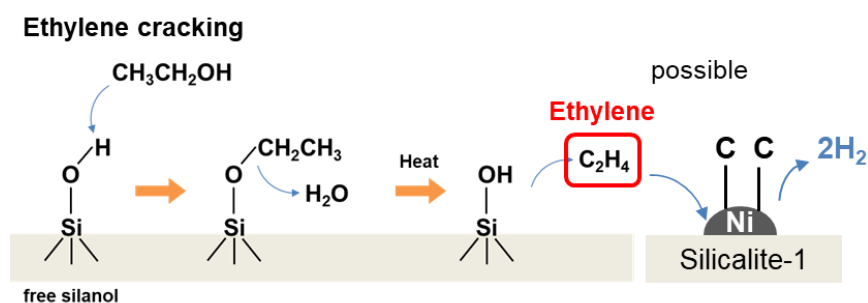
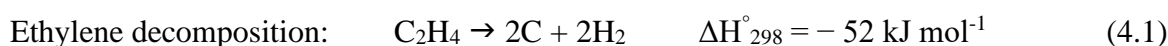


**Figure 4.3.** Possible coke formation pathway from ethylene decomposition.

Coke formation from ethylene which proceeds via decomposition or polymerization are likely to occur at the temperature above 450 °C (600 -700 °C for pyrolysis). The process starts with adsorption and dissociation to C on the metal surface, diffusion through metal as bulk diffusion or surface diffusion (for Ni active site: Ni<sub>3</sub>C formation), then nucleation, and precipitation as a crystalline carbon structure. Ethylene polymerization and filamentous coke formation are illustrated in Figure 4.4. Over Ni-Silicalite-1, coke forms only when Ni exists (catalytic coke formation) and amorphous coke is favored in high ethanol concentration condition.

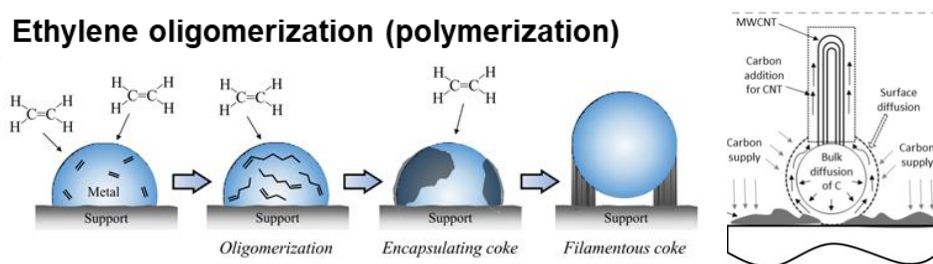


**Figure 4.4.** Possible coke formation pathway from ethylene polymerization [91].

## 4.2. Experimental

### 4.2.1. ESR activity test

ESR activity tests were conducted in a quartz fixed bed reactor. The experimental set up diagram is shown in Figure 4.5. The 0.1 g of catalyst, pellet size of 300 – 850  $\mu\text{m}$ , was packed between pieces of quartz wool. The pretreatment before reaction test was conducted. Catalyst oxidation was conducted at 850  $^{\circ}\text{C}$  for 30 min in air stream. After that, the catalyst was purged with  $\text{N}_2$  to remove the remaining oxygen before the reduction process. Afterward, the catalyst was reduced at 850  $^{\circ}\text{C}$  in 20%  $\text{H}_2$  in  $\text{N}_2$  (total gas flow rate of 50 mL/min) for 1 h. The reason choosing the reduction temperature of 850  $^{\circ}\text{C}$  is to ensure the reduction of all Ni species on the catalysts. The catalyst was purged again with  $\text{N}_2$  to remove all remaining  $\text{H}_2$  from reduction. The furnace temperature was adjusted to the reaction temperature and waited until stabilized which took around 15 – 20 mins. The reaction test was started by feeding the mixture of ethanol and water, steam-to-ethanol molar ratio (S/E) of 3:1, with a syringe pump. The feed flow rate was set to be 0.49 mL/h (0.2 g<sub>Ethanol</sub>/h). The liquid feed was vaporized with the heating element set at temperature of 150  $^{\circ}\text{C}$ . The reaction conditions were listed as follows.

#### Pretreatment:

- oxidation for 1 h at 850  $^{\circ}\text{C}$
- reduction 20%  $\text{H}_2/\text{N}_2$  for 1 h at 850  $^{\circ}\text{C}$

#### Reaction Condition:

- Pressure: atmospheric pressure, continuous flow
- Carrier gas for the reaction:  $\text{N}_2$  50 mL/min
- Reaction temperature: 500/600/700/800  $^{\circ}\text{C}$
- Feed Ethanol-to-water molar ratio = 1:3 and 1:1
- Liquid feed rate = 0.49 mL/h (0.2 g<sub>EtOH</sub>/h)
- Total gas flow rate (inlet) = 57.2 mL/min
- $p_{\text{EtOH}} = 3.18 \text{ kPa}$  (0.03 atm)
- $W/F = 0.5 \text{ h g}_{\text{catalyst}}/\text{g}_{\text{EtOH}}$

#### Time on stream:

- 30, 100, 170, 240 min (time on stream of 4 h)
- Every 60 min (time on stream of 10 h, as a long-time reaction)

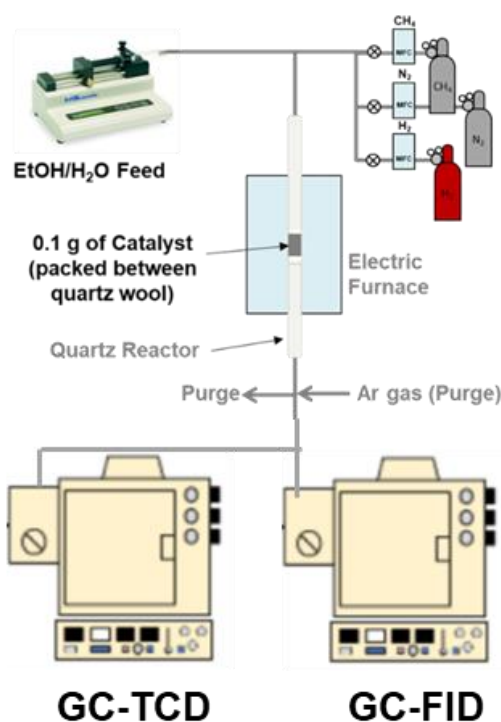


**Figure 4.5.** Experimental setup for ESR Reaction Test.

The gas effluent from the reactor was analyzed for a gas composition by online gas chromatography (GC). Two GCs were used in the experiment. The first one is coupled with a flame-ionized detector (FID) and PorapakQ column (GL Sciences, Japan) for the determination of hydrocarbon compound, C<sub>x</sub>H<sub>y</sub> and C<sub>x</sub>H<sub>y</sub>O<sub>z</sub>, obtained from the reaction. The second GC is coupled with a thermal conductivity detector (TCD) and a Shincarbon-ST column (Shinwa Co., Japan) for the determination of H<sub>2</sub>, CO, CO<sub>2</sub>, CH<sub>4</sub>, and C<sub>2</sub>H<sub>4</sub>. Since the separated GC system was used, the connection of amount of gas calculation is the amount of CH<sub>4</sub> between two channels with the N<sub>2</sub> flow rate of 50 mL/min.

The ethanol conversion, hydrogen yield, product gas selectivity, and product gas ratio were calculated using the following equations:

$$X_{Ethanol} = \frac{(F_{Ethanol,in} - F_{Ethanol,out})}{F_{Ethanol,in}} \quad (4.4)$$

$$Y_{H_2} = \frac{F_{H_2,out}}{(6 \times F_{Ethanol,in})} \times 100 \quad (4.5)$$

$$S_i = \frac{F_{i,out}}{v_i \times (F_{Ethanol,in} - F_{Ethanol,out})} \times 100 \quad (4.6)$$

where  $F_i$  is a molar flow rate of product  $i$  inlet or outlet of the reactor, and  $v_i$  is a stoichiometric coefficient of product  $i$  ( $i = \text{CO}, \text{CO}_2, \text{CH}_4, \text{C}_2\text{H}_4, \text{and } \text{CH}_3\text{CHO}$ ). Noted that, the molar flow rate of ethanol fed to the system was calculated from the liquid fed from the syringe pump.

The effect of Ni location on catalyst were focusing on the activity difference and coke formation at the representative temperature of 600 °C. This temperature is high enough to activate the reactant for further reaction and is the most severe temperature for coke formation among the reaction temperature that was tested in this study. After the difference was seen at a temperature, the catalytic difference in different reaction temperature is further evaluated from 500 – 800 °C. At low reaction temperature, the challenge is that the reaction is in a kinetic control condition which means the rate of production is up to the activation energy. Therefore, the catalytic performance of different catalysts can be investigated in this reaction condition. Various types of products can be observed at this temperature; hence the coke formation and suppression ability can be studied in this condition. On the other hand, the reaction at high reaction temperature reaches a thermodynamic control condition. Stable products are produced at this condition. Mostly, the information relating to catalytic stability can be extracted from the investigation in this reaction condition. Therefore, the stability of catalyst structure and Ni sites are the observation points in this study.

#### **4.2.2. Catalyst characterization (after the reaction test)**

The properties of spent catalysts after the reaction tests were evaluated with some of the same characterization techniques (refer to section 2.2.3.), and some more techniques as listed below:

1. X-ray Diffraction (XRD): surface morphology change (intensity or peak position).
2. N<sub>2</sub> physisorption: specific surface area, micropore volume, and crystallinity implementation change after the reaction
3. Scanning electron microscopy (SEM): Zeolite crystal size and surface morphology appearance change after reaction test. The observation on morphology of coke formation can also be observed.
4. Transmission Electron Microscopy (TEM): Ni size changes are observed to compare the result of Ni sintering resistance ability between catalysts. Coke morphology in terms of formation type and size can also be observed.
5. Thermogravimetric analysis (TG): The amount of coke formation on the spent catalysts are quantified by the net weight change of sample (TG curve), which was combusted in air from 250 – 900 °C using thermogravimetric/differential thermal analyzer (TG-DTA; Thermoplus EVO/TG 8120, Rigaku Co., Ltd., Japan). Moreover, the brief information about carbon type can be interpret from combustion behavior (peak temperature and combustion time) in DTA curve.

### 4.3. Results and discussion

#### 4.3.1. Effect of Ni location on catalysts towards ethanol conversion and product selectivity in different reaction temperature

The study examined the catalytic performance of ESR under varying reaction temperatures (ranging from 500 to 800 °C) using three materials: Silicalite-1 (without Ni) as a blank standard without Ni metal, Ni/Silicalite-1 (Ni impregnated on the zeolite surface, conventional preparation method), and Ni@Silicalite-1 (Ni encapsulated within the primary zeolite particles). The catalyst preparation conditions are listed below in Table 4.1.

**Table 4.1.** Catalysts preparation conditions of the catalyst used in this experiment.

| Sample Name     | Preparation method             | Ni loading<br>(wt %) | Preparation condition  |
|-----------------|--------------------------------|----------------------|--|
| Silicalite-1    | Hydrothermal synthesis (HTS)   | -                    | HTS (180 °C 72 h)<br>H <sub>2</sub> O : Si ratio = 50  |
| Ni/Silicalite-1 | Incipient wetness impregnation | 0.82                 |  |
| Ni@Silicalite-1 | 2-step HTS                     | 0.91                 | Calcined Ni-PS<br>dissolution time = 18 h<br>Zeolite HTS at 100 °C 72 h<br>H <sub>2</sub> O : Si ratio = 100 |

Several characterizations have been done, to verify the properties of catalyst before and after reaction for comparison. Figure 4.6 displays X-ray diffraction (XRD) patterns for various samples: Ni-PS precursor, Silicalite-1 (used as a reference), Ni/Silicalite-1, and Ni@Silicalite-1. The pattern of Ni-PS precursor differs from others due to its composition, which is primarily Ni-containing amorphous silica (SiO<sub>2</sub>). During the hydrothermal synthesis, the Ni-PS precursor dissolves and contributes to zeolite formation in the solution containing Ni-PS, TEOS, and TPAOH. Successful synthesis of Ni@Silicalite-1 resulted in a well-crystallized Ni-containing MFI zeolite, as indicated by patterns closely resembling those of MFI zeolite. The slightly reduced intensity in the Ni@Silicalite-1 pattern is attributed to the presence of the Ni-containing amorphous silica precursor, with a possibility of a small portion not fully converting into zeolite. Additionally, the zeolite particle size might be marginally larger compared to the reference Silicalite-1. Regarding peak identification in the enlarged patterns, no discernible diffraction peaks corresponding to Ni species (either NiO or

Ni-phyllsilicate) were detected. This is likely due to the minimal amount of Ni incorporated in all samples (ranging from 0.9 to 2.4 wt% nominal) and the effective dispersion of small-sized Ni particles within the catalysts.

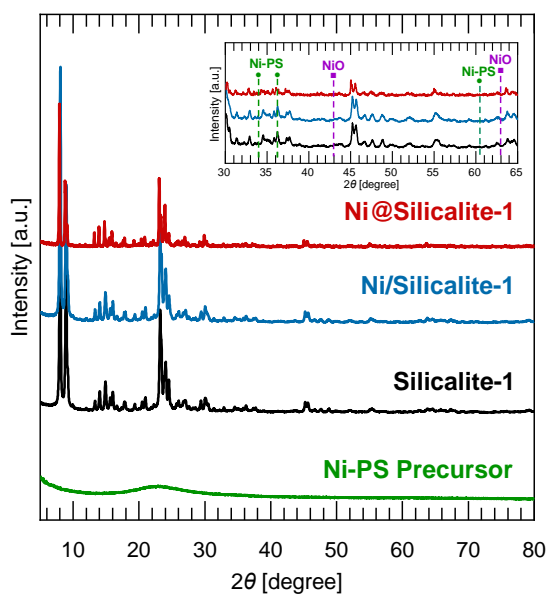


**Figure 4.6.** XRD patterns of prepared Ni catalysts, Silicalite-1, and Ni-PS precursor.

Figure 4.7 illustrates the N<sub>2</sub> physisorption characteristics of the produced materials. The surface area and micropore volume, determined through the BET technique and t-plot analysis, respectively, are detailed in Table 4.2.

**Table 4.2.** Surface properties of synthesized Ni catalysts, Silicalite-1, and Ni-PS Precursor.

| Sample          | Surface area ( $S_{\text{BET}}$ )<br>( $\text{m}^2/\text{g}_{\text{sample}}$ ) | Micropore Volume<br>( $\text{cm}^3(\text{STP})/\text{g}$ ) |
|-----------------|--|--|
| Ni-PS Precursor | 8.23   | 0.001  |
| Silicalite-1    | 483.00   | 0.19   |
| Ni/Silicalite-1 | 421.76   | 0.18   |
| Ni@Silicalite-1 | 447.33   | 0.14   |

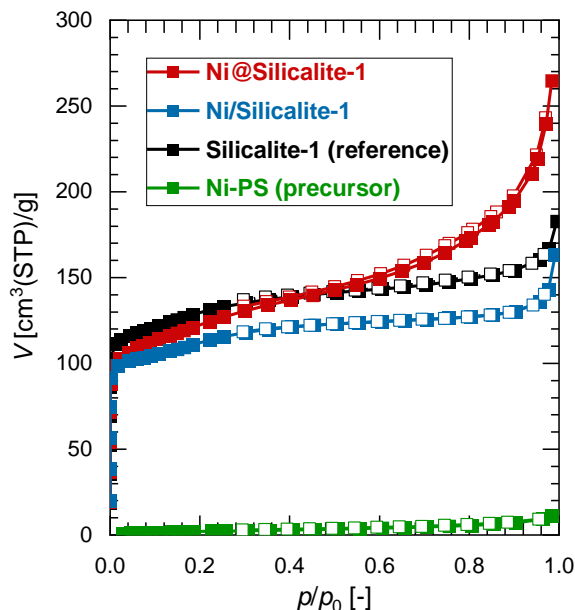


**Figure 4.7.** N<sub>2</sub> physisorption profiles of prepared Ni catalysts, Silicalite-1, and Ni-PS precursor.

The Ni-PS precursor exhibits minimal adsorption volume and an almost negligible micropore volume, indicating its classification as a non-porous amorphous silica material. Conversely, the other three materials demonstrate Type II adsorption isotherm characteristics, which is a typical form of MFI-type zeolites. Additionally, these materials display consistent adsorption in the low-pressure region, reflective of single-layered adsorption, indicating good microporosity. These results suggest a well-developed crystallinity of MFI zeolite. Introducing Ni onto the zeolite slightly reduces the surface area and micropore volume of the sample. In the case of Ni@Silicalite-1, there is increased adsorption in the mid-to-high range of relative adsorption pressure, suggesting the presence of diverse pore sizes on the surface, possibly due to the incorporation of amorphous silica from the precursor.

The surface characteristics of the produced materials are evident in the SEM images depicted in Figure 4.8. Silicalite-1 and Ni/Silicalite-1 exhibit a smooth external surface, while Ni@Silicalite-1 displays a rougher surface. This rough surface could be attributed to SiO<sub>2</sub> remnants that did not integrate into the zeolite structure during the hydrothermal synthesis process. This observation aligns with the N<sub>2</sub> physisorption profile. Furthermore, the crystal size of Ni@Silicalite-1 was found to be slightly larger (approximately 400 nm) compared to Ni/Silicalite-1 (approximately 250 nm), consistent with the lower intensity observed in the XRD patterns.

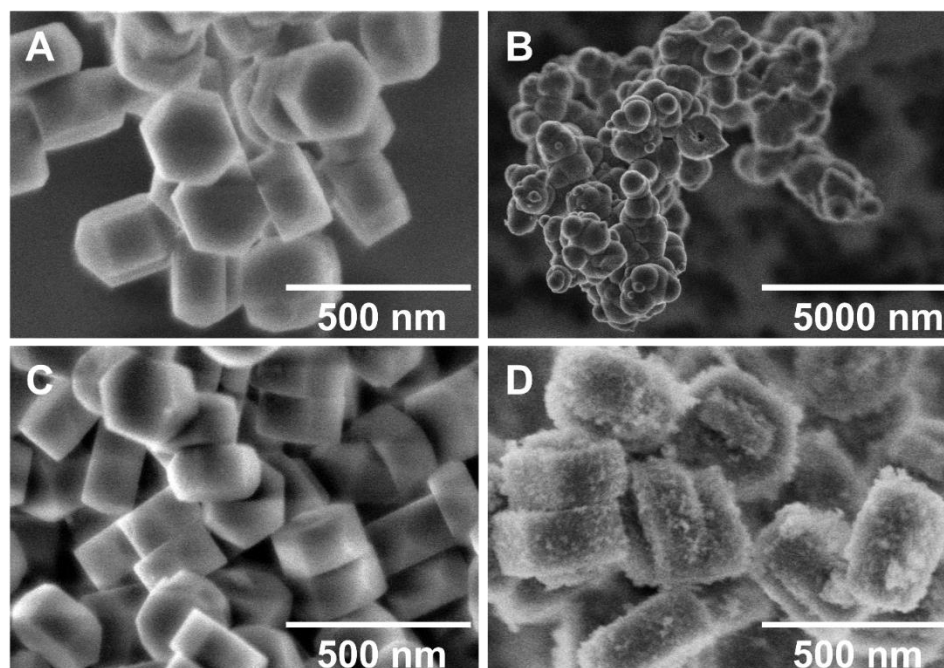


**Figure 4.8.** SEM images of synthesized materials: (A) Silicalite-1, (B) Ni-PS precursor, (C) Ni/Silicalite-1, and (D) Ni@Silicalite-1 (after calcination at 500 °C).

The next part of the characterization of materials is about the active species on the catalysts which are Ni active sites. The properties of Ni are evaluated in temperature-programmed reduction ( $H_2$ -TPR),  $N_2O$ -pulse chemisorption, and TEM.

The temperature-programmed reduction ( $H_2$ -TPR) profiles for the Ni-based materials are illustrated in Figure 4.9. The presence of Ni species is evidenced by the reduction process, and the varying reduction temperatures indicate differences in reduction behavior, reflecting the metal-support interaction within the catalyst. For Ni species, reduction initiates at around 400 °C and extends to approximately 600 – 650 °C is the reduction temperature of NiO. A higher reduction in temperature indicates a more difficult reduction of active sites, signifying a stronger metal-support interaction. This high reduction temperature is possible with fine Ni particles or well-structured Ni species like Ni-phyllsilicate, which is reducible in the range of 700 – 850 °C. In the synthesized Ni-PS precursor, the reduction peak ranges from 450 – 850 °C, displaying a left-tailed behavior. This suggests that the Ni-PS precursor primarily comprises Ni-phyllsilicate as a major component, with a smaller amount of NiO. In Ni/Silicalite-1, two regions of reduction peaks are observed. The peaks at 400 – 520 °C align with the standard NiO reduction temperature, while the peak at 810 °C indicates the potential presence of small Ni particles acquired during the incipient wetness impregnation process. Conversely, Ni@Silicalite-1



displays a single reduction peak, implying heightened metal-support interaction resulting from Ni-phyllsilicate formation in the prepared catalyst after calcination. Considering the reduction profiles of the samples, a reduction temperature of 850 °C was selected for the catalyst reduction process.

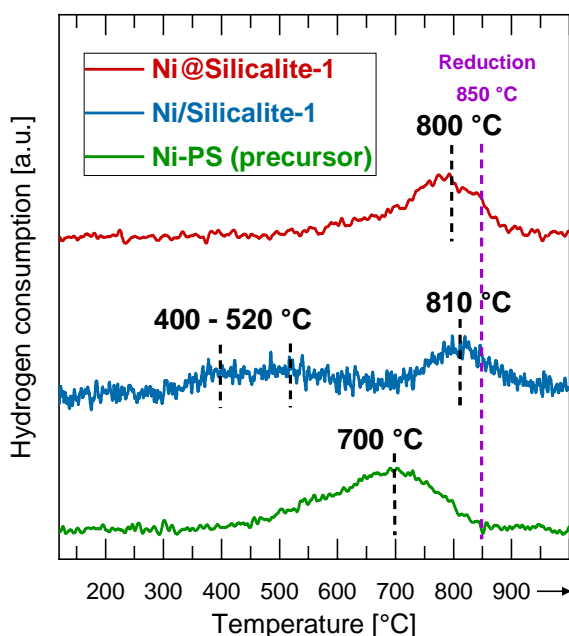


**Figure 4.9.** H<sub>2</sub>-TPR Profiles of prepared Ni-PS precursor and Ni catalysts.

Table 4.3 presents an overview of Ni properties on both Ni-PS precursors and Ni catalysts, including Ni loading, Ni dispersion, and Ni particle size (determined through N<sub>2</sub>O titration and TEM after reduction; TEM images displayed in Figure 4.13.). The Ni catalysts were prepared with a nominal Ni loading of approximately 1 wt%. In both cases, the average Ni particle size post-reduction, determined from TEM images, was approximately 3.7 – 3.8 nm. The calculated Ni particle size after reduction through N<sub>2</sub>O titration followed a similar trend to the apparent values observed in TEM images. Obviously, the N<sub>2</sub>O titration values were notably larger due to N<sub>2</sub>O's accessibility to the metal Ni surface on zeolites. In the case of Ni/Silicalite-1, the larger value was attributed to metal sintering effects, while for Ni@Silicalite-1, it was due to potential silica coating on the Ni surface which limits Ni accessibility. A distinct contrast can be observed in Ni dispersion and Ni particle size distribution. Ni/Silicalite-1 displayed low Ni dispersion with a broader size distribution. TEM images revealed agglomerated Ni particles ranging from 14 – 24 nm on Ni/Silicalite-1 since the reduction stage, aligning with the lower Ni dispersion. Conversely, Ni@Silicalite-1 exhibited highly dispersed Ni particles with a smaller size of 3 – 4 nm and a narrow size

dispersion. This high Ni dispersion allowed for better reactant accessibility to the Ni surface, facilitating reactions. The smaller Ni size on the support surface established a robust metal-support interaction, enhancing catalytic activity. Based on these findings, Ni@Silicalite-1 is anticipated to demonstrate superior catalytic performance. The encapsulation structure achieved through hydrothermal synthesis using Ni-PS precursor is expected to enhance ESR reaction activity.

**Table 4.3.** Properties of Ni catalysts.

| Sample          | Ni loading <sup>a</sup><br>(wt%) | Ni Dispersion <sup>b</sup><br>(%) | Ni particle size (nm)      |                                  |
|-----------------|----------------------------------|-----------------------------------|----------------------------|----------------------------------|
|                 |                                  |                                   | Before reaction            |                                  |
|                 |                                  |                                   | N <sub>2</sub> O titration | TEM observation <sup>c</sup>     |
| Ni-PS Precursor | 2.35                             | -                                 | -                          | -                                |
| Ni/Silicalite-1 | 0.82                             | 0.88                              | 115.61                     | 3.8 ± 2.6<br>(large: 14 – 24 nm) |
| Ni@Silicalite-1 | 0.91                             | 6.54                              | 15.47                      | 3.7 ± 0.6                        |

<sup>a</sup> measured by XRF

<sup>b</sup> measured by N<sub>2</sub>O pulse chemisorption, fresh catalyst (before using in reaction test)

<sup>c</sup> catalyst after reduction at 700°C 1 h in reduction gas (H<sub>2</sub>/N<sub>2</sub>)

The outcomes, illustrating the ethanol conversion, H<sub>2</sub> production, and carbon products formation yield, are shown in Figure 4.10. After examining the ethanol conversion and product selectivity, it becomes apparent that the reaction can be categorized into two distinct regions. At a low reaction temperature of 500 – 600 °C, variation in reactant conversion, product selectivity, and coke formation from the various reaction pathways can be observed. Hence, the reaction is under kinetic control. At elevated reaction temperatures ranging from 700 to 800 °C, complete ethanol conversion and minimal variations in product selectivity are noticeable, signifying that the reaction attains thermodynamic equilibrium. Under this state of thermodynamic equilibrium, it is possible to directly assess the stability of the catalyst at these reaction temperatures. In addition to analyzing ethanol conversion, product yield, and selectivity, the study also examined the catalysts' properties before and after the reaction. This was done to demonstrate their capability to suppress coke formation and maintain structural stability.

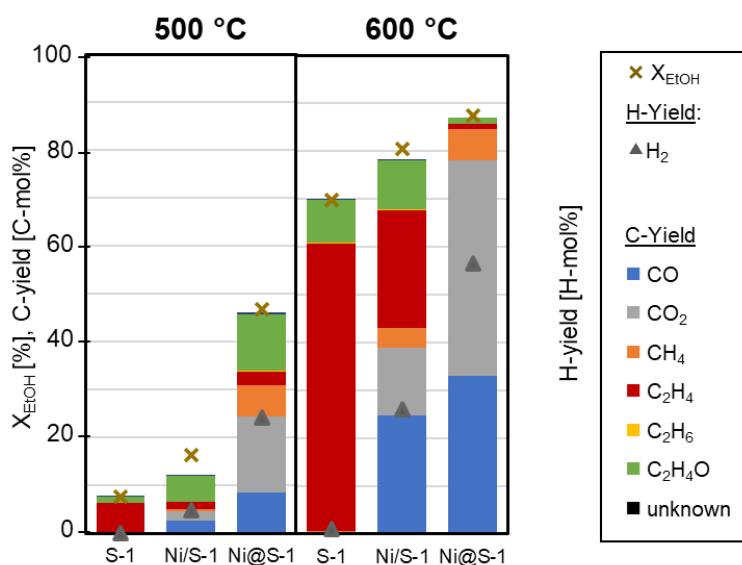


**Figure 4.10.** Ethanol conversion, H-yield, and C-yield in ESR activity test over Silicalite-1, Ni/Silicalite-1, and Ni@Silicalite-1, respectively, at 500 – 600 °C (time on stream of 4 h) (inlet ethanol-water mixture of 0.49 mL/h (0.2 g<sub>Ethanol</sub>/h), S/E=3, p<sub>EtOH</sub> = 0.03 atm, total inlet gas flow rate of 57.2 mL/min, and W/F = 0.5 h<sup>-1</sup>).

Consider the catalytic activity of ESR at a low reaction temperature (500 – 600 °C), which is in a kinetic control condition. For the case of pure support, Silicalite-1 without Ni, it is clearly that the primary reaction pathway involves the dehydration of ethanol to form ethylene (involving the cleavage of C-O bonds), while a minor pathway involves the dehydrogenation of ethanol to produce acetaldehyde. The presence of Ni catalyst accelerates three key processes: the dehydrogenation of ethanol to acetaldehyde (involving O-H bonds cleavage), C-C bonds cleavage leading to a steam reforming pathway, and subsequent water-gas shift reaction that produces C1 products along with hydrogen.

At 500 °C, the reaction temperature is insufficient to activate the reactants for effective progression, resulting in a low ethanol conversion. Notably, the catalytic activity of Ni@Silicalite-1 surpasses that of Ni/Silicalite-1, exhibiting approximately threefold higher in ethanol conversion, fivefold higher in H<sub>2</sub> yield, and a greater proportion of C1 products. This enhanced performance is attributed to the encapsulation of small-sized Ni particles within the zeolite structure of Ni@Silicalite-1, which expedites dehydrogenation, steam reforming, and the water-gas shift reaction even at lower reaction temperatures.

At 600 °C, similar reaction pathways are observed on both Silicalite-1 and Ni impregnated on Silicalite-1. At this temperature, sufficient activation of reactants occurs, leading to a significant increase in ethanol conversion, with relatively minor differences

observed among the three materials. The steam reforming pathway is notably enhanced on both Ni-impregnated Silicalite-1 and Ni encapsulated within Silicalite-1 due to the presence of Ni and the influence of the reaction temperature. Consequently, there is an increase in the selectivity of C1 products, including CH<sub>4</sub>, CO, and CO<sub>2</sub>, surpassing the results observed at 500 °C. Ni@Silicalite-1 demonstrates superior capability in converting C2 compounds into C1 products and generating more H<sub>2</sub>, this phenomenon is attributed to the smaller size of encapsulated Ni. Conversely, Ni/Silicalite-1 converts only half of the C2 compounds into C1 products and yields a lower amount of H<sub>2</sub>.

The variation in product distribution within the reaction medium suggests differing reaction pathways for ESR and the phenomenon of coke formation on the catalysts after use. On Silicalite-1 without Ni, numerous C2 precursors were generated, yet no carbon formation was detected on the Silicalite-1 following ESR. This suggests that coke formation only takes place in the presence of Ni sites on the catalyst. The amount of coke formation on the spent catalyst is listed in Table 4.4. On Ni/Silicalite-1, Ni exists on zeolite surface with a low Ni-support interaction, it makes C2 conversion in steam reforming pathway to be lower, therefore, the reaction medium primarily contains ethylene and acetaldehyde. These C2 compounds experience decomposition and polymerization, resulting in coke formation on the used catalysts. Ni@Silicalite-1 demonstrates significantly lower coke formation, approximately 2 to 3 times less than that observed in Ni/Silicalite-1. The smaller Ni size and encapsulation structure prove advantageous for both the reaction's activity and its propensity for coke formation.

**Table 4.4.** Amount of coke formation on spent Ni catalysts (wt %).

| Reaction Condition |      | Ni/Silicalite-1 | Ni@Silicalite-1 |
|--------------------|------|-----------------|-----------------|
| 500 °C             | 4 h  | 9.40            | 3.37            |
|                    | 10 h | 15.31           | 6.28            |
| 600 °C             | 4 h  | 12.35           | 4.16            |
| 700 °C             | 4 h  | 4.96            | 0.99            |
| 800 °C             | 4 h  | 0.00            | 0.00            |

Next experiments are conducted to explore ESR at elevated temperatures ranging from 700 to 800 °C using three materials: Silicalite-1, Ni/Silicalite-1, and Ni@Silicalite-1. The resulting data, illustrated in Figure 4.11, are compared with the calculated thermodynamic equilibrium composition, in the same manner as done in the experiment in 500 – 600 °C.

The experimental results were shown in Figure 4.11. At a reaction temperature of 700 °C, the reaction environment leans towards equilibrium over kinetics, and reaching thermodynamic equilibrium at 800 °C. Complete ethanol conversion was achieved at both temperatures. At 700 °C, on Silicalite-1 without Ni, the dehydration of ethanol to ethylene was notably enhanced, accompanied by a minor production of acetaldehyde through ethanol dehydrogenation. A small amount of C1 products and hydrogen evolved due to thermally activated steam reforming reactions or thermal decomposition of acetaldehyde to CH<sub>4</sub> and CO. Unlike the low-temperature experiments, no coke formation was observed on the spent Silicalite-1, affirming that coke formation only occurred with Ni active sites exist.

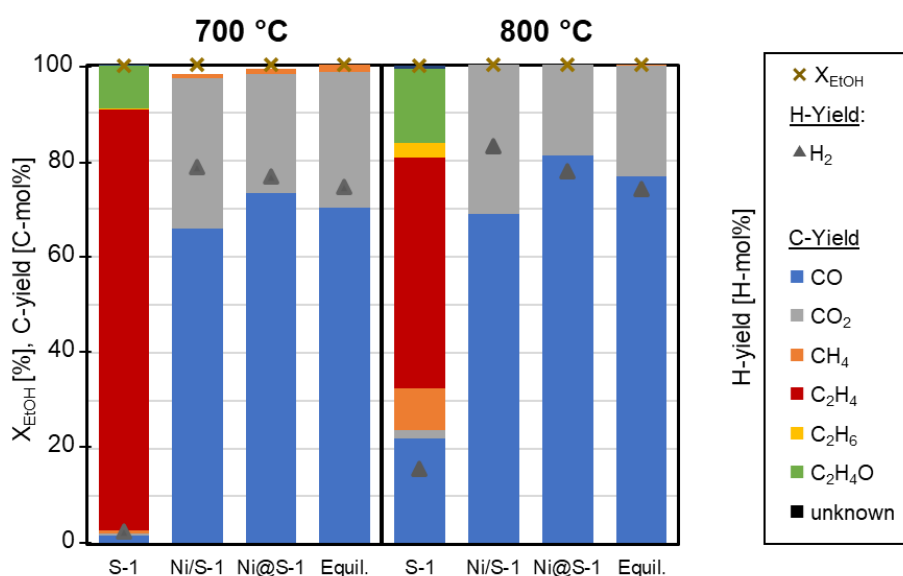


**Figure 4.11.** Ethanol conversion, H-yield, and C-yield in ESR activity test over Silicalite-1, Ni/Silicalite-1, and Ni@Silicalite-1, respectively, at 700 – 800 °C (time on stream of 4 h) (inlet ethanol-water mixture of 0.49 mL/h (0.2 g<sub>Ethanol</sub>/h), S/E=3, p<sub>EtOH</sub> = 0.03 atm, total inlet gas flow rate of 57.2 mL/min, and W/F = 0.5 h<sup>-1</sup>).

In catalysts containing Ni sites, the absence of C2 species in the reaction medium was observed, and the product gases were H<sub>2</sub>, CO, and CO<sub>2</sub>. This indicates the progression of the steam reforming pathway under these reaction conditions. The product distributions on both catalysts deviated from the calculated values for the thermodynamic equilibrium composition. For Ni/Silicalite-1, higher H<sub>2</sub> production compared to the calculated equilibrium composition was achieved due to coke formation through ethylene or methane decomposition pathways. Moreover, the reduced CO production stemmed from coke formation through the Boudouard reaction, where CO is consumed to produce CO<sub>2</sub> along with coke. In contrast, Ni@Silicalite-1 exhibited heightened activity, yielding a higher quantity of C1 products. The H<sub>2</sub> yield,

however, decreased compared to Ni/Silicalite-1 due to a reverse water-gas shift reaction that consumes  $H_2$  and  $CO_2$ , producing  $CO$  and  $H_2O$ . This reverse reaction was enhanced on smaller Ni sites and within the encapsulation structure.

At 800 °C, the temperature is sufficiently elevated to manifest reaction pathways influenced by temperature effects. Thermal decomposition of the reactants occurred, along with a thermal steam reforming reaction, resulting in reforming products observed on Silicalite-1 without Ni. The thermal ethanol dehydrogenation process was intensified due to the higher reaction temperature, surpassing ethanol dehydration to ethylene and yielding a greater quantity of acetaldehyde. Additionally, thermal decomposition of acetaldehyde took place at this temperature, leading to the evolution of  $CH_4$  and  $CO$ . The catalysts exhibited a similar pattern of product yields as observed at 700 °C, but with an enhanced effect due to the higher reaction temperature. No coke formation was detected on any of the spent catalysts at this reaction temperature, as indicated in Table 4.4. This outcome is attributed to the temperature's impact, which amplifies both the steam reforming pathway (reducing the formation of coke precursors) and the coke gasification process (elimination of coke). Based on the preceding analysis, it was observed that the formation of coke on Ni@Silicalite-1 was lesser compared to Ni/Silicalite-1 across all tested temperatures. Hence, the encapsulation structure of Ni within the zeolite not only improves the catalyst's capability for C-C bond cleavage, resulting in higher catalytic activity, but also offers resistance against coke formation on the Ni surface.

#### **4.3.2. Effect of steam-to-carbon ratio in feed**

Steam to carbon ratio in feed is one of the operating conditions that control the coke formation on the spent catalyst after reaction which is one of ESR catalyst deactivation. In this experiment, the molar ratio of ethanol-to-water in feed was varied to compare the performance of encapsulation catalyst. The ratio varies as the ideal stoichiometric coefficient of 1:3 and the severe condition of lower water content of 1:1, to illustrate the coke formation tolerance. Also, the lower reaction temperature that is severe in terms of coke formation due to the concentrated of coke precursor can be found in the reaction media. The catalytic activity in terms of ethanol conversion, product selectivity, hydrogen yield is shown in Figure 4.12. The amount of coke formation on the spent catalyst is listed in Table 4.5. For comparison, the experimental results of Ni/Silicalite-1 impregnation catalyst tested with 1:3 molar ratio of ethanol-to-water are shown along as well.

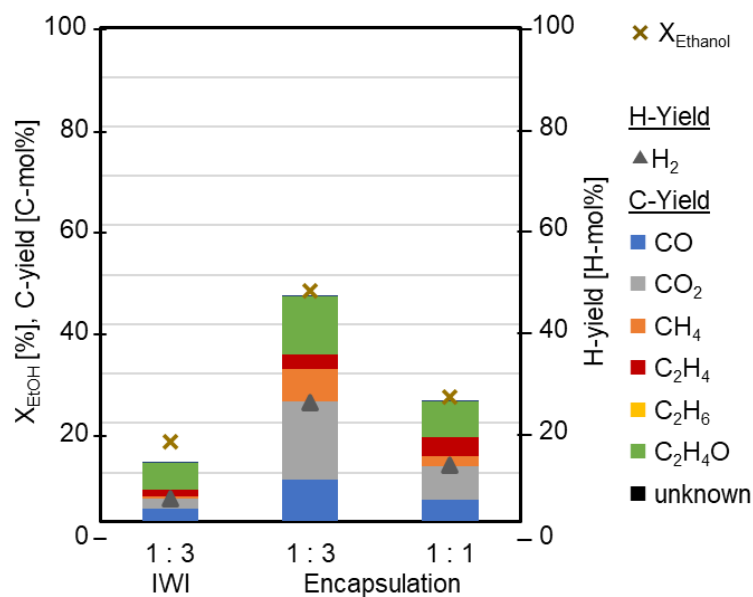


**Figure 4.12.** Reaction results of the different steam-to-carbon ratio on Ni@Silicalite-1 with the comparison of impregnation catalyst.

In a low steam reaction, encapsulation structure can provide a catalytic reactivity higher than the conventional impregnation catalyst. With the lower steam content, the ethanol conversion of Ni@Silicalite-1 are reduced in half of the stoichiometric ratio condition, with the higher ratio of C<sub>2</sub> species in the reaction media due to the production in non-steam reforming pathway from lack of reactant, water, obviously the formation of ethylene from ethanol dehydration. Interestingly, the encapsulation structure shows a good performance in coke suppression, as in Table 4.5, only a slight increase of coke formation observed on the spent catalyst. Consideration the surface area and micropore volume change after low-steam condition as shown in Table 4.6, the coke formation mechanism on the catalyst might be a little different from the case with higher steam content, which can alter the catalyst surface by increasing the surface area and pore volume.

**Table 4.5.** The amount of coke formation on spent catalyst in different steam-to-carbon ratio.

| Sample          | Reaction condition | Coke<br>mg/0.1 g cat |
|-----------------|--------------------|----------------------|
| Ni/Silicalite-1 | 1:3 (4 h)          | 9.40                 |
| Ni@Silicalite-1 | 1:3 (4 h)          | 3.37                 |
|                 | 1:1 (4 h)          | 3.42                 |

**Table 4.6.** surface area and micropore volume change of Ni@Silicalite-1 after the various reaction test (after coke removal process).

|           | Surface area<br>( $\text{cm}^2/\text{g}_{\text{sample}}$ ) | Micropore Volume<br>( $\text{cm}^3(\text{STP})/\text{g}$ ) |
|-----------|--|--|
| Fresh     | 447.330  | 0.1396   |
| 1:3 (4 h) | 406.726  | 0.1246   |
| 1:1 (4 h) | 496.873  | 0.1852   |

In conclusion, the encapsulation catalyst can function in severe conditions that are prone to coke formation such as low reaction temperature and also low steam content. This catalyst structure is interesting to evaluate in the different types of deactivations, which can be done in further study.

#### 4.3.3. Stability Test

The stability assessment of ESR was conducted under two distinct reaction conditions. The initial condition involved ESR at 500 °C with a time on stream of 10 hours. This examination compared the catalytic activity at a lower reaction temperature and evaluated the catalyst's capability to suppress coke formation, given that the reaction medium at this temperature is enriched with active coke precursors and C2 compounds.

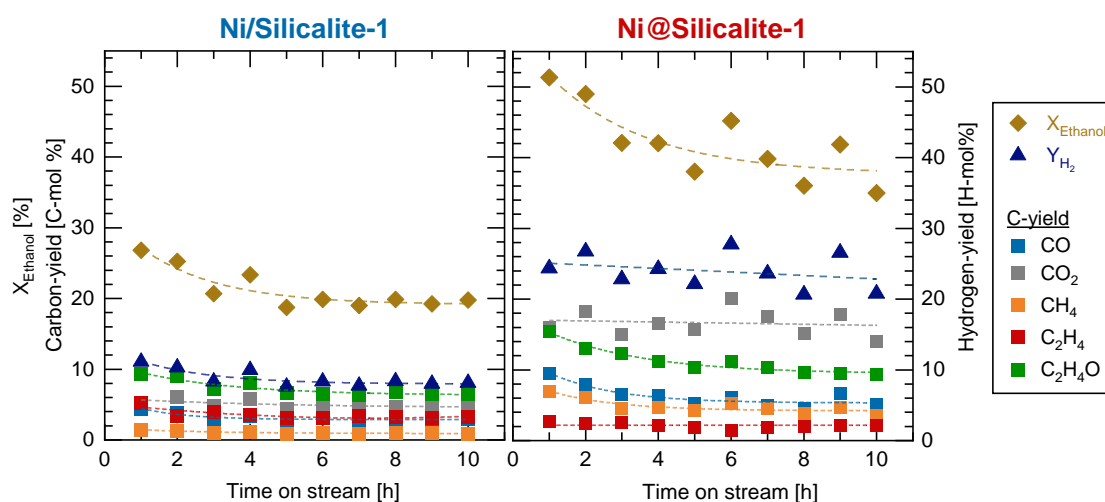


**Figure 4.13.** Ethanol conversion, H-yield, and C-yield in ESR stability test over Ni/Silicalite-1 and Ni@Silicalite-1 at 500 °C for 10 h (inlet ethanol-water mixture of 0.49 mL/h (0.2  $\text{g}_{\text{Ethanol}}/\text{h}$ ),  $S/E=3$ ,  $p_{\text{EtOH}} = 0.03$  atm, total inlet gas flow rate of 57.2 mL/min, and  $W/F = 0.5 \text{ h}^{-1}$ ).



The comparison of reaction performance and product stability is illustrated in Figure 4.13. Ni/Silicalite-1 initiated with an ethanol conversion rate of 27%, which then declined to 20% after 10 hours, indicating a 30% reduction in ethanol conversion over the specified period. Hydrogen yield ranged between 8% and 11%. Conversely, Ni@Silicalite-1 showcased a higher initial ethanol conversion of 51%, decreasing to 35% after 10 hours. The reduction in conversion was comparable to that of an impregnation catalyst, at approximately 30%, but over the 10-hour time on stream, the reduction rate was twice as high. Additionally, Ni@Silicalite-1 yielded a greater and more consistent hydrogen production over time (21% to 24% H<sub>2</sub> yield, with a 12.5% reduction over time)

Regarding coke formation, the quantity of coke formed on the spent catalysts after 10 hours of ESR at 500 °C is detailed in Table 4.4. A significantly greater amount of coke was observed on Ni/Silicalite-1, being 2.5 times higher compared to Ni@Silicalite-1. The SEM images illustrating the spent Ni/Silicalite-1 and Ni@Silicalite-1 after 10 hours of ESR at 500 °C are presented in Figure 4.14A and 4.14B, respectively.

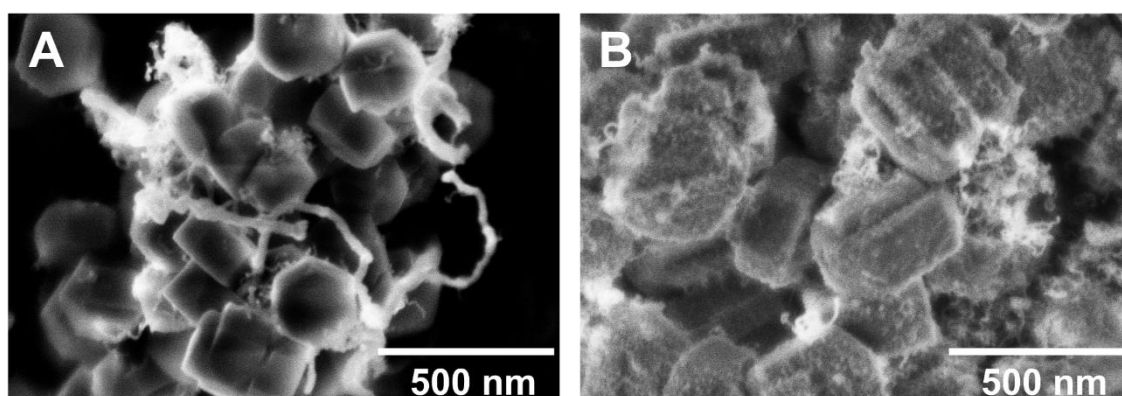


**Figure 4.14.** SEM images of the spent Ni/Silicalite-1 (A) and Ni@Silicalite-1 (B), after ESR stability test at 500 °C 10 h.

Filamentous coke was observed on the catalyst surface in both Ni/Silicalite-1 and Ni@Silicalite-1, but in different manners, i.e., in varying amounts and sizes. Ni/Silicalite-1 exhibited a substantial presence of filamentous coke with diverse diameters, aligning with the amount of coke determined from TG analysis. The different amount of coke formation is the result from the activity of the Ni active sites promotes the different reaction pathways, consequently the different coke precursors. The coke formation also affects the reaction activity by decreasing product selectivity with the reaction time due to the reduction of active surface area via physisorption or chemisorption of carbon species which hinder the access of

the reactant towards the Ni active sites. The different size of filamentous coke originates from the sites of coke origin, together with the growth mode. The larger coke diameters stemmed from the Ni's significant size, prompting a tip-growth mode of coke formation (metal size  $\geq 5$  nm). This raised the risk of Ni site loss from the catalyst surface during the reaction and subsequent regeneration processes. On the other hand, Ni@Silicalite-1 displayed a smaller amount of filamentous coke on its surface. This growth of filamentous coke indicated the presence of carbon growth sites, which in our study correspond to Ni. Consequently, it implies that Ni@Silicalite-1 in this study is not entirely encapsulated, and trace amounts of Ni remain on the catalyst surface. Fortunately, these Ni particles are small, resulting in minimal coke formation with smaller diameters compared to the case of an impregnation catalyst. Given the small growth sites on the surface, these cokes are likely to grow in a base-growth mode, making them easier for gasification. Additionally, there is a higher likelihood for Ni to persist and function as an active Ni after catalyst regeneration.

The stability of Ni within the catalysts was assessed by examining particle size change post-reaction, providing insights into the catalyst's resistance to sintering. TEM images of the catalysts after 10 hours of ESR at 500 °C are presented in Figure 4.15B and 4.15D. The Ni particle size on each catalyst did not exhibit significant changes from its reduction stage. The observed Ni sizes were approximately 4 – 6 nm, with larger particles measuring 20 – 35 nm on Ni/Silicalite-1, and around 4 – 5 nm on Ni@Silicalite-1. At this stage, clear indications of sintering resistance were not observed. Therefore, an investigation into the stability at high temperatures was conducted, focusing on the specific effect of Ni sintering, especially considering the absence of coke formation on the spent catalysts after exposure to 800 °C.

As previously mentioned, the investigation of the catalyst's sintering resistance was specifically focused on 800 °C condition. TEM images of the spent Ni@Silicalite-1 and Ni/Silicalite-1 are displayed in Figure 4.15C and 4.15F, respectively. Ni sites within Ni@Silicalite-1 maintained a size of approximately 4.1 nm, evenly dispersed within the catalyst particles. A few larger Ni particles, around 7 – 10 nm in size, were observed near the outer edge of the zeolite particles. In contrast, Ni/Silicalite-1 exhibited significant agglomeration, with Ni sites sintering from 4 to 10 nm and agglomerated particles reaching sizes of 30 – 40 nm on the catalyst particles. The observed Ni particle sizes corresponded to the amount and diameter of coke, as previously described in the results. The small Ni sizes in Ni@Silicalite-1 are encapsulated within the Silicalite-1, serving as a barrier that separates Ni sites, preventing agglomeration while allowing gas passage for catalytic reactions. Therefore,

the encapsulation structure of Ni inside zeolite proves advantageous for ESR, enhancing catalytic activity while demonstrating sintering resistance and coke suppression across varying reaction conditions.

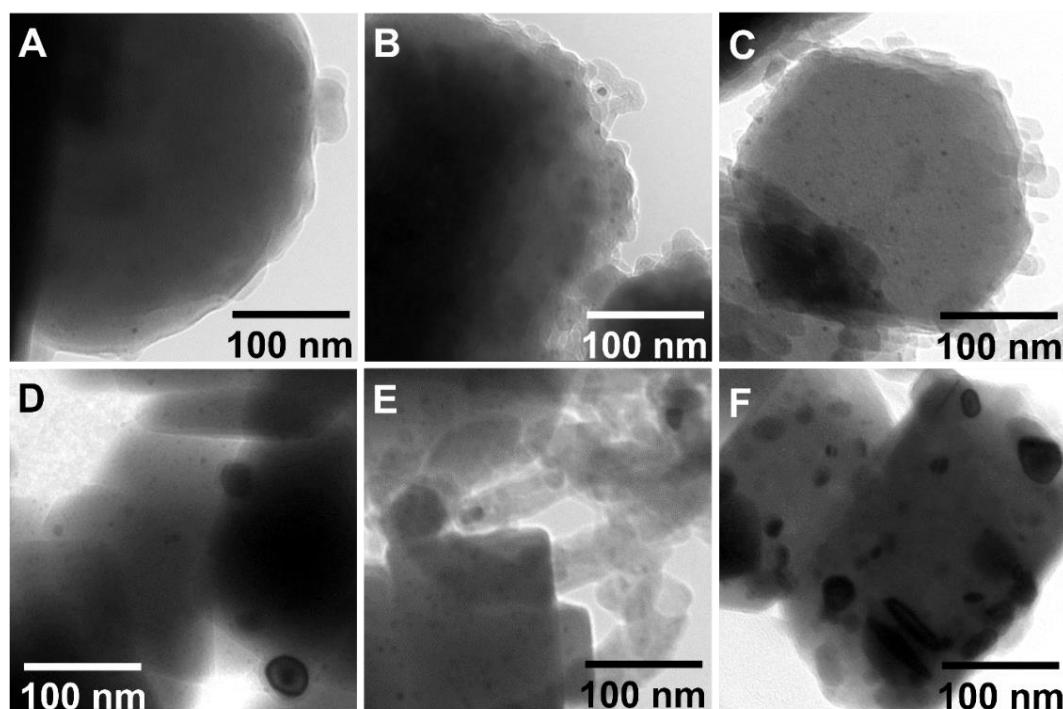


**Figure 4.15.** TEM images of Ni catalysts: Ni@Silicalite-1 (A, B, and C), Ni/Silicalite-1 (D, E, and F): after reduction at 700 °C (A and D), after reaction at 500 °C for 10 h (B and E), 800 °C for 4 h (C and F), left-to-right, respectively.

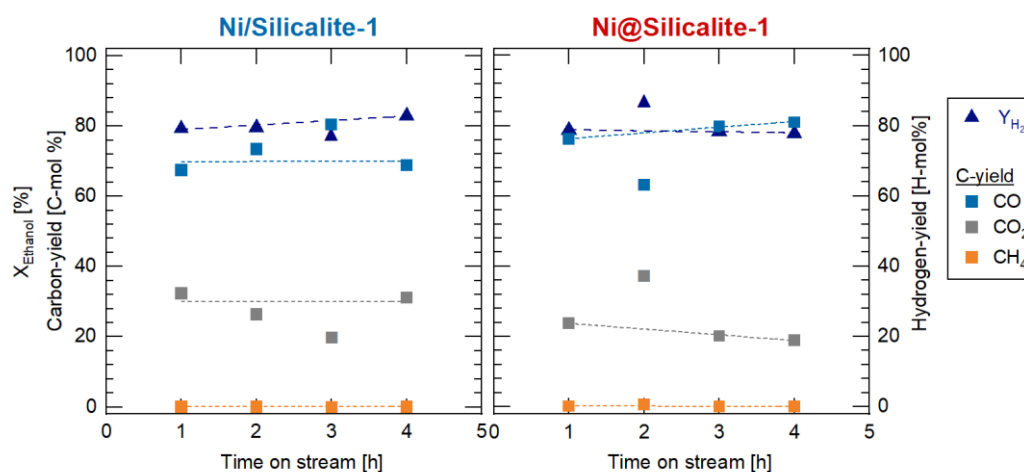


**Figure 4.16.** Ethanol conversion, H<sub>2</sub>-yield, and C-yield in ESR stability test over Ni/Silicalite-1 and Ni@Silicalite-1 at 800 °C for 4 h (inlet ethanol-water mixture of 0.49 mL/h (0.2 g<sub>Ethanol</sub>/h), S/E=3, p<sub>EtOH</sub> = 0.03 atm, total inlet gas flow rate of 57.2 mL/min, and W/F = 0.5 h<sup>-1</sup>).

**Table 4.7.** Surface area and micropore volume of the spent catalysts.

| Sample         | Time on stream (h) | Reaction temperature (°C) | Ni/Silicalite-1 | Ni@Silicalite-1 |
|----------------|--------------------|---------------------------|-----------------|-----------------|
| Fresh catalyst | -                  | -                         | 421.8 (0.18)    | 447.3 (0.14)    |
| Spent catalyst | 4 h                | 500                       | 441.0 (0.19)    | 406.7 (0.12)    |
|                |                    | 600                       | 399.3 (0.15)    | 349.4 (0.11)    |
|                |                    | 700                       | 427.6 (0.18)    | 421.1 (0.13)    |
|                |                    | 800                       | 414.5 (0.18)    | 397.2 (0.12)    |
|                | 10 h               | 500                       | 406.0 (0.17)    | 343.0 (0.11)    |

\* Micropore volumes are listed in parenthesis (-).

Another element of maintaining catalyst stability concerns the thermal durability of the catalyst structure. ESR is acknowledged as a severe reaction environment due to its elevated temperature and abundant steam, intended to enhance activity while minimizing coke formation. An effective catalyst for ESR should excel not only in catalytic activity, resistance to Ni sintering, and coke formation but also in preserving its structure under these rigorous reaction conditions. The N<sub>2</sub> physisorption data for the spent Ni catalyst under various reaction conditions is presented in Table 4.7. The reduction in surface area and micropore volume of the spent catalysts is a phenomenon indicating deterioration of the catalyst surface due to either reaction temperature or time on stream. Notably, the surface area and micropore volume remain relatively stable for Ni/Silicalite-1. Silicalite-1 support, being a crystalline material, demonstrates resilience in harsh conditions such as high reaction temperature and a steam-rich atmosphere. Considering of the observed coke formation behavior, it can be inferred that the substantial coke formation observed in the SEM images is primarily on the Ni sites that remain on the catalyst surface, without significantly affecting the surface properties of the catalyst during the time on stream in this study.

A notable alteration in surface area and micropore volume was observed in Ni@Silicalite-1. The encapsulation structure effectively suppresses the formation of extensive filamentous coke, as previously discussed. However, other forms of coke, like amorphous coke, may develop to a slight extent on the Ni surface or at the Ni-silica interface during the progression of the reaction, potentially leading to minor modifications in the surface area and micropore volume of the catalyst. Furthermore, the characterization results revealed the presence of amorphous silica on the surface of Ni@Silicalite-1, which could contribute to the degradation of the catalyst structure. The incomplete incorporation of Ni-PS

precursor during zeolite formation left trace amounts of silica on the surface, hindering the crystallization of the catalyst surface compared to the well-structured interior of the catalyst particle. The well-structured portion of Ni@Silicalite-1 displayed commendable catalytic activity, resistance to Ni sintering, and resistance to coke formation, as demonstrated in the preceding sections. As mentioned in the analysis of coke formation behavior, the synthesized Ni@Silicalite-1 in this study does not represent a fully encapsulated Ni structure within zeolite. This could be attributed to the residual amorphous silica present on the catalyst surface. These Ni particles containing amorphous silica or silica-coated Ni are partially exposed on the surface of Ni@Silicalite-1. As the reaction progresses, the silica begins to deform, and the Ni surface becomes exposed to the reaction medium without adequate protection. Consequently, it acts as a site for carbon growth on the surface.

In summary of Chapter 4, the investigation of catalytic activity of Ni@Silicalite-1 was performed in comparison with Ni/Silicalite-1, and Silicalite-1, in the aspect of Ni location, and Ni existence, respectively. The reaction tests were conducted at 500 – 800 °C, covering the range of kinetic control condition and thermodynamic equilibrium conditions. The catalysts properties including surface morphology and active sites properties were together investigated. Ni@Silicalite-1, the catalyst with Ni encapsulation structure, shows superior performance in all investigating reaction temperatures. It exhibits larger ethanol conversion, higher selectivity towards the complete steam reforming products, noticeably lower coke formation, and sintering resistance. The encapsulation structure provides the improvement of metal-support interaction, obtaining the small Ni particle size, securing inside zeolite structures. Considering between Ni particles inside zeolite, the crystalline zeolite structure acts as a porous barrier between each Ni NPs, so that sintering resistance can be achieved on Ni@Silicalite-1, together allowing the reactants to reach the small Ni active sites. Another aspect, considering the encapsulated Ni near the zeolite surface, the crystalline zeolite also secures from losing to the outer surface, metal sintering and coke formation can be suppressed at the same time. By the way, the obtained Ni@Silicalite-1 catalyst still required further development in preparation for a better encapsulation and lower the coke formation or even further to obtain coke-free catalyst.

## Chapter 5 : Conclusion and recommendations

The study on the production of hydrogen and syngas from biomass-derived alcohols using zeolite-encapsulated nickel catalysts was investigated through the preparation and utilization of Ni nanoparticles encapsulated Silicalite-1 catalysts in bioethanol steam reforming reaction. The development of Ni@Silicalite-1 catalysts were investigating in various preparation conditions, including the different precursors (the utilization of solid precursors, porosity, and calcination state) and hydrothermal synthesis condition (water-to-silica ratio and hydrothermal synthesis temperature). According to the studied conditions, the Ni@Silicalite-1 with the best properties was prepared by two-step method using non-porous calcined precursor in a mother liquor of water-to-silica ratio of 100 and was hydrothermal synthesis at 100 °C for 72 h. The obtained catalysts were further used in catalytic activity testing in ethanol steam reforming at 500 – 800 °C, compared to conventional Ni/Silicalite-1, and pure Silicalite-1, for reaction activity on a different Ni location, and reaction pathways investigation.

The catalytic activity of Ni over Silicalite-1 for ethanol steam reforming was enhanced by the encapsulation structure. The encapsulation structure of ultrafine Ni inside Silicalite-1 zeolite provides a direct advantage for the catalyst activity and suppressing coke formation. The small active sites provide a strong metal-support interaction, which helps in catalytic activity for reactant activation, adsorption, C-C bond cleavage, and desorption. The small Ni NPs highly dispersed in zeolite help reduce coke formation due to its activity towards steam reforming pathway which can reduce the coke precursor in a reaction media, consequently, reduce coke formation. The encapsulation structure provides benefits towards the reaction in two aspects, it suppresses sintering with the barrier structure of crystalline zeolite between Ni particles, which avoids agglomeration, which clearly observed in the severe condition as high reaction temperature. Moreover, the encapsulation structure with zeolite framework on the outer most surface can prevent a severe filamentous coke formation which is a main cause of ESR catalyst deactivation. Along with the filamentous coke suppression, the chance of active sites leaching after regeneration can also be suppressed.

The high crystallinity of catalyst structure provides stability under severe reaction conditions including high reaction temperature and steam atmosphere. The preparation condition of Ni@Silicalite-1, both precursor dissolution and hydrothermal synthesis condition can contribute to the structure formation. The proper dissolution of the precursor provides a nice configuration of zeolite precursors and can be nucleated and crystallized to form a highly crystalline structure. The calcined non-porous precursor can maintain a proper

dissolution from the stronger structure, and less contact surface for dissolution. On the other hand, too little precursor dissolution leads to the remaining amorphous silica (also containing Ni), too much dissolution leads to the individual Ni existing on zeolite surface. The proper hydrolysis condition that matches well with the mother liquor state helps make a highly crystalline zeolite with Ni encapsulated inside. The higher driving force from high alkalinity, high concentration of species leads the too fast nucleation and crystallization before the proper state of precursor dissolved and presence in the proper state, yielding the lower crystallinity of zeolite with the presence of Ni-amorphous silica. Too high hydrolysis temperature leads to the redissolution and recrystallization, Ni can be encapsulated inside high crystallinity zeolite but with the trace amount of Ni present on the outer surface.

For the further outlooks of this research, the successfully synthesized Ni@Silicalite-1 with a highly crystalline zeolite and fully encapsulated Ni inside Silicalite-1 will be a potential catalyst for the bioethanol steam reforming, also for other hydrocarbon reforming in a real application. It is indispensable to control the size and location of Ni active sites on the catalyst, together with the high crystallinity of the zeolites to deal with the severe reaction condition. The optimal preparation condition leads to the ideal catalyst properties which can overcome the difficulties in ethanol steam reforming reaction, especially sintering and coke formation. As the result in this study, the synthesis parameters for Ni@Silicalite-1 can be further improved. Considering the preparation procedure, especially a dissolution of Ni-PS and recrystallization to form Ni-containing zeolite. Fine tuning in dissolution time in the recent hydrolysis condition can be further studied, the optimal total dissolution time of Ni-PS might be in 12 – 15 hours in mother liquor preparation before hydrothermal synthesis. Moreover, the surface modification, for example, surface functional group modification, or Silanol group defect reduction, might be further studied, in order to obtain a stronger surface withstanding the outside-in structure collapse from the high temperature steam reaction.

## References

1. Bossel U, Eliasson B (2003) Energy and the Hydrogen Economy. Altern Fuels Data Cent
2. IEA (2023) Clean energy can help to ease the water crisis. <https://www.iea.org/commentaries/clean-energy-can-help-to-ease-the-water-crisis>
3. Fuel Cell and Hydrogen Energy Association (FCHEA) (2020) ROAD MAP TO A US HYDROGEN ECONOMY
4. Dincer I, Acar C (2014) Review and evaluation of hydrogen production methods for better sustainability. *Int J Hydrogen Energy* 40:11094–11111. <https://doi.org/10.1016/j.ijhydene.2014.12.035>
5. Abuadala A, Dincer I, Naterer GF (2010) Exergy analysis of hydrogen production from biomass gasification. *Int J Hydrogen Energy* 35:4981–4990. <https://doi.org/10.1016/j.ijhydene.2009.08.025>
6. Das D, Veziroglu TN (2008) Advances in biological hydrogen production processes. *Int J Hydrogen Energy* 33:6046–6057. <https://doi.org/10.1016/j.ijhydene.2008.07.098>
7. Koutrouli EC, Kalfas H, Gavala HN, et al (2009) Hydrogen and methane production through two-stage mesophilic anaerobic digestion of olive pulp. *Bioresour Technol* 100:3718–3723. <https://doi.org/10.1016/j.biortech.2009.01.037>
8. Tolga Balta M, Dincer I, Hepbasli A (2009) Thermodynamic assessment of geothermal energy use in hydrogen production. *Int J Hydrogen Energy* 34:2925–2939. <https://doi.org/10.1016/j.ijhydene.2009.01.087>
9. Zhang X, Yang W, Blasiak W (2011) Modeling study of woody biomass: Interactions of cellulose, hemicellulose, and lignin. *Energy and Fuels* 25:4786–4795. <https://doi.org/10.1021/ef201097d>
10. Nahar G, Dupont V (2012) Hydrogen via steam reforming of liquid biofeedstock. *Biofuels* 3:167–191. <https://doi.org/10.4155/BFS.12.8>
11. Willige A (2022) The colors of hydrogen: Expanding ways of decarbonization. In: *Spectra*. <https://spectra.mhi.com/the-colors-of-hydrogen-expanding-ways-of-decarbonization>
12. Sanchez N, Ruiz R, Hacker V, Cobo M (2020) Impact of bioethanol impurities on steam reforming for hydrogen production: A review. *Int J Hydrogen Energy* 45:11923–11942. <https://doi.org/10.1016/j.ijhydene.2020.02.159>
13. Lazar MD, Senila L, Dan M, Mihet M (2019) Crude bioethanol reforming process: The advantage of a biosource exploitation. Elsevier Inc.



14. Song H (2012) Catalytic Hydrogen Production from Bioethanol. In: Lima MAP (ed) Bioethanol. IntechOpen
15. Rossetti I, Compagnoni M, Finocchio E, et al (2016) Syngas production via steam reforming of bioethanol over Ni–BEA catalysts: A BTL strategy. *Int J Hydrogen Energy* 41:16878–16889. <https://doi.org/10.1016/j.ijhydene.2016.07.149>
16. Abdalazeez A, Wang W, Abuelgasim S (2021) Syngas production from chemical looping reforming of ethanol over iron-based oxygen carriers: Theoretical analysis and experimental investigation. *Chinese J Chem Eng* 38:123–131. <https://doi.org/10.1016/j.cjche.2021.02.012>
17. Pashchenko D (2019) Thermochemical recuperation by ethanol steam reforming: Thermodynamic analysis and heat balance. *Int J Hydrogen Energy* 44:30865–30875. <https://doi.org/10.1016/j.ijhydene.2019.10.009>
18. Dong X, Peng L, Xiaoyou Y (2019) Process modeling, optimization, and heat integration of ethanol reforming process for syngas production with high H<sub>2</sub>/CO ratio. *Processes* 7:.. <https://doi.org/10.3390/PR7120960>
19. Arregi A, Lopez G, Amutio M, et al (2018) Regenerability of a Ni catalyst in the catalytic steam reforming of biomass pyrolysis volatiles. *J Ind Eng Chem* 68:69–78. <https://doi.org/10.1016/j.jiec.2018.07.030>
20. Du J, Gao J, Gu F, et al (2018) A strategy to regenerate coked and sintered Ni/Al<sub>2</sub>O<sub>3</sub> catalyst for methanation reaction. *Int J Hydrogen Energy* 43:20661–20670. <https://doi.org/10.1016/j.ijhydene.2018.09.128>
21. Arregi A, Amutio M, Lopez G, et al (2018) Evaluation of thermochemical routes for hydrogen production from biomass: A review. *Energy Convers Manag* 165:696–719. <https://doi.org/10.1016/j.enconman.2018.03.089>
22. Lopez G, Artetxe M, Amutio M, et al (2018) Recent advances in the gasification of waste plastics. A critical overview. *Renew Sustain Energy Rev* 82:576–596. <https://doi.org/10.1016/j.rser.2017.09.032>
23. Khamhaeng P, Laosiripojana N, Assabumrungrat S, Kim-Lohsoontorn P (2021) Techno-economic analysis of hydrogen production from dehydrogenation and steam reforming of ethanol for carbon dioxide conversion to methanol. *Int J Hydrogen Energy* 46:30891–30902. <https://doi.org/10.1016/j.ijhydene.2021.04.048>
24. Elias KFM, Lucrédio AF, Assaf EM (2015) Study of Sr Addition on Ni/Al<sub>2</sub>O<sub>3</sub> Catalysts Applied in Ethanol Steam Reforming. *J Chem Eng Chem Res* 2:488–496
25. Cifuentes B, Valero MMF, Conesa J a. J, et al (2015) Hydrogen Production by Steam

- Reforming of Ethanol on Rh-Pt Catalysts: Influence of CeO<sub>2</sub>, ZrO<sub>2</sub>, and La<sub>2</sub>O<sub>3</sub> as Supports. *Catalysts* 5:1872–1896. <https://doi.org/10.3390/catal5041872>
26. Guerrero L, Castilla S, Cobo M (2014) Advances in ethanol reforming for the production of hydrogen. *Quim Nova* 37:850–856. <https://doi.org/10.5935/0100-4042.20140137>
  27. Hou T, Zhang S, Chen Y, et al (2015) Hydrogen production from ethanol reforming: Catalysts and reaction mechanism. *Renew Sustain Energy Rev* 44:132–148. <https://doi.org/10.1016/j.rser.2014.12.023>
  28. Konsolakis M, Ioakimidis Z, Kraia T, Marnellos G (2016) Hydrogen Production by Ethanol Steam Reforming (ESR) over CeO<sub>2</sub> Supported Transition Metal (Fe, Co, Ni, Cu) Catalysts: Insight into the Structure-Activity Relationship. *Catalysts* 6:39. <https://doi.org/10.3390/catal6030039>
  29. Kumar A, Prasad R, Sharma YC (2014) Steam Reforming of Ethanol: Production of Renewable Hydrogen. *Int J Environ Res Dev* 4:2249–3131
  30. Olafadehan OA, Ayoola AA, Akintunde OO, Adeniyi VO (2015) MECHANISTIC KINETIC MODELS FOR STEAM REFORMING OF CONCENTRATED CRUDE ETHANOL ON NI/AL<sub>2</sub>O<sub>3</sub> CATALYST. 10:633–653
  31. Vargas JC, Ivanova S, Thomas S, et al (2012) Influence of Gold on Ce-Zr-Co Fluorite-Type Mixed Oxide Catalysts for Ethanol Steam Reforming. *Catalysts* 2:121–138. <https://doi.org/10.3390/catal2010121>
  32. Ogo S, Sekine Y (2020) Recent progress in ethanol steam reforming using non-noble transition metal catalysts: A review. *Fuel Process Technol* 199:106238. <https://doi.org/10.1016/j.fuproc.2019.106238>
  33. Liguras DK, Kondarides DI, Verykios XE (2003) Production of hydrogen for fuel cells by steam reforming of ethanol over supported noble metal catalysts. *Appl Catal B Environ* 43:345–354. [https://doi.org/10.1016/S0926-3373\(02\)00327-2](https://doi.org/10.1016/S0926-3373(02)00327-2)
  34. Lin J, Chen L, Choong CKS, et al (2015) Molecular catalysis for the steam reforming of ethanol. *Sci China Chem* 58:60–78. <https://doi.org/10.1007/s11426-014-5262-0>
  35. Dalena F, Giglio E, Marino A, et al (2022) Steam Reforming of Bioethanol Using Metallic Catalysts on Zeolitic Supports: An Overview. *Catalysts* 12:.. <https://doi.org/10.3390/catal12060617>
  36. Masuda T, Fujikata Y, Mukai SR, Hashimoto K (1998) Changes in catalytic activity of MFI-type zeolites caused by dealumination in a steam atmosphere. *Appl Catal A Gen* 172:73–83. [https://doi.org/10.1016/S0926-860X\(98\)00120-3](https://doi.org/10.1016/S0926-860X(98)00120-3)

37. Gusev AA, Psarras AC, Triantafyllidis KS, et al (2017) Effect of steam deactivation severity of ZSM-5 additives on LPG olefins production in the FCC process. *Molecules* 22:. <https://doi.org/10.3390/molecules22101784>
38. Arayawate S (2018) Hydrogen Production from Ethanol Steam Reforming and Ammonia Decomposition. Sirindhorn International Institute of Technology, Thammasat University
39. Palmaa V, Castaldo F, Ruoccoa C, et al (2015) Low temperature-ethanol steam reforming over Ni-based catalysts supported on CeO<sub>2</sub>. *J Power Technol* 95:54–66
40. Muroyama H, Nakase R, Matsui T, Eguchi K (2010) Ethanol steam reforming over Ni-based spinel oxide. *Int J Hydrogen Energy* 35:1575–1581. <https://doi.org/10.1016/j.ijhydene.2009.12.083>
41. Fajardo H V., Longo E, Mezalira DZ, et al (2010) Influence of support on catalytic behavior of nickel catalysts in the steam reforming of ethanol for hydrogen production. *Environ Chem Lett* 8:79–85. <https://doi.org/10.1007/s10311-008-0195-5>
42. Mondal T, Pant KK, Dalai AK (2015) Catalytic oxidative steam reforming of bio-ethanol for hydrogen production over Rh promoted Ni/CeO<sub>2</sub>-ZrO<sub>2</sub> catalyst. *Int J Hydrogen Energy* 40:2529–2544. <https://doi.org/10.1016/j.ijhydene.2014.12.070>
43. Ramrez-Hernandez GY, Viveros-Garcia T, Fuentes-Ramirez R, Galindo-Esquivel IR (2016) Promoting behavior of yttrium over nickel supported on alumina-yttria catalysts in the ethanol steam reforming reaction. *Int J Hydrogen Energy* 41:9332–9343. <https://doi.org/10.1016/j.ijhydene.2016.04.080>
44. Ma H, Zhang R, Huang S, et al (2012) Ni/Y<sub>2</sub>O<sub>3</sub>-Al<sub>2</sub>O<sub>3</sub> catalysts for hydrogen production from steam reforming of ethanol at low temperature. *J Rare Earths* 30:683–690. [https://doi.org/10.1016/S1002-0721\(12\)60112-4](https://doi.org/10.1016/S1002-0721(12)60112-4)
45. Li Z, Li M, Bian Z, et al (2016) Design of highly stable and selective core/yolk-shell nanocatalysts-review. *Appl Catal B Environ* 188:324–341. <https://doi.org/10.1016/j.apcatb.2016.01.067>
46. Azancot L, Bobadilla LF, Santos JL, et al (2019) Influence of the preparation method in the metal-support interaction and reducibility of Ni-Mg-Al based catalysts for methane steam reforming. *Int J Hydrogen Energy* 44:19827–19840. <https://doi.org/10.1016/j.ijhydene.2019.05.167>
47. Yao D, Yang H, Chen H, Williams PT (2018) Investigation of nickel-impregnated zeolite catalysts for hydrogen/syngas production from the catalytic reforming of waste polyethylene. *Appl Catal B Environ* 227:477–487.

- <https://doi.org/10.1016/j.apcatb.2018.01.050>
48. Kim JH, Suh DJ, Park TJ, Kim KL (2000) Effect of metal particle size on coking during CO<sub>2</sub> reforming of CH<sub>4</sub> over Ni-alumina aerogel catalysts. *Appl Catal A Gen* 197:191–200. [https://doi.org/10.1016/S0926-860X\(99\)00487-1](https://doi.org/10.1016/S0926-860X(99)00487-1)
  49. Kobayashi T, Furuya T, Fujitsuka H, Tago T (2019) Synthesis of Birdcage-type zeolite encapsulating ultrafine Pt nanoparticles and its application in dry reforming of methane. *Chem Eng J* 377:120203. <https://doi.org/10.1016/j.cej.2018.10.140>
  50. Fujitsuka H, Kobayashi T, Tago T (2021) Development of Silicalite-1-encapsulated Ni nanoparticle catalyst from amorphous silica-coated Ni for dry reforming of methane: Achieving coke formation suppression and high thermal stability. *J CO<sub>2</sub> Util* 53:101707. <https://doi.org/10.1016/j.jcou.2021.101707>
  51. Zhang Y, Takahashi R, Kimura K, et al (2023) Development of Silicalite-1-Encapsulated Ni Catalyst from Ni Phyllosilicate for Dry Reforming of Methane. *Catal Surv from Asia* 27:56–66. <https://doi.org/10.1007/s10563-022-09379-3>
  52. Cundy CS, Cox PA (2003) The hydrothermal synthesis of zeolites: History and development from the earliest days to the present time. *Chem Rev* 103:663–701. <https://doi.org/10.1021/cr020060i>
  53. Hosokawa M, Nogi K, Naio M, Yokoyama T (2008) CONTROL OF NANOSTRUCTURE OF MATERIALS. In: *Nanoparticle Technology Handbook*. Elsevier B.V
  54. Moshoeshoe M, Silas Nadiye-Tabbiruka M, Obuseng V (2017) A Review of the Chemistry, Structure, Properties and Applications of Zeolites. *Am J Mater Sci* 2017:196–221. <https://doi.org/10.5923/j.materials.20170705.12>
  55. Grand J, Awala H, Mintova S (2016) Mechanism of zeolites crystal growth: New findings and open questions. *CrystEngComm* 18:650–664. <https://doi.org/10.1039/c5ce02286j>
  56. Buschmann Â, Kirschhock CEA, Kremer S, et al (2001) Zeosil Nanoslabs : Building Blocks in nPr 4 N ‡ -. *Communications* 3010:2637–2640
  57. Umeda T, Yamada H, Ohara K, et al (2017) Comparative Study on the Different Interaction Pathways between Amorphous Aluminosilicate Species and Organic Structure-Directing Agents Yielding Different Zeolite Phases. *J Phys Chem C* 121:24324–24334. <https://doi.org/10.1021/acs.jpcc.7b07745>
  58. Kacirek H, Lechert H (1975) Growth of the zeolite type NaY. *J Phys Chem* 79:1589–1593. <https://doi.org/10.1021/j100582a024>

59. Zheng B, Wan Y, Yang W, et al (2014) Mechanism of seeding in hydrothermal synthesis of zeolite Beta with organic structure-directing agent-free gel. *Chinese J Catal* 35:1800–1810. [https://doi.org/10.1016/S1872-2067\(14\)60089-9](https://doi.org/10.1016/S1872-2067(14)60089-9)
60. Xie B, Zhang H, Yang C, et al (2011) Seed-directed synthesis of zeolites with enhanced performance in the absence of organic templates. *Chem Commun* 47:3945–3947. <https://doi.org/10.1039/C0CC05414C>
61. Dumas A, Mizrahi M, Martin F, Requejo FG (2015) Local and Extended-Order Evolution of Synthetic Talc during Hydrothermal Synthesis: Extended X-ray Absorption Fine Structure, X-ray Diffraction, and Fourier Transform Infrared Spectroscopy Studies. *Cryst Growth Des* 15:5451–5463. <https://doi.org/10.1021/acs.cgd.5b01076>
62. Tao M, Meng X, Lv Y, et al (2016) Effect of impregnation solvent on Ni dispersion and catalytic properties of Ni/SBA-15 for CO methanation reaction. *Fuel* 165:289–297. <https://doi.org/10.1016/j.fuel.2015.10.023>
63. Shakhshiri BZ, Dirreen GE, Juergens F (1980) Tested demonstrations: Color, solubility, and complex ion equilibria of nickel (II) species in aqueous solution. *J Chem Educ* 57:900–901. <https://doi.org/10.1021/ed057p900>
64. Birk J (2023) Characteristic Reactions of Nickel Ions ( $\text{Ni}^{2+}$ )
65. Xu Y, Sun X, Wu D, et al (2007) Ammonia catalyzed hydrolysis-condensation kinetics of tetraethoxysilane/ dimethyldiethoxysilane mixtures studied by  $^{29}\text{Si}$  NMR and SAXS. *J Solution Chem* 36:327–344. <https://doi.org/10.1007/s10953-006-9117-y>
66. Fatsikostas AN, Verykios XE (2004) Reaction network of steam reforming of ethanol over Ni-based catalysts. *J Catal* 225:439–452. <https://doi.org/10.1016/j.jcat.2004.04.034>
67. Zanchet D, Santos JBO, Damyanova S, et al (2015) Toward understanding metal-catalyzed ethanol reforming. *ACS Catal* 5:3841–3863. <https://doi.org/10.1021/cs5020755>
68. Tripodi A, Compagnoni M, Rossetti I (2016) Kinetic Modeling and Reactor Simulation for Ethanol Steam Reforming. *ChemCatChem* 8:3804–3813. <https://doi.org/10.1002/cctc.201601075>
69. Yeh YH, Gorte RJ, Rangarajan S, Mavrikakis M (2016) Adsorption of Small Alkanes on ZSM-5 Zeolites: Influence of Brønsted Sites. *J Phys Chem C* 120:12132–12138. <https://doi.org/10.1021/acs.jpcc.6b03855>
70. Luo T, Zhang R, Zeng WW, et al (2021) Alkoxylation Reaction of Alcohol on Silica

- Surfaces Studied by Sum Frequency Vibrational Spectroscopy. *J Phys Chem C* 125:8638–8646. <https://doi.org/10.1021/acs.jpcc.1c02418>
71. Luts T, Katz A (2012) Chemisorption and dehydration of ethanol on silica: Effect of temperature on selectivity. *Top Catal* 55:84–92. <https://doi.org/10.1007/s11244-012-9771-9>
  72. Shinohara Y, Nakajima T, Suzuki S (1999) A theoretical study of the dehydration and the dehydrogenation processes of alcohols on metal oxides using MOPAC. *J Mol Struct THEOCHEM* 460:231–244. [https://doi.org/10.1016/S0166-1280\(98\)00321-2](https://doi.org/10.1016/S0166-1280(98)00321-2)
  73. Jiménez MJ, Lissarrague MS, Bechthold P, et al (2022) Ethanol adsorption on Ni doped Mo<sub>2</sub>C(001): a theoretical study. *Top Catal* 65:839–847. <https://doi.org/10.1007/s11244-022-01596-4>
  74. Xu J, Zhang X, Zenobi R, et al (1991) Ethanol decomposition on Ni(111): observation of ethoxy formation by IRAS and other methods. *Surf Sci* 256:288–300. [https://doi.org/10.1016/0039-6028\(91\)90872-P](https://doi.org/10.1016/0039-6028(91)90872-P)
  75. Gates SM, Russell JN, Yates JT (1986) Bond activation sequence observed in the chemisorption and surface reaction of ethanol on Ni(111). *Surf Sci* 171:111–134. [https://doi.org/10.1016/0039-6028\(86\)90565-0](https://doi.org/10.1016/0039-6028(86)90565-0)
  76. Vaidya PD, Wu YJ, Rodrigues AE (2018) Kinetics of ethanol steam reforming for hydrogen production. In: *Ethanol: Science and Engineering*. Elsevier Inc., pp 341–354
  77. El-Salamony RA (2023) Catalytic Steam Reforming of Ethanol to Produce Hydrogen: Modern and Efficient Catalyst Modification Strategies. *ChemistrySelect* 8:. <https://doi.org/10.1002/slct.202203195>
  78. Mattos L V., Jacobs G, Davis BH, Noronha FB (2012) Production of hydrogen from ethanol: Review of reaction mechanism and catalyst deactivation. *Chem Rev* 112:4094–4123. <https://doi.org/10.1021/cr2000114>
  79. Li MR, Chen J, Wang GC (2016) Reaction Mechanism of Ethanol on Model Cobalt Catalysts: DFT Calculations. *J Phys Chem C* 120:14198–14208. <https://doi.org/10.1021/acs.jpcc.6b04036>
  80. Ferrin P, Simonetti D, Kandoi S, et al (2009) Modeling ethanol decomposition on transition metals: A combined application of scaling and brønsted-evans-polanyi relations. *J Am Chem Soc* 131:5809–5815. <https://doi.org/10.1021/ja8099322>
  81. Bai Y, Kirvassilis D, Xu L, Mavrikakis M (2019) Atomic and molecular adsorption on Ni(111). *Surf Sci* 679:240–253. <https://doi.org/10.1016/j.susc.2018.08.004>
  82. Sharma YC, Kumar A, Prasad R, Upadhyay SN (2017) Ethanol steam reforming for

- hydrogen production: Latest and effective catalyst modification strategies to minimize carbonaceous deactivation. *Renew Sustain Energy Rev* 74:89–103.  
<https://doi.org/10.1016/j.rser.2017.02.049>
83. Stanciakova K, Weckhuysen BM (2021) Water–active site interactions in zeolites and their relevance in catalysis. *Trends Chem* 3:456–468.  
<https://doi.org/10.1016/j.trechm.2021.03.004>
  84. Zhang L, Chen K, Chen B, et al (2015) Factors that Determine Zeolite Stability in Hot Liquid Water. *J Am Chem Soc* 137:11810–11819.  
<https://doi.org/10.1021/jacs.5b07398>
  85. Malola S, Svelle S, Bleken FL, Swang O (2012) Detailed reaction paths for zeolite dealumination and desilication from density functional calculations. *Angew Chemie - Int Ed* 51:652–655. <https://doi.org/10.1002/anie.201104462>
  86. Ochoa A, Bilbao J, Gayubo AG, Castaño P (2020) Coke formation and deactivation during catalytic reforming of biomass and waste pyrolysis products: A review. *Renew Sustain Energy Rev* 119:. <https://doi.org/10.1016/j.rser.2019.109600>
  87. Gohier A, Ewels CP, Minea TM, Djouadi MA (2008) Carbon nanotube growth mechanism switches from tip- to base-growth with decreasing catalyst particle size. *Carbon N Y* 46:1331–1338. <https://doi.org/10.1016/j.carbon.2008.05.016>
  88. Machado BF, Bacsá RR, Rivera-c C, Serp P (2019) Preparation of Few-Layer Graphene / Carbon. *J Carbon Res* 5:. <https://doi.org/10.3390/c5020028>
  89. Gayubo AG, Valecillos J, Iglesias-Vázquez S, et al (2021) Insights into the reaction routes for H<sub>2</sub> formation in the ethanol steam reforming on a catalyst derived from NiAl<sub>2</sub>O<sub>4</sub> spinel. *Energy and Fuels* 35:17197–17211.  
<https://doi.org/10.1021/acs.energyfuels.1c01670>
  90. Cumming KA, Wojciechowski BW (1996) Hydrogen transfer, coke formation, and catalyst decay and their role in the chain mechanism of catalytic cracking. *Catal Rev - Sci Eng* 38:101–157. <https://doi.org/10.1080/01614949608006455>
  91. Hamzah N, Mohd Yasin MF, Mohd Yusop MZ, et al (2019) Growth region characterization of carbon nanotubes synthesis in heterogeneous flame environment with wire-based macro-image analysis. *Diam Relat Mater* 99:107500.  
<https://doi.org/10.1016/j.diamond.2019.107500>

## Biography

|                      |   |
|----------------------|---|
| <b>Name</b>          | Miss Sirintra Arayawate   |
| <b>Date of Birth</b> | July 31, 1993   |
| <b>Education</b>     | 2016: Bachelor of Engineering (Chemical Engineering) Sirindhorn<br>International Institute of Technology, Thammasat University, TH<br>2018: Master of Science (Engineering and Technology) Sirindhorn<br>International Institute of Technology, Thammasat University, TH<br>2019 - Present: Doctor of Engineering (Chemical Science and Engineering)<br>Tokyo Institute of Technology, JP |

## Publications

- **Arayawate, S.**, Yokosawa, T., Kimura, K., Fujitsuka, H., & Tago, T. (2023). Development of Ni nanoparticle encapsulated with Silicalite-1 catalyst for high activity steam reforming of bioethanol with high sintering resistance and coke suppression. *Journal of Chemical Engineering of Japan*.  
<https://doi.org/10.1080/00219592.2023.2269226>
- Vacharapong, P., **Arayawate, S.**, Katanyutanon, S., & Toochinda, P. (2020). Enhancement of Ni Catalyst Using CeO<sub>2</sub>-Al<sub>2</sub>O<sub>3</sub> Support Prepared with Magnetic Inducement for ESR. *Catalysts*, 10(11), 1357.
- Vacharapong, P., **Arayawate, S.**, Henpraserttae, S., Katanyutanon, S., Charojrochkul, S., Lawtrakul, L., & Toochinda, P. (2019). Effect of Magnetic Inducement in Preparation of Ni/Ce-doped Al<sub>2</sub>O<sub>3</sub> for Ammonia Decomposition. *ChemistrySelect*, 4(40), 11913–11919.
- Samarasinghe, D., Gadavanij, I., Soontornpakornkit, N., Muangkumbutr, N., Katanyutanon, S., **Arayawate, S.**, & Toochinda, P. (2019). Effects of Magnetic Inducement on Cu-Zn/Al<sub>2</sub>O<sub>3</sub> Catalyst for Methanol Steam Reforming. *Proceedings of The Pure and Applied Chemistry International Conference 2019 (PACCON 2019)*, CS75–CS79.
- Saimala, S., Srisasanarat, R., Chevangkool, P., Tananilgul, T., **Arayawate, S.**, Sinlikhitkul, N., ... Toochinda, P. (2019). Preparation of Menthol/ $\beta$ -Cyclodextrin and Menthol/Methylated- $\beta$ -Cyclodextrin Inclusion Complexes to Enhance Aqueous Solubility and Stability. *Proceedings of The Pure and Applied Chemistry International Conference 2019 (PACCON 2019)*, IC19–IC23.



- Maneewongvatana, D., Manatmethikun, M., Tiyapornsuwan, P., **Arayawate, S.**, Toochinda, P., Vachrapong, P. (2018). Effect of doped support and urea on catalytic activity and coke prevention from Ni catalyst for ethanol steam reforming reaction. *Proceedings of The Pure and Applied Chemistry International Conference 2018 (PACCON 2018)*. pp. 287-290
- Babel, S., **Arayawate, S.**, Faedsura, E., & Sudrajat, H. (2018). Microwave-Assisted Transesterification of Waste Cooking Oil for Biodiesel Production. *Utilization and Management of Bioresources*, 165–174.
- **Arayawate, S.**, Vacharapong, P., Songkrasin, P., Sirinimnuankul, P., Viphustien, P., Toochinda, P. (2017). Effect of support on Ni catalyst used for ethanol steam reforming reaction. *Proceedings of The Pure and Applied Chemistry International Conference 2017 (PACCON2017)*. pp. 1234–1239. (Oral Presentation)
- Babel, S., **Arayawate, S.**, Faedsura, E., Sudrajat, H. (2016). Production of Biodiesel from Waste Cooking Oil Using Transesterification, with the KOH on Carbon Support from Waste Material and Eggshell, as the Catalyst. *Environ. Nat. Resour. J.*, 14 (2), 60–68.

#### Presentation (2019 – present)

- 化学工学会 第 54 回秋季大会 (2023 年 9 月 12 日)  
“ゼオライト内包 Ni 微粒子触媒を用いたエタノール水蒸気改質反応”  
横澤 つき, Arayawate Sirintra, 高野 真那, 木村 健太郎, 多湖 輝興
- 化学工学会 第 88 回年会 (2023 年 3 月 17 日)  
“バイオエタノールからの高効率水素製造を目的としたゼオライト内包 Ni 微粒子触媒の開発”  
横澤 つき, Arayawate Sirintra, 木村 健太郎, 多湖 輝興
- 第 52 回石油・石油化学討論会 (2022 年 10 月 27 日)  
“高温水蒸気雰囲気下で優れた耐久性を示すゼオライト内包 Ni 微粒子触媒の開発とエタノール水蒸気改質反応への適用”  
横澤 つき, Arayawate Sirintra, 藤墳 大裕, 木村 健太郎, 多湖 輝興
- 化学工学会 第 53 回秋季大会 (2022 年 9 月 14 日)  
“Silicalite-1 ゼオライト内包 Ni 微粒子触媒によるエタノールの水蒸気改質反応”

横澤 つき, Arayawate Sirintra, 藤墳 大裕, 木村 健太郎, 多湖 輝興

- The 12th International Conference on Environmental Catalysis (ICEC2022) (2022/08/01)  
“Development of Ni nanoparticle encapsulated with Silicalite-1 catalyst for high activity steam reforming of bioethanol with coke suppression ability”  
Sirintra Arayawate, Tsuki Yokosawa, Hiroyasu Fujitsuka, Teruoki Tago
- The 9th Tokyo Conference on Advanced Catalytic Science and Technology (TOCAT9) (2022/07/25)  
“Preparation of Ni nanoparticles encapsulated with Silicalite-1 catalyst for high activity and coke suppression for Ethanol Steam Reforming”  
Sirintra ARAYAWATE, Tsuki YOKOSAWA, Hiroyasu FUJITSUKA, Teruoki TAGO
- 第 129 回触媒討論会 (2022 年 3 月 30 日)  
“Synthesis of Ni nanoparticles encapsulated Silicalite-1 for enhancing ethanol steam reforming activity”  
Sirintra Arayawate · Tsuki Yokosawa · Hiroyasu Fujitsuka · Teruoki Tago
- 第 24 回化学工学学会学生発表会 (2022 年 3 月 5 日)  
“金属微粒子内包ゼオライト触媒によるエタノール水蒸気改質反応”  
横澤つき, Arayawate Sirintra, 藤墳 大裕, 多湖 輝興
- 石油学会 第 25 回 JPIJS ポスターセッション (2021 年 5 月 24 日)  
“Development of Silicalite-1 encapsulated Ni nanoparticle catalysts for steam reforming of ethanol with high activity”  
Sirintra Arayawate, Hiroyasu Fujitsuka, Teruoki Tago